



GEORG-AUGUST-UNIVERSITÄT  
GÖTTINGEN

**PROBING ROLES OF TRPML  
IN *DROSOPHILA* HEARING**

Dissertation

for the award of the degree

“Doctor rerum naturalium”

of the Georg-August-Universität Göttingen

within the doctoral program (Sensory and Motor Neuroscience)

of the Georg-August University School of Science (GAUSS)

submitted by

Seol-hee Joo

from Seoul, South Korea

Göttingen 2014

### **Members of the Thesis Committee**

Prof. Dr. Martin Göpfert (Supervisor)

Georg-August-University Göttingen, Cellular Neurobiology

Prof. Dr. André Fiala

Georg-August-University Göttingen, Molecular Neurobiology of Behavior

Dr. Tina Pangrsic

Georg-August-University, Neurobiology

Oral examination: 21.01.2015

I herewith declare that the Ph.D. thesis entitled “Probing roles of TRPML in *Drosophila* hearing” has been written independently and with no other sources and aids than quoted.

Seol-hee Joo

Göttingen, November 2014

# Table of contents

Abstract .....	3
Table of figures.....	4
List of tables .....	5
1 Introduction.....	6
1.1 Hearing in <i>Drosophila melanogaster</i> .....	6
1.1.1 Structural basis of <i>Drosophila</i> hearing .....	6
1.1.2 <i>Drosophila</i> as a model for hearing research.....	8
1.2 TRP channels in <i>Drosophila</i> hearing.....	12
1.2.1 Transient Receptor Potential (TRP) channels.....	12
1.2.2 Putative mechanotransduction channels in <i>Drosophila</i> ear .....	14
1.2.3 Mucolipin, TRPML.....	16
2 Materials and Methods .....	20
2.1 Generation of transgenic flies and verification of mutants .....	20
2.1.1 Generation of transgenic flies .....	20
2.1.2 Verification of mutants.....	22
2.2 Probing auditory function in <i>Drosophila</i> – electrophysiological approach.....	23
2.2.1 Free fluctuation .....	23
2.2.2 Sound-evoked responses.....	24
2.2.3 Gating compliance .....	25
2.3 Immunohistochemistry .....	27
2.3.1 Tissue preparation.....	27
2.3.2 Antibody staining.....	27
2.3.3 Confocal microscopy and image processing.....	28
2.4 Motif search/prediction .....	28
2.5 Fly husbandry .....	29
2.6 List of chemicals .....	29
2.7 List of materials for molecular biology work.....	31
3 Results .....	33

3.1	Mutant analysis for active process in JO .....	33
3.1.1	Characterization of hearing phenotypes of <i>trpm1</i> <sup>1</sup> mutants .....	33
3.1.2	Genomic rescue .....	37
3.1.3	Effects of <i>trpm1</i> mutation on morphology and cellular health of JO.....	39
3.2	TRPML, the place of action.....	42
3.2.1	GAL4XUAS rescue .....	43
3.2.2	Cellular expression.....	46
3.2.3	Intracellular localization? .....	47
3.3	Efforts to find the molecular mechanisms of TRPML action on hearing.....	50
3.3.1	Analysis of gating compliance in <i>trpm1</i> <sup>1</sup> mutants .....	50
3.3.2	Epistatic analysis of TRPML and TRPV channels.....	53
4	Discussion.....	58
4.1	Neuronal expression of TRPML in the <i>Drosophila</i> ear .....	59
4.2	Intracellular localization of TRPML in <i>Drosophila</i> : on the lysosomes, on the plasma membrane and on the ciliary membrane?.....	59
4.3	TRPML mechanisms of action on fly hearing .....	61
4.3.1	TRPML-TRPV interaction in the amplificatory gain and signal propagation .....	62
4.3.2	TRPML on the correlates of transducer gating.....	62
5	Conclusions.....	66
6	References.....	67
7	Supplementary data .....	79
	List of abbreviations .....	81
	Acknowledgement.....	82
	Curriculum vitae .....	83

## Abstract

Several transient receptor potential (TRP) channels have been implicated in *Drosophila* hearing, including the TRPN channel NOMPC, the TRPVs Nan and lav, and the TRPA members Pyx and Pain. Here I report that fly hearing also involves TRPML mucolipin channels, mutations in which are implicated in the neurodegenerative disorder mucopolipidosis type IV (TRPML1) in humans and hearing impairments in *varitint-waddler* mice (TRPML3) (Di Palma et al. 2002). The latter hearing impairments arise from a point mutation that render TRPML3 constitutively open (Grimm et al. 2007, Kim et al. 2007, Nagata et al. 2008, van Aken et al. 2008), yet hearing remains uncompromised by the loss of this channel (Jörs et al. 2010), leaving the auditory relevance of TRPMLs elusive. In contrast to the mammalian system, where different TRPML channels may compensate for each other, *Drosophila* has only one TRPML member (*trpml*; dTRPML), facilitating physiological investigations. Here, I show that *Drosophila* TRPML is expressed in auditory neurons and required for sensitive hearing. Investigations of the fly's auditory mechanics revealed that mechanical amplification by auditory neurons is disrupted by null mutation in *trpml*, linearizing the mechanics of the fly's antennal sound receiver, reducing its fluctuation power and its mechanical sensitivity, and increasing its mechanical best frequency. This loss of mechanical amplification is associated with a reduced sensitivity of auditory nerve responses to both sound stimuli and sound-induced receiver displacements. A genomic *trpml* rescue construct partially restored normal amplification and auditory sensitivity in mutant flies, and so did the selective expression of *trpml* in the auditory neurons. Promoter fusions revealed that *trpml* is expressed in the fly's auditory neurons, and mutant defects in mechanotransduction were identified when I analyzed correlates of mechanical ion channel gating. Epistatic analyses place TRPML parallel to Nan-lav TRPV channels, which impede mechanical amplification by auditory neurons whereas TRPML facilitates this amplification. This establishes a role of TRPML mucolipin channels in hearing, auditory organ physiology, and auditory neuron function. Results providing first hints on the relation between lysosomal defects and hearing deficits in *trpml* mutants are also presented and discussed.

## Table of figures

FIGURE 1. DROSOPHILA EAR.....	7
FIGURE 2. FOUR DEFINING FEATURES OF THE ACTIVE PROCESS IN THE INNER EAR.....	10
FIGURE 3. GATING SPRING MODEL IN THE DROSOPHILA EAR. ....	11
FIGURE 4. PHYLOGENIC TREE OF REPRESENTATIVE TRP CHANNELS. ....	13
FIGURE 5. EXPERIMENTAL SETUP FOR PROBING AUDITORY FUNCTION IN DROSOPHILA. ....	24
FIGURE 6. ANTENNAL FREE FLUCTUATION IS REDUCED IN TRPML <sup>1</sup> MUTANTS.....	34
FIGURE 7. SOUND-EVOKED RESPONSES IN TRPML <sup>1</sup> MUTANTS SUGGEST IMPAIRMENT IN SENSITIVE HEARING. ....	35
FIGURE 8. INTRODUCTION OF GENOMIC RESCUE CONSTRUCT PARTIALLY RESTORES SENSITIVE HEARING IN TRPML <sup>1</sup> MUANTS.....	37
FIGURE 9. GROSS MORPHOLOGICAL INTEGRITY WAS MAINTAINED IN TRPML <sup>1</sup> MUTANT JO. ....	40
FIGURE 10. LIPOFUSCIN WAS NOT DETECTED IN TRPML <sup>1</sup> MUTANT JO.....	41
FIGURE 11. AUTOPHAGOSOMAL MARKER WAS NOT DETECTED IN TRPML <sup>1</sup> MUTANT JO.....	42
FIGURE 12. NEURONAL EXPRESSION OF TRPML PARTIALLY RESCUES THE HEARING PHENOTYPES IN TRPML <sup>1</sup> MUANTS. ....	43
FIGURE 13. GFP EXPRESSION DRIVEN BY TRPML-GAL4 SUGGESTS NEURONAL EXPRESSION OF TRPML IN JO. ....	46
FIGURE 14. TARGETING MOTIF PREDICTION SUGGEST PLASMA MEMBRANE AND LYSOSOMAL ASSOCIATION. ....	48
FIGURE 15. EXPRESSION OF TRPML WITH DIFFERENT TAGS MIGHT SUGGEST LYSOSOMAL LOCALIZATION.....	49
FIGURE 16. TRPML <sup>1</sup> MUTATION AFFECTS THE NONLINEAR GATING COMPLIANCE IN THE FLY'S ANTENNA. ....	51
FIGURE 17. NOMPC AND IAV ARE LOCALIZED PROPERLY IN TRPML <sup>1</sup> MUTANTS. ....	52
FIGURE 18. DOUBLE MUTANTS OF TRPML <sup>1</sup> AND IAV <sup>1</sup> CHANNELS SHOW INTERMEDIATE MECHANICAL AMPLIFICATION OF EACH SINGLE MUTANTS. ....	53
FIGURE 19. GATING COMPLIANCE IN DOUBLE MUTANTS OF TRPML <sup>1</sup> AND IAV <sup>1</sup> REFLECT BOTH ASPECTS FROM SINGLE MUTANTS.....	55

## List of tables

TABLE 1. MATERIALS AND CONDITIONS FOR GENERATION OF CONSTRUCTS.....	21
TABLE 2. PRIMERS AND CONDITIONS FOR GENOTYPING PCR.....	22
TABLE 3. COMPARISON OF HEARING PHENOTYPES IN CONTROL ( $w^{1118}$ ), TRPML <sup>1</sup> MUTANTS, AND GENOMICALLY RESCUED TRPML <sup>1</sup> MUTANTS (N=5). SG, SENSITIVITY GAIN.....	39
TABLE 4 . COMPARISON OF HEARING PHENOTYPES IN CONTROL ( $w^{1118}$ ), TRPML <sup>1</sup> MUTANTS, AND UBIQUITOUSLY AND NEURONALLY RESCUED TRPML <sup>1</sup> MUTANTS (N=5). SG, SENSITIVITY GAIN.....	45
TABLE 5. COMPARISON OF PARAMETERS OF GATING SPRING MODEL WITH TWO TYPES OF CHANNELS IN CONTROL ( $w^{1118}$ ( $R^2=0.9398$ )) AND TRPML <sup>1</sup> MUTANTS ( $R^2=0.9473$ ).....	51
TABLE 6. COMPARISON OF HEARING PHENOTYPES IN CONTROL (CANTONS), TRPML <sup>1</sup> AND IAV <sup>1</sup> SINGLE AND DOUBLE MUTANTS.....	54
TABLE 7. COMPARISON OF PARAMETERS OF GATING SPRING MODEL WITH TWO TYPES OF CHANNELS IN CONTROL (CANTONS ( $R^2=0.9398$ )), SINGLE MUTANTS (TRPML <sup>1</sup> ( $R^2=0.9473$ ) AND IAV <sup>1</sup> ( $R^2=0.9245$ )) AND DOUBLE MUTANTS (IAV <sup>1</sup> ;TRPML <sup>1</sup> ( $R^2=0.9134$ )).	56



# 1 Introduction

## 1.1 Hearing in *Drosophila melanogaster*

Hearing in the fruit fly *Drosophila melanogaster* primarily serves conspecific communication. Male flies court females with songs they generate by fanning one of their wings. These songs increase female receptivity, which is drastically reduced by hearing impairments (Burnet et al. 1971). The ear of *Drosophila* is formed by its antenna, whose distal part vibrates in response to the particle velocity component of sound and serves as a sound receiver. Whereas eardrums are moved by the sound pressure, this detection of the sound-particle velocity is advantageous for close-range acoustic communication, allowing for intimate courtship song (Bennet-Clark 1971, Göpfert and Robert 2008).

### 1.1.1 Structural basis of *Drosophila* hearing

The fly's antenna is composed of three segments, scape, pedicel and funiculus (Figure 1a-b). The third antennal segment (a3) funiculus is rigidly coupled to the feather-like projection arista, together forming the sound receiver. In response to sound stimulus, a3 vibrates about the longitudinal axis of the antenna by the torque exerted by the back and forth movement of the arista. This vibration is transferred to a chordotonal organ called Johnston's organ (JO) in the pedicel (a2) via a flexible a2-a3 joint (Göpfert and Robert, Nature 2001), compressing and stretching the organ. The *Drosophila* JO consists of 227 multicellular scolopidia (Kamikouchi et al. 2006), each comprising two to three sensory neurons, one scolopale cell, and one cap cell and a ligament cell (Eberl and Boekhoff-Falk 2007; Figure 1c-d). While a scolopale cell ensheathes the dendritic region of the neurons, a cap cell and a ligament cell connect the scolopidium apically and basally to a2 and a3, respectively. In total, JO consists of  $447 \pm 24$  mechanosensory neurons (JONs) (Kamikouchi et al. 2006). These neurons are bipolar and monodendritic (Lu et al. 2009), with an axon projecting to the antennal mechanosensory and motor center (AMMC) and a single dendrite that, spanning across the a2-a3 joint, connects to a3. The dendrite bears an inner and an outer segment. The latter is ciliated, displaying a 9 + 0 axoneme and a

swelling at half its length, the ciliary dilation. This dilation is filled with a paracrystalline structure (Todi et al. 2004, Kernan 2007) and compartmentalizes the cilium into a proximal and a distal region (Figure 1d). The cilium is surrounded by actin-based scolopale rods that are formed by the scolopale cell and a tightly sealed scolopale space (Carlson et al. 1997a, 1997b, Todi et al. 2004). The apical tip of the cilium is connected to the cap cell via an extracellular dendritic cap that contains the extracellular matrix protein NOMPA secreted by the scolopale cells.

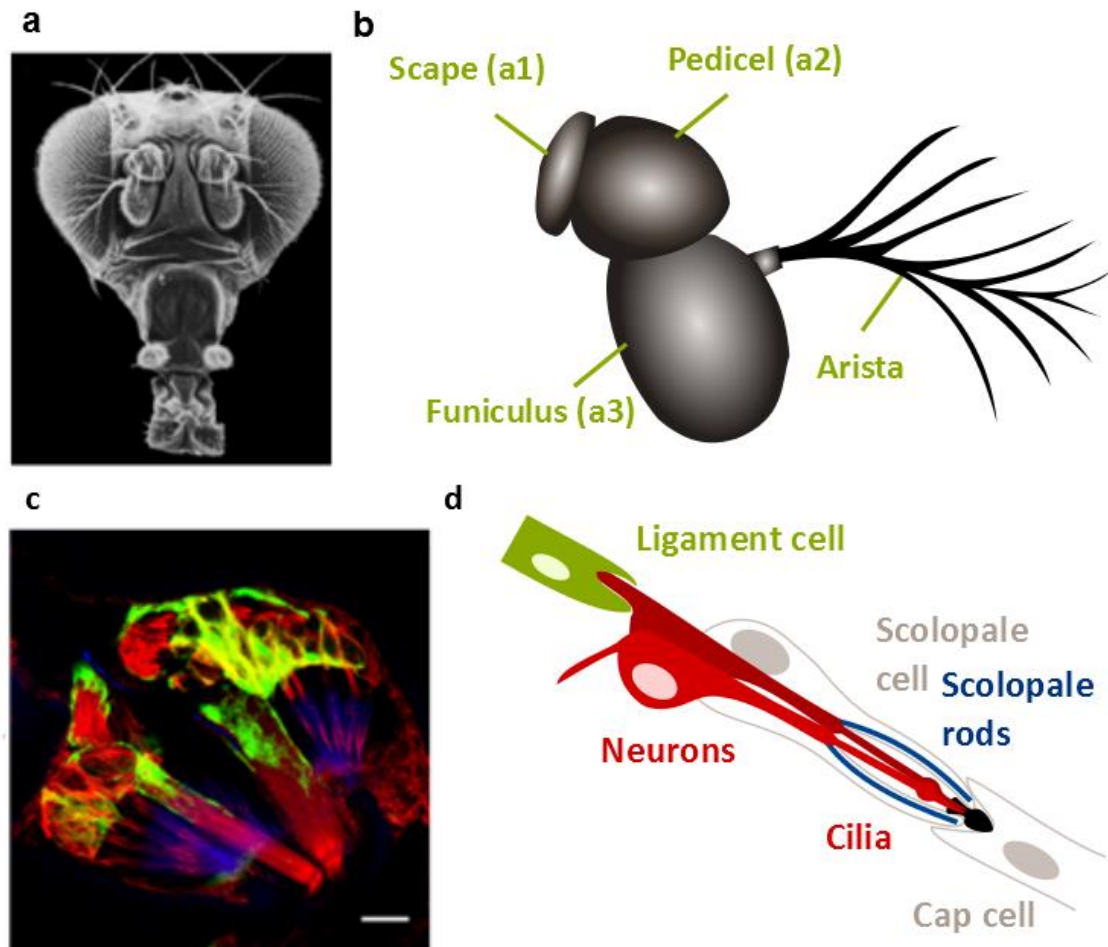


**Figure 1. *Drosophila* ear.**

**a.** Scanning electron microscope image of wild-type fly head (by Dr. Rudi Turner, inserted with permission). The antennae are located between two eyes **b.** Illustration of the antenna. Johnston's organ, the hearing organ, is located in the pedicel. The arista serves as the sound receiver, making the rigidly-coupled third segment (funiculus) vibrate in response to sound. Only the scape contains muscles. **c.** Confocal image of Johnston's organ. Johnston's organ neurons are marked with  $\alpha$ -Tubulin antibody (red), the scolopale rods are labelled with Phalloidin (blue), and the ligament cells are visualized by driving GFP via an Ir94b-GAL4 promoter fusion construct. **d.** Schematic representation of scolopidium (adapted from Chung et al. 2001). Structures marked in c are highlighted in the respective color.

JON cilia are specialized mechanosensory organelles, as is exemplified by the deafness of mutants with ciliary phenotypes ranging from a severe structural disruption of the cilia to the subtle mislocalization of ciliary proteins: Mutants missing functional Rfx, a transcription factor regulating ciliogenesis (Han et al. 2003, Cachero et al. 2011) or NOMPB, which is required for intraciliary transport, for example, lack cilia, and hence, hearing. Loss of Spam, an extracellular shielding material, causes a massive cellular deformation of JO neurons followed by hearing loss upon heat-induced osmotic imbalance (Cook et al. 2008). Auditory function is also disrupted by mutations in genes that contribute to cilium assembly, including the transcription factor *fd3f* (Newton et al. 2012), *unc* (Kernan et al. 1994, Eberl et al. 2000, Baker et al. 2004), *tilB* (Kavlie et al. 2010), as well as genes that are implicated in the proper organization of the ciliary dilation such as *btv* (Eberl et al. 2000, Newton et al. 2012) and *dcx-emap* (Bechstetdt et al. 2010). Mislocalization of the putative mechanotransduction channels NOMPC, Inactive (*lav*) and Nanchung (*Nan*) also leads to hearing defects (Göpfert et al. 2006, Cheng et al. 2010a, Park et al. 2013).

### **1.1.2 *Drosophila* as a model for hearing research**

Notwithstanding the anatomical differences and the evolutionary distance, the fly ear exhibits genetic as well as mechanical parallels with the mammalian cochlea (reviewed in Eberl et al. 2000, Kernan 2007, Göpfert and Robert 2008), allowing to exploit the genetic tractability of the *Drosophila* ear to explore the genetics and mechanisms of hearing.

#### **1.1.2.1 Genetic parallels**

Each scolopidium is developmentally derived from a single sensory precursor (SOP) cell. During development, mechanosensory specification is directed by a basic helix-loop-helix (bHLH) proneuronal transcription factor Atonal (Jarman et al. 1995), whose mouse homolog Atoh1 is essential for the development of cochlear hair cells (Bermingham et al. 1999). Interestingly, fly Atonal and mouse Atoh1 can complement each other's function, i.e. *atonal* can rescue the defects in cochlear development when introduced into mouse *atoh1* mutant and vice versa (Ben-arie et al. 2000, Wang et al. 2002).

Furthermore, *atonal* was recently shown to fine-tune the development of chordotonal organs by regulating the two transcription factors Rfx and Fd3f, which in turn regulate general ciliogenesis and chordotonal-specific cilium differentiation, respectively (Cachero et al. 2011, Newton et al. 2012), and these downstream regulatory genes might be also conserved. Although cochlear hair cells are endowed with actin-rich stereocilia, their kinocilium has ciliary structure (Kikuchi et al. n.d., Ake Flock and Duvall 1965), providing a ground to look for genetic equivalence. Vertebrate Rfx3 is implicated in ciliogenesis, although its impact on hair cell development is yet to be proven (Thomas et al. 2010). For example, Fd3d shares target genes related to ciliary motility Foxj even though their homology is rather low (Mazet et al. 2003, Larroux et al. 2008, Jacquet et al. 2009, Newton et al. 2012, Jarman 2014).

In addition to genes in developmental pathways, some other components also show parallels. Loss of Crinkled, for example, disturbs the arrangement and attachment of JO neurons, which is in accordance with the function of its mammalian counterpart, Myosin VIIA, which is necessary for the stair case-like organization of hair cell stereocilia (Todi et al. 2008). Mutations in TRPVs IAV and NAN as well as in one of their mammalian homologs, TRPV4, result in hearing impairments (Kim et al. 2003, Gong et al. 2004, Tabuchi et al. 2005, Zimoń et al. 2010). Tectorins, components of extracellular matrix in the cochlea have ZP domains as the aforementioned cap protein NompA, and their respective losses lead to hearing impairments (Killick et al. 1995, Legan et al. 1997). These genetic parallels suggest that *Drosophila* can be a powerful tool to decipher mechanisms underlying deafness in humans (Boekhoff-Falk 2005, Göpfert and Robert 2008, Jarman 2014).

### **1.1.2.2 Functional parallels**

The performance of our inner ear is immensely augmented by an active process that is defined by four features: 1) amplification, which boosts the ears' mechanical response more than 100-fold; 2) frequency selectivity, which reflects the selective enhancement of the ear's mechanical input and sharpens frequency tuning; 3) compressive nonlinearity, which compresses a broad range of stimulus amplitudes into a narrow range of mechanical responses, and 4) spontaneous otoacoustic emission, sound generated by unprovoked-ear in a quiet environment (Göpfert and Robert 2008, Hudspeth 2008; Figure 2). This active process exists in *Drosophila*, whose antennal sound receiver displays all these four characteristics. The *Drosophila* ear exhibits power gain, reflecting the active energy contributions and its mechanical responses to low intensity sounds is maximally amplified, with amplification gains

of around 10 (Göpfert et al. 2006). This compressive nonlinearity allows the flies to sense a wide range of sound intensities and facilitates sound detection when sound is faint (Göpfert and Robert 2003). The active tuning of the sound receiver vanishes during anoxia (Göpfert and Robert 2002), and in TRPV mutants lacking *iav* and *nanchung* the sound receiver displays self-sustained oscillations, the mechanical analogue of spontaneous otoacoustic emissions arising from excess amplification (Göpfert et al. 2006).

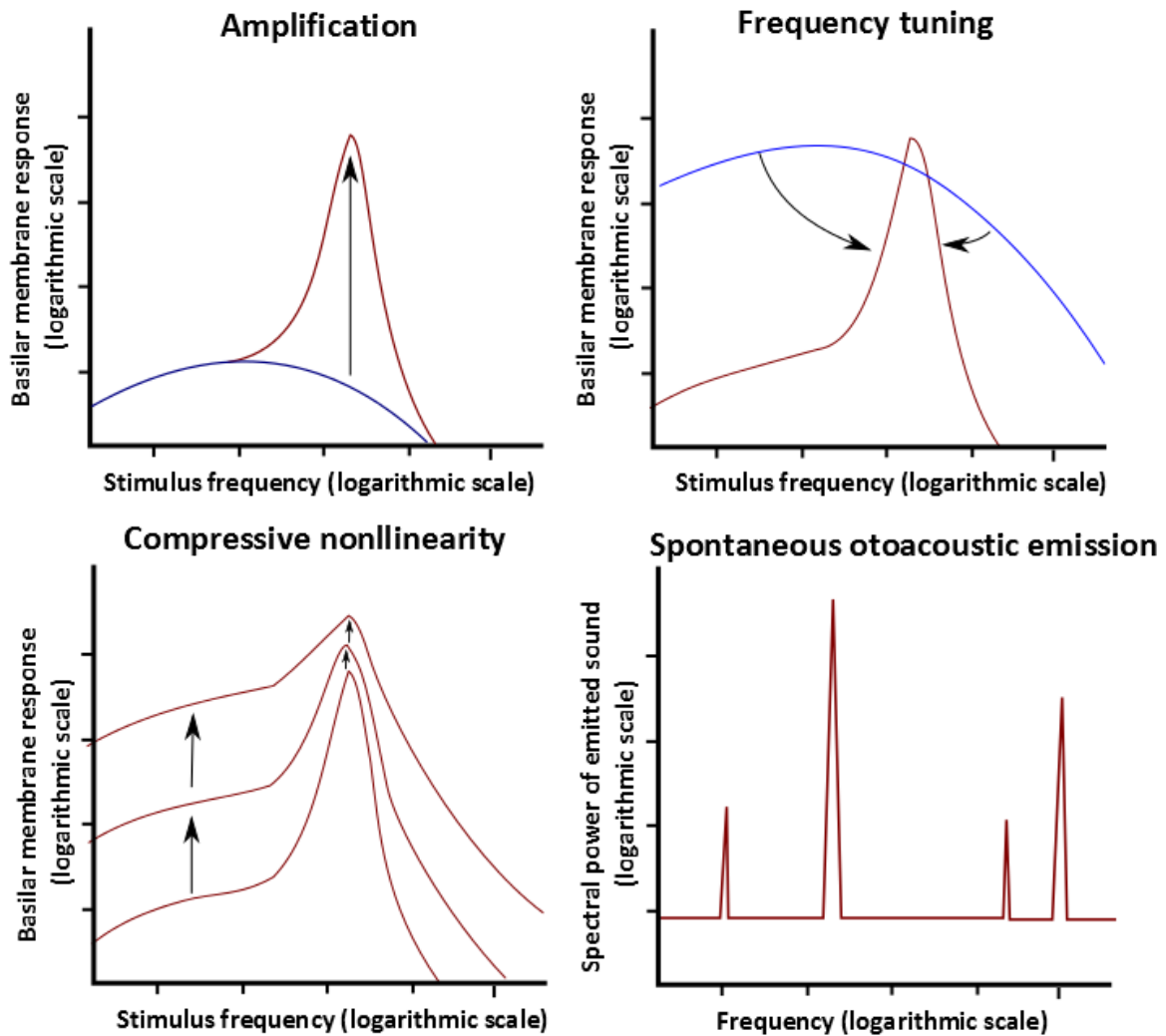


**Figure 2.** Four defining features of the active process in the inner ear.

**a.** Amplification. **b.** Sharpened frequency tuning. **c.** Compressive nonlinearity. **d.** Spontaneous otoacoustic emission (taken and retouched from Hudspeth 2008 with permission).

Mechanotransduction in *Drosophila* relies on mechanically-gated ion channels (Albert et al. 2007). The mechanical opening of force-gated channels introduces a nonlinear gating compliance in the antennal

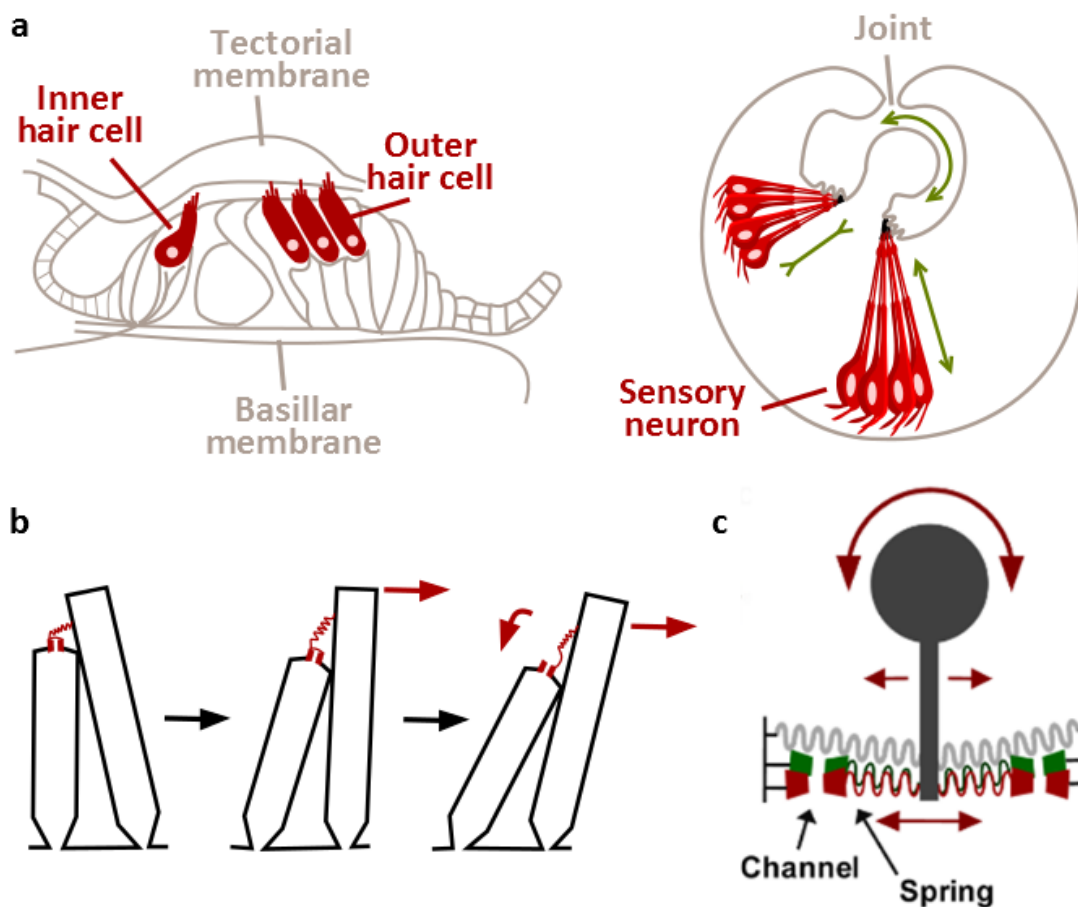


**Figure 3. Gating spring model in the *Drosophila* ear.**

**a.** Structural basis for gating spring model in vertebrate (left) and *Drosophila* (right) ears (modified from Bechstedt and Howard 2008), with each structure for model application highlighted. **b.** Gating compliance in hair cell stereocilia. Application of force (green arrow) to a hair bundle put strains on the gating spring, which conveys the force to open the channel (orange arrow), relaxing the spring, and this relaxation moves the whole bundle further more (red arrow) (modified from Hudspeth et al. 2000). **c.** Schematics of gating spring model for *Drosophila* ear. The model comprises two opposing populations of channels symmetrically connected to the oscillator via gating spring. Note that the channels are illustrated with two different colors, which indicates two groups of channels with different sensitivities to sound stimulus. This is the modification applied to the original model with only one type of channels to better fit the experimental data in *Drosophila*. (adapted from Nadrowski et al. 2008 and modified according to Effertz et al. 2012).

mechanics that can be described by gating spring model for vertebrate auditory transduction (Figure 3b-c). This model posits that the mechanotransducers in hair cells are mechanically activated via gating

springs that convey forces to gates of the channels. When the channels open, the gating springs relax, resulting in nonlinear gating compliance, which is a reduction in the stiffness of the antenna that occurs over the range of displacement/force at which the channels gate (Albert et al. 2007; Figure 3b). This model in flies assumes that two opposing populations of channels symmetrically connected to the oscillator via gating springs and this is arranged in parallel with linear spring. According to the gating spring model, the displacement-dependent stiffness of the antenna ( $K(x)$ ) reflects a linear elasticity of stiffness ( $K_{par}$ ) and the combined stiffness of the gating springs ( $K_{GS}$ ). Both of these elasticities determine the asymptotic stiffness  $K_{\infty}$ , that the antenna assumes when it is deflected far. The gating spring model relates the stiffness of the system, ( $K(x)$ ), to the open probability of the channels ( $P_o$ ) (Howard and Hudspeth 1988):

$$K(x) = K_{\infty} - \left( \frac{Nz^2}{k_B T} \right) * P_o(1 - P_o).$$

A recent study has shown that the mechanics of the fly's antenna betrays the mechanical gating of at least two different types of, that are sensitive (s) and less sensitive (i), channels (Effertz et al. 2012), yielding

$$K(x) = K_{\infty} - \left( \frac{N_s z_s^2}{k_B T} \right) * P_{0s}(1 - P_{0s}) - \left( \frac{N_i z_i^2}{k_B T} \right) * P_{0i}(1 - P_{0i}).$$

## 1.2 TRP channels in *Drosophila* hearing

### 1.2.1 Transient Receptor Potential (TRP) channels

The transient receptor potential (TRP) channel superfamily is exceptionally diverse in its responsiveness to different stimuli, ranging from temperature, pH, ligands, osmolarity and even stretch. Additionally, multiple gating mechanisms can coexist in a single channel. Varying degrees of cation selectivities, together with the homo- and hetero-multimerization of TRPs, further expand the diversity of this ion channel family. These diverse features suggest the role of TRPs in signal integration at the cellular level, which is crucial for cells to detect and respond to changes in their local environment, as well as for different sensory processes at the organism level, which includes vision, olfaction, nociception, thermo- and hygro-sensation, touch, and hearing (Venkatachalam and Montell 2007).

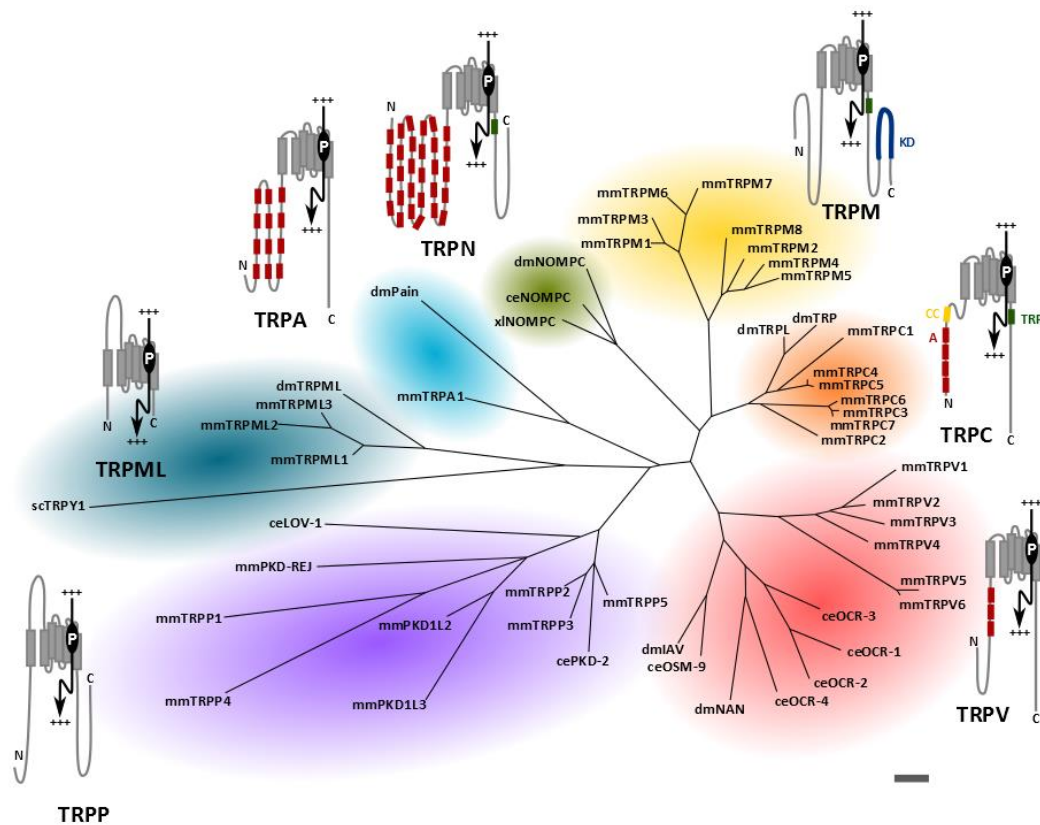


**Figure 4. Phylogenetic tree of representative TRP channels.**

TRP channels can be categorized into seven groups, including TRPC (canonical), TRPV (vanilloid), TRPM (melanostatin), TRPN (NOMPC), TRPA (ankyrin) and more distantly related TRPML (mucolipin) and TRPP (polycystin). Predicted membrane topology for each group is illustrated including distinct domain features: A, ankyrin; cc, coiled-coil domain; TRP domain; KD, protein kinase domain. Prefixes of gene names indicate species: *ce*, *Caenorhabditis elegans*, *dm*, *Drosophila melanogaster*, *mm*, *Mus Musculus*, *sc*, *Saccharomyces cerevisiae*, *xl*, *Xenopus laevis*. Scale bar: 0.2 nucleotide substitutions/site. (phylogenetic tree adapted from Christensen and Corey (2007) with permission and topology adapted from Venkatachalam and Montell (2007)).

Members of the TRP family are evolutionarily conserved among organisms ranging from yeast to invertebrates and vertebrates. Based on sequence homology, TRP channels can be categorized into two groups, whereby group 1 is subdivided into the TRPC (canonical), TRPV (vanilloid), TRPM (melanostatin), TRPN (NOMPC), TRPA (ankyrin) subfamilies, and group 2 comprises TRPMLs (mucolipins) and TRPPs (polycystins) (Figure 4). Both groups share structural features of voltage-gated potassium channels (Harteneck et al. 2000): they form tetrameric complexes, with each monomer showing a six-transmembrane helix topology (S1-S6). S5 and S6 line the pore and the reentrant loop



between S5-6 forms the selectivity filter (Kedei et al. 2001, Yu and Catterall 2004, Hellmich and Gaudet 2014).

A large extracellular loop between S1 and S2 is the key characteristics separating group 2 from group 1 (Venkatachalam and Montell 2007). The channels show high diversity in their intracellular regions- especially both N- and C-termini contain several different domains. One of the distinct domains includes N-terminal ankyrin repeats, which are present in the TRPC, TRPA, TRPV and TRPN subfamilies. The 33-amino acid ankyrin repeat forms helix-turn-helix structure, with side-by-side packing of each repeats forming a surface for protein-protein interaction (Sedgwick and Smerdon 1999, Mosavi et al. 2004). Ankyrin repeats appear in wide variety of proteins, involved in plethora of cellular processes, including development, cell signaling, and cell cycle regulation (Latorre et al. 2009). Interestingly, studies showed that ankyrin repeats in TRPA and TRPN bear the appropriate stiffness properties required for the gating springs in the hearing apparatus (Sotomayor et al. 2005, Lee et al. 2006). In accordance of these data, two TRPA channels painless and pyrexia were implicated in gravity sensation and a TRPN channel NOMPC in hearing (Göpfert et al. 2006, Sun et al. 2009, Effertz et al. 2011).

## **1.2.2 Putative mechanotransduction channels in *Drosophila* ear**

Christensen and Corey (2007) suggests several criteria for a protein to be a reasonable candidate mechanotransduction channel: 1) Direct gating of the channel by force which can be assessed by the activation kinetics and mechanical correlates of the channel gating, 2) requirement of the channel for mechanotransduction, which is a matter of correct expression and localization of the protein, 3) whether it confers mechanosensitivity when expressed in a heterologous system, 4) presence of pore-forming and force-sensing structure, which becomes apparent when those structures are mutated. According to these criteria, there are three candidates for the mechanotransduction channel in *Drosophila* hearing, NOMPC (No mechanoreceptor potential C), and two TRPVs IAV (Inactive), and NAN (Nanchung).

### **1.2.2.1 NOMPC**

NOMPC is expressed and localized to the distal cilia of all JONs (Lee et al. 2010, Cheng et al. 2010a, Liang et al. 2011). A 29 ankyrin repeat domain at the N'-terminus of NOMPC has been suggested to be a gating spring, based on its helical structure and predicted elastic properties (Sotomayor et al. 2005, Lee et al. 2006). Also, the existence of microtubule-membrane connection of *Drosophila* mechanoreceptors are NOMPC-dependent and the modeling approach revealed that the connection shows characteristics of ankyrin repeats (Liang et al. 2013), suggesting NOMPC could be providing the force-sensing structure. Ectopic expression of NOMPC confers mechanosensitivity to otherwise touch-insensitive cells and the channel with a mutation in putative selective filter shows altered permeation properties (Yan et al. 2013, Gong et al. 2013), indicating that NOMPC indeed is a mechanically gated ion channel. These reports suggest that NOMPC might be the mechanotransducer in the ear of *Drosophila*.

The consequences of loss of the channel in JO, however, leave a room for disputes on whether NOMPC is the fly's auditory mechannotransduction channel. Loss of NOMPC abolishes active amplification (Göpfert et al. 2006), which seems to be linked to transduction (Nadrowski et al. 2008, Zanini and Göpfert 2014), suggesting that NOMPC might be the transduction channel in JONs. Two observations, however, complicate this hypothesis. First, the NOMPC null mutation lowers the amplitude and sensitivity of sound-evoked nerve response but the nerve response to antennal displacement is not completely lost (Göpfert et al. 2006). Second, giant fiber neurons are shown to be coupled to an unknown number of sound-sensing JONs via gap junction (Kamikouchi et al. 2009, Lehnert et al. 2013) and the subthreshold signals recorded from the giant fiber neurons were still detectable in the NOMPC null mutants (Lehnert et al. 2013). These results might be due to the existence of second type of mechano-transduction channel with lower sensitivity than NOMPC. JONs can be categorized into two different groups based on their preferential response to different stimuli, sound and gravity/wind (Kamikouchi et al. 2009, Effertz et al. 2011). Not only are the latter JONs NOMPC-independent for their gravity/wind sensing function, but also ablation of those cells did not affect mechanical amplification and sensitive hearing (Kamikouchi et al. 2009, Effertz et al. 2011). Also, mechanical correlates of channel gating in the fly ear suggest that JONs have mechanically gated channel types of two different sensitivities, with the gating of the more sensitive type being dependent on NOMPC (Effertz et al. 2012). Taken together, NOMPC seems to be required in the auditory JONs for transduction and there seems to be a second transduction channel in some JONs that awaits its identification.

### **1.2.2.2 IAV/NAN**

Two TRPV channels IAV and NAN expressed in JON are localized to the proximal region of the cilia (Kim et al. 2003, Gong et al. 2004). Correct localization of these channels are interdependent, suggesting IAV and NAN form a heteromultimeric channel (Gong et al. 2004). Heterologous expression of NAN (Kim et al. 2003) or IAV (Gong et al. 2004) produced currents induced by hypo-osmotic stress in the cells, suggesting that the TRPVs might be mechanosensitive. In the null mutants of either of the TRPV channels, auditory nerve response is completely abolished (Kim et al. 2003, Gong et al. 2004) and the subthreshold recordings from the giant fiber neurons showed abolished response (Lehnert et al. 2013), suggesting IAV and NAN might mediate auditory transduction in the fly. But the mutants exhibit excess feedback amplification (Göpfert et al. 2006), which indicate intact transduction (Zanini and Göpfert 2014), leaving the conclusions open.

Based on the findings above on NOMPC, IAV and NAN, two models of TRP function in *Drosophila* auditory transduction has been proposed (Zanini and Göpfert 2014). In NOMPC transducer model, mechanical stimuli are coupled to the NOMPC channel in auditory JONs and less sensitive type of channel in gravity/wind-receptor JONs, which transduces the vibrations to cellular signals, whereas NAN/IAV acts downstream of transduction to propagate the signals. In sound-sensitive JONs, NOMPC interacts with adaptation motors leading to mechanical amplification, which is negatively regulated by NAN/IAV (Göpfert et al. 2006, Effertz et al. 2011, 2012). In NAN/IAV transducer model, antennal vibrations directly gate NAN/IAV channels, which transduce them into cellular signals in both types of JONs. NOMPC acts on mechanical amplification in auditory JONs, enhancing the mechanical input to NAN/IAV, thus promoting transduction (Lehnert et al. 2013, Zanini and Göpfert 2014).

### **1.2.3 Mucolipin, TRPML**

#### **1.2.3.1 Lysosomal processes and autophagy**

Lysosomes are membrane-enclosed organelles characterized by their acidic lumen. The lumen is filled with more than 50 powerful acid hydrolases devoted to digestion of specific substrates, together

degrading most of the cellular waste (Kroemer and Jäätelä 2005). Due to this distinctive feature, lysosome has been considered as waste processors clearing and recycling the cellular waste since the first characterization of the organelle with 'electron dense core' by Christian de Duve 50 years ago (Novikoff et al. 1956). Recent advances, however, are revealing much wider involvement of lysosomes in cellular processes, including membrane repair, secretion, neurite outgrowth, cellular metabolism, and cell death (Blott and Griffiths 2002, Guicciardi et al. 2004, McNeil and Kirchhausen 2005, Laplante and Sabatini 2012).

There are two incoming routes to lysosomes: endocytotic and autophagic pathways. Extracellular materials destined for degradation are internalized into primary endocytic vesicles. The vesicles undergo maturation into early endosomes (EE) and later, late endosomes (LE). The membrane of EEs and LEs can sort ubiquitinated proteins into invaginating buds, which pinch off into the lumen of the vesicle, giving rise to multivesicular bodies (MVBs). Those intraluminal vesicles are eventually exposed to the degradative enzymes after the LEs fuse with lysosomes (Hurley and Emr 2006). Cytoplasmic components/organelles for degradation, on the other hand, are first sequestered into autophagosomes. Autophagosomes fuse with LEs forming the amphisome, which subsequently matures into MVBs. MVBs merge with lysosome eventually to form autolysosomes where they get degraded (Moreau et al. 2013). This autophagic process plays essential roles in disposal of damaged organelles and recycling of cellular resources, which become significant in the metabolic control under stress conditions (Mariño et al. 2014).

Lysosomal exocytosis and lysosome to trans-Golgi network (TGN) trafficking constitute two major exits from lysosomes. Lysosomal exocytosis is a fusion between lysosomal and plasma membrane, which can exocytose bulk materials from the lysosomal lumen and transfer membrane materials for plasma membrane repair (Settembre et al. 2013). Trafficking of pinched-off vesicles from lysosome to TGN makes it possible for lysosomes to selectively remove and transport endosomal membrane proteins and lipids, and the digested materials can be used to synthesize cellular components (Alberts et al. 2008).

To perform these tasks, lysosomes are equipped with specialized membrane proteins in addition to the acidic lumen with digestive enzymes and protective glycocalyx lining on the interior of lysosomes (Reitsma et al. 2007). For regulated trafficking and fusion, molecules comprising membrane fusion machineries such as SNAREs and Rabs (Peterson et al. 1999, Mullock et al. 2000), a  $Ca^{2+}$  channel, most probably Mucolipin-1, to trigger the fusion (LaPlante et al. 2002), as well as the lysosomal markers like LAMP1 to facilitate recognition by the fusion machineries (Chen and Whiteheart 1999) are present on the lysosomal membrane. Niemann-Pick C1 (NPC1) is involved in cholesterol efflux (Lloyd-Evans et al.

2008) whereas lysosomal amino acid transporter 1 (LAAT1) is required for amino acid discharge from the lysosomes (Liu et al. 2012), which are crucial for the cellular lipid and amino acid homeostasis, respectively. Interestingly, on the lysosomal membrane, there is a feature directly coupling the lysosomes to the autophagic control, LYNUS (Settembre et al. 2013).

The lysosomal nutrient sensing (LYNUS) is a multiprotein complex containing mTOR, which detects the nutrient availability in the cells (Settembre and Ballabio 2014). The complex is activated upon sensing nutrients, portrayed by the kinase activity of mTOR. Active mTOR phosphorylates TFEB, which inhibits the protein (Peña-Llopis et al. 2011). TFEB is a transcription factor that binds to a consensus known as CLEAR motifs (the coordinated lysosomal expression and regulation) (Sardiello et al. 2009), which are frequently found in the promoter region of the genes involved in the cellular clearance. Under starvation condition, mTOR becomes inactive, losing the control on TFEB. Then TFEB is released to enter the nucleus and upregulate the target genes, which facilitate the lysosome biogenesis, endocytotic as well as exocytotic flow, and autophagy (Settembre et al. 2011).

### **1.2.3.2 TRPML in hearing?**

Mucopolin-1, the founding member of TRPML family channels was first identified as the causative gene for the lysosomal storage disorder mucopolipidosis IV (MLIV) (Sun et al. 2000). MLIV is characterized by psychomotor retardation and progressive retinal degeneration. Cells from the patients exhibit enlarged vacuoles and accumulation of lipids in endosomal compartments. Mammals have TRPML homologs and increasing evidence supports that all these channels are cation channels, which play roles at different steps along the endolysosomal path (Cheng et al. 2010b). Also, the channels predominantly reside on the endosomal membranes, revealed by overexpression with tagged proteins and gradient fractionation approaches (Puertollano and Kiselyov 2009). Reports on biophysical properties of mammalian and *Drosophila* TRPML channels revealed that the activity of the channels were augmented by low pH and PI(3,5)P<sub>2</sub> which represent the endolysosomal conditions (Dong et al. 2010, Feng et al. 2014), implying that those channels are located in those intracellular compartments. Recent advances in endolysosomal biology puts TRPML in a central position with multifaceted involvement. For example, relatively well-studied Mucopolin-1 is implied in endosome maturation, lysosome to TGN trafficking, autophagosome-lysosome fusion, and lysosomal exocytosis (Wang et al.

2014). Importantly, two reports link TRPML with the control of autophagy and hence metabolic control (Kim et al. 2009, Wong et al. 2012).

*Varitint-waddler* mouse shows hearing defect derived from a gain-of-function mutation in TRPML3 (Di Palma et al. 2002, Grimm et al. 2007, Kim et al. 2007, Nagata et al. 2008, van Aken et al. 2008). Also, Takumida and Anniko (2010) reported that the channel is expressed on the stereociliary membrane as well as in the endosomal compartments in the inner hair cells. Null mutation of TRPML3, however, didn't have any impact on hearing (Jörs et al. 2010), leaving the auditory involvement of TRPML unclear. Hence, in this study, I investigated the involvement of TRPML in the *Drosophila* system with the advantage of having single homolog and possible mechanisms of TRPML action in the process.

## 2 Materials and Methods

### 2.1 Generation of transgenic flies and verification of mutants

#### 2.1.1 Generation of transgenic flies

Making transgenic flies included the cloning of constructs into a proper vector, the injection of the constructs into *Drosophila* embryos and the balancing of the progenies carrying the insertion to establish stable lines.

Cloning included to five main steps: 1) the designing of primers, 2) the amplification and/or purification of templates, 3) polymerase chain reaction (PCR), 4) verification of the sequences, and 5) ligation to appropriate vectors. Primers were designed using a primer design tool provided by ncbi (<http://www.ncbi.nlm.nih.gov/tools/primer-blast>). The melting temperature was set between 55 to 65°C. The primers were chosen so that they don't have similar sequences in the templates, except for the primers targeting in-frame sequences. Restriction sites were added to some primers to facilitate the ligation into target vectors. The final melting temperature and possibilities for hairpin formation, self- and hetero-dimerization were checked using oligoanalyzer 3.1 (<http://eu.idtdna.com/analyzer/Applications/OligoAnalyzer>). Genomic DNA templates were prepared from one of the wild-type strains (*CantonS* or *w<sup>1118</sup>*) using a genomic DNA extraction kit (DNeasy Blood & Tissue Kit, Qiagen), following manufacturer's instruction. RNAs were extracted using a RNA purification kit (RNeasy mini kit, Qiagen) and then reverse transcribed with a reverse transcription kit (LongRange 2Step RT-PCR Kit, Qiagen) to generate cDNA templates. *Bac* clones were purified using mini prep kit (Invisorb® Spin Plasmid Mini Two, 1010140400, Invitex), following a modified protocol from manufacturer's. PCRs were performed with designed primers and templates of which the primers are based on (Table 1), using high-fidelity DNA polymerase (Phusion high-fidelity DNA polymerase, F-530L, Thermo Scientific). The PCR products were purified with a PCR purification kit (QIAquick PCR Purification Kit (50), 28104, Qiagen) according to manufacturer's instructions and then ligated to pCR2.1 TOPO vector (pCR®2.1-TOPO®, Invitrogen). Chemically competent cells (XL-1 Blue, 200-236 Stratagene) were transformed with the ligation products following the standard heat-shock

procedures and single colonies were inoculated from the plates to separate tubes containing LB medium with ampicillin, incubated overnight at 37°C for amplification, and then the DNA was purified from the harvested cells using mini prep kit. After verifying correct clones with enzyme restriction pattern resolved on agarose gels followed by sequencing, the DNA was digested with restriction enzymes (FastDigest, Thermo Scientific), separated on agarose gels, eluted from the gels using gel extraction kit (QIAquick Gel Extraction Kit (250), 28706, Qiagen) and ligated (T4 DNA ligase, Thermo Scientific) with the right vectors (Table 1). After the amplification and verification steps of ligation products as in the TOPO vector cloning described above, the constructs in pPTGAL or pUAST-attB were sent for injection into *Drosophila* embryos to a service provider (Bestgene Inc. Chino Hills, CA, USA).

**Table 1. Materials and conditions for generation of constructs.**

f, forward; r, reverse; Ta, annealing temperature

Construct		Direction	Primers	Template	Ta (°C)	Sub-cloning vector	Restriction enzyme	Final vector
trpml-GAL4		f	AGGAGCAGGATGGAAAGGAT	BACR23N10	62	NA	Stu1	pPTGAL
		r	CGATGTGCTCCTCCTTCGTT				Kpn1	
GFP-TRPML	GFP	f	GGTGAGATCTTAAACCATGGCTAGC AAAGGAGAAG	pTracer-CMV	60	pCR2.1	Bgl2	pUAST
		r	GTCGCGGCCGCATCCATGCCATGTG TAATCCCAG				Not1	
	TRPML	f	AGGCGGCCGCGATGCAGAGCTACG GCCCGG	cDNA	65	pCR2.1	Not1	
		r	CGCCTCGAGTTACTTCATAATACTA GAAAGGCTGGT				Xho1	
TRPML-GFP	TRPML	f	ACGGCGGCCGCGCACATCGAGATG CAGAGCTACGGCCCC	cDNA	67	pCR2.1	Not1	pUAST-attB
		r	CACCGGTACCCTTCATAATACTAGA AAGGCTGGTGTAACCACTGTTGG				Kpn1	
	GFP	f	GAACGGTACCATGGCTAGCAAAGG AGAAGAAC	pTracer-CMV	60	pCR2.1	Kpn1	
		r	GGTTCTAGACTAATCCATGCCATGT GTAATCCCAGCAG				Xba1	
GST-TRPMLC'-11XHis	TRPMLC'	f	ATGGATCCGATGGCTTTCCACCAC	pUAST-GFPTRPML	63	pCR2.1	BamH1	pGEX-4T-2
		r	CCAGGAATTCCTTCATAATACTAGA AAGGC				EcoR1	
	11XHis	f	GAATTCCTGGAAGTTCTGTTCCAGG GGCCCCATCATCACCATCACC	Overlapping PCR	70	pCR2.1	EcoR1	
		r	GCGGCCGCTCAGTGATGGTGATGA TGTTGGTGATGGTGATGATGGG				Not1	



## 2.1.2 Verification of mutants

Genotypes of the mutants were verified by PCR or PCR followed by gel electrophoresis and/or sequencing, depending on the size of the mutational lesion. The procedure started from the purification of total DNA from the flies using a genomic DNA extraction kit (DNeasy Blood & Tissue Kit, Qiagen), following the manufacturer's instruction. PCRs were performed with designed primers (Table 2) and high-fidelity DNA polymerase (Phusion high-fidelity DNA polymerase, F-530L, Thermo Scientific) on the extracted genomic DNA. The PCR products were purified with a PCR purification kit (QIAquick PCR Purification Kit (50), 28104, Qiagen) according to the manufacturer's instructions. Large deletion of *trpm1*<sup>l</sup> was verified by simply resolving the PCR products on agarose gels with the *w*<sup>1118</sup> as control, whereas a point mutation in *iav* mutants was checked by subsequent sequencing (MPI-Sequencing Facility in Hermann-Rein-Str. 3, 37075 Göttingen, Germany) of the products.

**Table 2. Primers and conditions for genotyping PCR**

Gene	Primers			Annealing temperature (°C)
	Direction	Sequence	ID	
<i>trpm1</i>	forward	TGTACGTCCATGTAGCGTCG	33024	62
	reverse	AAATCCCCTGACCACGATG	33025	62
	forward	CGTCCATGTAGCGTCGATGA	33026	62
	reverse	ACCTTTTCTTGGTCGCCAGT	33027	62
<i>iav</i>	forward	TGATCCTGCACATGGTGGTC	33068	62
	reverse	GGTATCGGTGTCGCCAATCA	33069	62
	forward	CAACCAGACGGGACTGACTC	33070	62
	reverse	GAAATGGAATGCACGCCAGG	33071	62

## **2.2 Probing auditory function in *Drosophila* – electrophysiological approach**

The electrophysiological methods to probe auditory function used in this thesis were established by Jörg T. Albert, Martin C. Göpfert, Björn Nadrowski and Thomas Effertz (Göpfert et al. 2006, Albert et al. 2007, Effertz et al. 2012).

Hearing in *Drosophila* was probed for three different aspects as described earlier. First, fluctuation of the sound receiver was recorded without any sound stimulus. Then responses to sound corresponding to the individual best frequency were monitored. Finally, gating compliance was assessed by displacing antenna with electrostatic force steps.

Preparation of fly involved fixing body parts to minimize the movements that were not related to hearing. Briefly, the fly was anesthetized with CO<sub>2</sub> and mounted on a Teflon pole with bee wax. After clipping the wings off, the position of the head, proboscis, legs, halteres and the joint between the scape-pedicle of the antenna to be measured were fixed with dental glue. Flies were also anesthetized by lowering the body temperature on ice instead of CO<sub>2</sub> to test the possibility that hearing in the mutant flies were irreversibly affected by CO<sub>2</sub>, which was excluded.

The experimental setup (Figure 5) was placed on a vibration isolation table. For measurements, only young flies of ages 1-3 days were measured unless specified.

### **2.2.1 Free fluctuation**

Movement of the sound receiver in the absence of sound stimulus were measured. This fluctuation is driven both by Brownian motion and the active process in the auditory nerves and provides a brief first look on the integrity of the auditory machinery.

Vibrations of the sound receiver were detected at the tip of the arista using a laser Doppler vibrometer (PSV-400, Polytec GmbH, Waldbronn, Germany). The amplitude components of 60 to 100 Fourier transforms were averaged to estimate the spectral density of the receiver's vibrations. The individual best frequency of the fly's receiver was determined based on the power spectrum. Data were processed and analyzed using PSV-VIB (Polytec), Excel 2007 (Microsoft), Prism (GraphPad).

## 2.2.2 Sound-evoked responses

Pure tones matching the individual best frequency (iBF) of the receiver in different intensities were applied via a loudspeaker placed approximately 10 cm behind the fly. The sound particle velocity applied was again monitored using a microphone (Emkay NR 3158 pressure gradient microphone, distributed by Knowles Electronics Inc., Itasca, Illinois, USA). Simultaneously, antennal displacement was recorded using the laser Doppler vibrometer (LDV) and the nerve response via an electrode (electrolytically etched tungsten wire) inserted between two pedicels with reference to the electrode positioned into the thorax (Figure 5a). Those three signals were sampled at a rate of 3.2 kHz and 1-second time windows were Fourier-transformed. Then they were averaged 5 to 10 times to determine the Fourier amplitudes of the microphone and the laser signals at the frequency of stimulation and nerve signals at twice the frequency of pure tone.

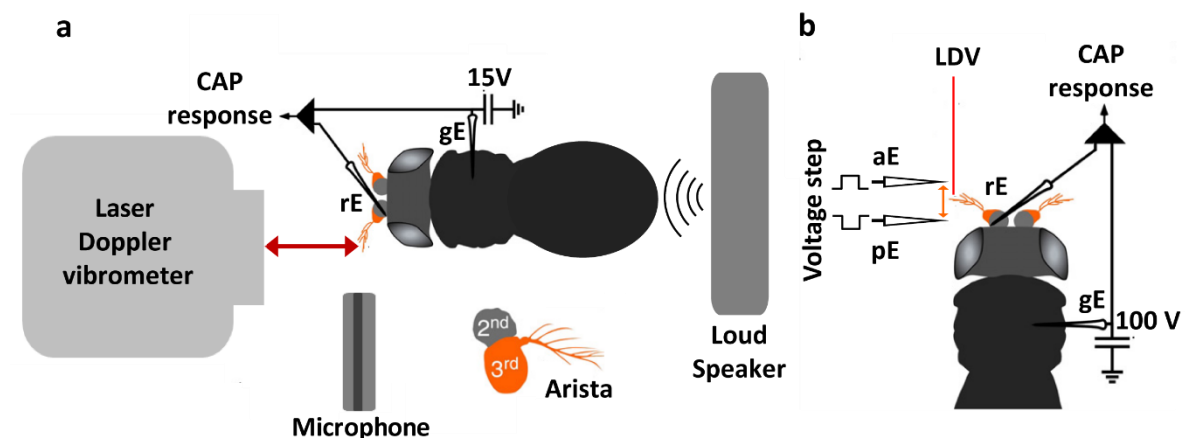


**Figure 5. Experimental setup for probing auditory function in *Drosophila*.**

**a.** Setup for measuring responses to sound stimuli. Loud speaker was placed ~10 cm behind the fly to apply sound stimulus, which was monitored via microphone. While laser Doppler vibrometer (LDV) was detecting antennal displacement, the nerve responses as compound action potential (CAP) was recorded via an electrode inserted between the two antennae (recording electrode, rE) with reference to the ground electrode put into thorax (grounding electrode, gE). **b.** Setup with electrostatic force steps. Bipolar stereotrodes were positioned anterior (aE) and posterior (pE) to the sound receiver to apply force steps. Displacement of the arista and the nerve responses were recorded via LDV and rE, respectively. (Adapted and modified from Albert et al. 2007.)

To quantify compressive nonlinearity, antenna's displacement was normalized to the stimulus particle velocity (SPV). The sensitivity gain was then calculated as the ratio between the sensitivities obtained in the lower and in the upper linear regimes. From nerve signal data, values reflecting three aspects of sound-evoked responses were extracted. First, average of maximal CAP was calculated. After normalizing CAP response of individual sound receiver, the nerve response was plotted against stimulus intensity and against antennal displacement. The data were then fitted with a Hill-equation ( $f(x) = y_{min} + \frac{(y_{max}-y_{min})}{(1+|x/m|^n)}$ ). Threshold SPV or displacement was defined as the SPV or displacement corresponding to 10% of maximum CAP amplitude of the Hill-fit. SPV or displacement range matching 10%-90% of maximum CAP amplitudes of the Hill-fit was defined as dynamic range. Data were processed and analyzed using PSV-VIB (Polytec), Spike 2 (Cambridge Electronic Design), Excel 2004 (Microsoft), Prism (GraphPad) and Sigma-Plot 10 (Systat Software).

## 2.2.3 Gating compliance

### 2.2.3.1 Data acquisition and fitting

Sound receiver of *Drosophila* was deflected in the range of -10 to +10  $\mu\text{m}$  with electrostatic step forces of 28 stimulus resolution. This was done by charging the fly to 100V and applying the forces with bipolar tungsten stereotrodes (WE3ST31.0A5 and WE3ST31.0A10, Micro Probe, Inc.) aligned anterior and posterior to the arista (Figure 6b). The displacement responses were sampled with a LDV at a rate of 100 KHz. The time traces were extracted and processed according to the procedures described in Effertz et al. 2012., which involved outlier rejection followed by calculation of average displacements using Python-based programs developed by Simon Qianhao Lu (Lu 2011).

Steady-state stiffness of the receiver ( $K_{steady}$ ), which was deduced from the steady-state displacement, which is approached during prolonged forcing (Albert et al. 2007), was calculated as follows:

$$K_{steady} = \frac{\partial(m \cdot a_{onset})}{\partial x_{steady}},$$

whereas dynamic stiffness of the receiver ( $K_{peak}$ ), which was calculated at the initial displacement peak, was acquired as the following:

$$K_{peak} = \frac{\partial(m \cdot (a_{onset} - a_{peak}))}{\partial x_{peak}},$$

where the apparent mass of antenna ( $m$ ) was assumed to be 5 ng (Humphris et al. 2005). Both stiffness values were adjusted by correcting the mass to compensate the differences among individuals of each group (namely either of one genotype and/or experimental condition), such that the  $K_{steady}$  matched the average value acquired from the respective group and used directly to deduce the  $K_{par}$ . The  $K_{peak}$  values was pooled from each experimental group fitted to both of the gating spring models described earlier (1.1.2.2).

Data were processed and analyzed using PSV-VIB (Polytec), Spike 2 (Cambridge Electronic Design), Python-based programs developed by Simon Qianhao Lu (Lu 2011), Excel 2004 (Microsoft) and Matlab (MathWorks). Data from *CantonS* and *lav<sup>1</sup>* single mutants and MATLAB scripts for gating compliance fitting were kindly provided by Dr. Christian Spalhoff.

### 2.2.3.2 Model selection using Akaike information criterion

After fitting the slope stiffness data to both two-transducer type and one-transducer type models, better model was determined using Akaike information criterion (Effertz et al. 2012). Akaike information criterion with correction for finite sample size (AICc), which is a measure of goodness for fitting results (Burnham and Anderson 2002) was calculated for each model as follows:

$$AICc = AIC + \frac{2k(k+1)}{n-k-1} ,$$

where  $AIC = n * \ln\left(\frac{RSS}{n}\right) + 2k$ ,  $RSS$  is the respective sum of the squared residuals,  $n$  the number of data points,  $k$  the number of free parameters. Two transducer type model has 5 free parameters ( $N_s$ ,  $z_s$ ,  $N_i$ ,  $z_i$  and  $K_{inf}$ ), while one transducer type model has 3 free parameters ( $N$ ,  $z$  and  $K_{inf}$ ). To finally assess which model describes the data better, Akaike weights for both models were calculated. Akaike weights ( $w_i$ ) provide a measure for the discrepancy of which model approximates the true process better in the form of probability (Wagenmakers and Farrell 2004) and is defined as follows:

$$w_i = \frac{\exp(-\Delta_i/2)}{\sum_{r=1}^2 \exp(-\Delta_r/2)} ,$$

where  $\Delta_i = AICc_i - \min AICc$ .

## **2.3 Immunohistochemistry**

### **2.3.1 Tissue preparation**

#### **2.3.1.1 Antennal preparation**

First, flies were anesthetized on ice for 10 minutes. Heads were separated from the bodies and incubated in the tubes containing fixative (4% Formaldehyde and 1% Triton X-100 in PBS, pH7.4) on a rotator (Stuart rotator SB2, NeoLab) for an hour at RT. Next, the heads were slightly dried on a filter paper and embedded with the anterior up into pre-warmed (75°C) albumin-gelatin (24.2% albumin, 5.7% gelatin in in dH<sub>2</sub>O) solution in silicon molds. The blocks were chilled at 4°C for 10 minutes and then post-fixed in 6% Paraformaldehyde (in dH<sub>2</sub>O) for overnight at 4°C. Following incubation in methanol for 10-30 min, the blocks were first washed with PBS (pH 7.4), after which they could be kept at 4°C for further steps, and then sliced into 30-50 µm sections with vibratome (Leica VT 1000 S combined with Leica MS5 microscope) and the sections were washed 3 times with PBS (pH 7.4).

#### **2.3.1.2 Brain preparation**

After anesthetizing on ice, flies were fixed with two pins on a dissection dish containing modified HL-3.1 solution (70 NaCl, 5 KCl, 20 MgCl<sub>2</sub>, 10 NaHCO<sub>3</sub>, 0.5 CaCl<sub>2</sub>, 115 Sucrose, 5 Trehalose, 5 HEPES, in mM, in dH<sub>2</sub>O, pH 7.2). After detaching proboscis, head cuticle and trachea were removed with forceps while the brain was still attached to the body. Using glass spoids, brains were washed once with HL-3.1 and incubated in tinted glass dishes containing fixative (4% Formaldehyde and 0.3% Triton X-100 in PBS, pH 7.4) on a rotator for an hour at RT. Then the samples were washed three times with PBS (pH 7.4) for 20 minutes each at RT on a rotator.

### **2.3.2 Antibody staining**

Washed samples were blocked in blocking solution (5% Normal goat serum, 2% bovine serum albumin, 1% Triton X-100 in PBS, pH 7.4) for 30 minutes to 1 hour at RT on a rotator. Then the samples were

incubated in new blocking solution (unless specified) containing primary antibodies at 4°C for overnight. After washing with 1% PBT (1% Triton X-100 in PBS, pH 7.4) 3-4 times over an hour, the samples were incubated with secondary antibodies in 1% PBT at RT for 1-3 hours (In case of using primary antibodies conjugated with fluorophores, those primary antibodies were added at this step) or at 4°C for overnight. After washing 2-3 times with 1% PBT and 2-3 times with PBS at RT over 1 hour, the samples were mounted in DABCO on a slide glass and topped with cover slip (In case of brains, spacers were used to prevent deformation of the soft tissues). Information on the antibodies or toxins binding specific structures with or without conjugated fluorophore used are as follows:

Primary antibodies or toxins: rabbit anti-GFP (1:1000, ab 6556, Abcam), Phalloidin conjugated with Alexa Fluor® 633 (1:40, A-22287, Invitrogen), rabbit anti-HRP, anti-HRP conjugated with Fluor® 546 (1:500, Invitrogen), mouse anti-Futsch (1:20, 22C10, Hybridoma bank), rat anti-IAV (1:1000, kindly provided by Prof. Changsoo Kim, Chonnam University, Kwangju, South Korea), mouse anti-NOMPC (1:1000, kindly provided by Prof. Joe Howard, MPI-CBG, Dresden, Germany), mouse anti-myc Tag (05-724, Merck), mouse anti- $\alpha$ -Tubulin (1:20, AA4.3, Hybridoma bank), rabbit-anti-dATG8 (1:200, kindly shared by Katja Köhler, Institute of Molecular Systems Biology ETH, Zurich, Switzerland), DAPI (0.1  $\mu$ g/ml in PBS).

Secondary antibodies: Alexa Fluor® 488 goat anti-mouse (1:500, Invitrogen), Alexa Fluor® 488 goat anti-rabbit (1:500, Invitrogen), Alexa Fluor® 546 goat anti-mouse (1:500, Invitrogen), Alexa Fluor® 633 goat anti-mouse (1:500, Invitrogen), Alexa Fluor® 633 goat anti-rabbit (1:500, Invitrogen), Alexa Fluor® 633 goat anti-rat (1:500, Invitrogen).

### **2.3.3 Confocal microscopy and image processing**

The samples stained with antibodies were observed with laser scanning confocal microscopes (TCS-SP2 and TCS-SP8, Leica). All images were processed with ImageJ and Adobe Illustrator CS3.

## **2.4 Motif search/prediction**

Three different lysosomal targeting sequence motifs (YXX $\Phi$ , di-leucine (LL) and acidic di-leucine ((D/E)XXXL(L/I))) were searched using Python (Python™). Palmitoylation sites were predicted using CSS-Palm software (Ren et al. 2008). Part of the found motifs were excluded based on the overlap with

transmembrane (TM) or extracellular loops by topology prediction (<https://www.predictprotein.org> and <http://smart.embl-heidelberg.de/>) were excluded from candidates. Sequences were aligned using clustalw2 (<http://www.ebi.ac.uk/Tools/msa/clustalw2/>).

## 2.5 Fly husbandry

The flies were funneled into plastic vials ¼ filled with fly food and stored at 25 °C under 60% humidity in 12h/12h light/dark cycle. The procedure to cook the food was as follows:

For 7 liters of food, 500 g fresh yeast was added to a liter of boiled water. After boiling for 20 minutes, 500 g sugar and 20 g salt dissolved in a liter of water was added. Then 60g of agar and 250 g of flour were separately heated in a liter of water until they become homogeneous and added to the mixture. After removing the mixture from the heat, one liter of fruit juice was added and the volume was adjusted to 7 liters with water. After the temperature was cooled to 60°C, 30 ml propionic acid was mixed in. Then the warm liquid food was poured into 25mm vials with an Isomatic® MCP pump. After cooling the food overnight at room temperature, the vials were closed with mite-free plugs and could be stored for use up to 4 weeks at 4°C, which was warmed to room temperature before putting the flies onto them. For high protein diet experiments, first crosses were set up with 20-30 adult flies on fresh food. After letting them lay eggs for a week, the parents were removed from the vial and 20% yeast solution (w/v in dH<sub>2</sub>O) was added onto the media (Wong et al. 2012).

## 2.6 List of chemicals

Agarose (A21114.0500, Applichem)

Albumin (A5253, Sigma-Aldrich)

Ampicillin (835242, Roche)

Bovine serum albumin (A1391, Applichem)

Calcium chloride dihydrate (CaCl<sub>2</sub> · 2H<sub>2</sub>O, 10035-04-8, applichem)



Chloramphenicol (C0378, Sigma-Aldrich)

Cornmeal (Obermühle Rosdorf)

DABCO (1,4-diazabicyclo[2.2.2]octane, 0718, Roth)

DAPI (4',6-diamidino-2-phenylindole)

Disodium hydrogen phosphate dihydrate ( $\text{Na}_2\text{HPO}_4$ , A3905.0500, Biochemica)

Ethanol (8006, J.T.Baker)

Gelatin (G2500, Sigma-Aldrich)

Glycerol (2039.1000, Th.Geyer Chem solute® )

Hydrochloric acid (HCl, A6578.0500, Applichem)

Isopropanol (A3928.0500GL, Applichem)

Magnesium chloride ( $\text{MgCl}_2$ , 2170690, Merck)

Magnesium sulphate ( $\text{MgSO}_4$ , 1.05886, Merck)

Manganese chloride ( $\text{MnCl}_2$ , A475734, Merck)

Methanol (8388, Roth)

Normal goat serum (005-000-121, Jackson Immuno)

Paraformaldehyde (PFA, 104051000, Merck)

PIPES (A1079, Applichem)

Propionic acid (8006050100, Merck)

Potassium chloride (KCl, 7447-40-7, Applichem)

Potassium hydroxide (KOH, A3871, Applichem)

Sodium chloride ( $\text{NaCl}$ , A2942.1000, Applichem)

Sodium dihydrogen phosphate monohydrate (NaH<sub>2</sub>PO<sub>4</sub>·H<sub>2</sub>O, A1047.0500, Biochemica)

Sodium hydroxide (NaOH, A6829.0500, Applichem)

Treacle (1905, Hellmi)

Tris base (Applichem, A2264.1000)

Triton-X (A1388.0500, Applichem)

## **2.7 List of materials for molecular biology work**

Blood and tissue kit (69504, Qiagen)

dATP (55082, Invitrogen)

dCTP (55083, Invitrogen)

dGTP (55084, Invitrogen)

dTTP (55085, Invitrogen)

FastDigest BamH1 (FD0054, Fermentas)

FastDigest EcoR1 (FD0274, Fermentas)

FastDigest Xba1 (FD0684, Fermentas)

GenElute™ Plasmid Midiprep Kit (PLD35, Sigma-Aldrich)

GeneRuler DNA ladder mix (SM0321, ThermoScientific)

InvisorbR Spin Plasmid Mini Two (1010140400, Invitex)

Luria agar (L2897, Sigma-Aldrich)

Luria broth (LB, L3022, Sigma-Aldrich)

Phusion for high fidelity PCR (F-553S, ThermoScientific)

QIAquick DNA purification kit (28104, Qiagen)

Qiaquick Gel extraction kit (28704, Qiagen)

Quantitect Reverse Transcription kit (205311, Qiagen)

Rapid DNA Dephos & DNA ligation kit (04 898 117 001, Roch)

Roti-safe gelstain (3865.1, Carl Roth)

TOPO TA cloning kit (450641, Invitrogen)

Trypton (8952.2, Roth)

XL-1 Blue Competent Cells (200 236, Stratagene)

Yeast extract (2363.2, Roth)

ZR Tissue and Insect RNA microprep kit (R1060, ZymoResearch)

## 3 Results

### 3.1 Mutant analysis for active process in JO

First hints that TRP channels of the mucolipin (TRPML) subfamily are implicated in hearing were provided by *varitint-waddler* mice, which are deaf (Di Palma et al. 2002). This auditory phenotype was shown to arise from a point mutation in *trpml3* that renders the TRPML3 channel constitutively active (Grimm et al. 2007, Kim et al. 2007, Nagata et al. 2008, van Aken et al. 2008). Genetic inactivation of TRPML3, however, did not lead to hearing deficits (Jörs et al. 2010), leaving the involvement of TRPML subfamily members in normal hearing elusive. In the mammalian system, investigating the roles of TRPML channels can be complicated by the existence of three homologs, which could functionally complement each other. The *Drosophila* genome includes only one *trpml* gene (Flybase ID: CG8743; in this thesis, the translation product from this gene will be called dTRPML to distinguish it from the mammalian counterparts), simplifying the problem. This project started based on preliminary screening by Thomas Effertz (Effertz 2011), who observed apparent hearing defects in *trpml* mutant flies. In this report, I first reevaluated auditory function in mutant flies and show that hearing in the mutants can be partly rescued genetically, documenting that dTRPML is required for hearing in *Drosophila*.

#### 3.1.1 Characterization of hearing phenotypes of *trpml*<sup>1</sup> mutants

##### 3.1.1.1 Free fluctuation

The antennal sound receivers of wild-type *Drosophila* display mechanical fluctuations in the absence of external stimulation. These fluctuations arise from thermal bombardment and, in addition, from the

mechanical activity of JO neurons. This mechanical activity shifts the mechanical best frequency of the antenna down to ca. 200 Hz, which is the frequency that dominates the flies' courtship songs (Nadrowski and Göpfert 2009). It also enhances the antenna's fluctuation power, adding energy to the antenna's thermal fluctuations. I measured the free fluctuations of the antenna by means of LDV and calculated the respective power spectrum by Fourier-transforming the data. Integrating the power spectra for frequencies between 100 and 1000 Hz yielded a total fluctuation power of  $1817.3 \pm 493.2 \text{ nm}^2$  (N=5) for  $w^{1118}$  controls, and converting the power spectra into velocity spectra yielded an individual best frequency (iBF) of  $202.0 \pm 6.7 \text{ Hz}$  (N=5) (Figure 6). In *trpm1* null mutants ( $trpm1^l$ ), the total fluctuation power was reduced about ten-fold to  $114.7 \pm 16.6 \text{ nm}^2$  (N=5), and the antennal best frequency was shifted to  $463.6 \pm 23.2 \text{ Hz}$  (N=5) (Figure 6). Collectively, this drop in the antenna's fluctuation power and the increase of its mechanical best frequency show that the mechanical energy JO neurons contribute to the antenna's free fluctuations is lowered in *trpm1* mutants.

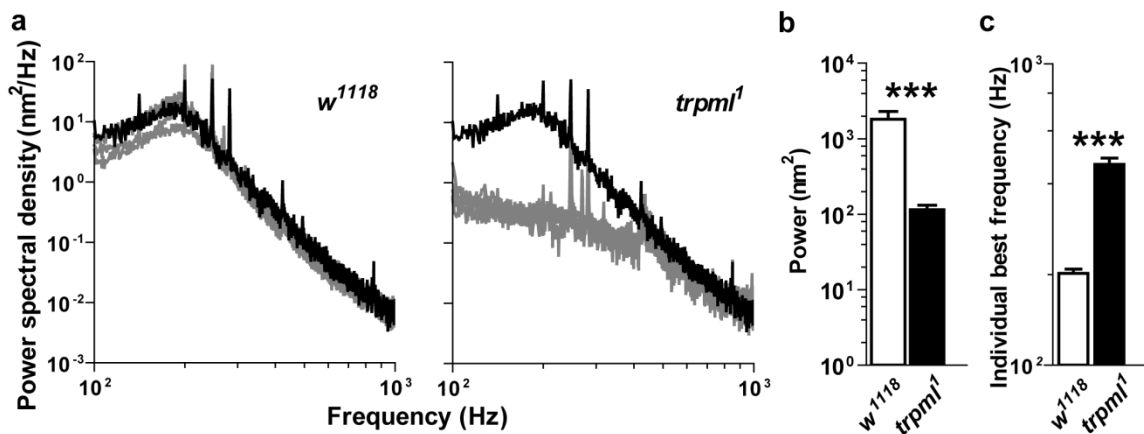


**Figure 6. Antennal free fluctuation is reduced in *trpm1<sup>l</sup>* mutants.**

**a.** Power spectra of the receiver's mechanical free fluctuations in the absence of sound stimuli in the control ( $w^{1118}$ ) and the mutant ( $trpm1^l$ ) strains. Traces: black, data from one  $w^{1118}$  control fly that is repeated in the right panel to facilitate comparisons. Grey, data obtained from other flies (N = 5 animals per strain). **b.** Total fluctuation power of the antennal receiver, calculated by integrating the individual power spectra shown in panel (a) for frequencies between 100 and 1,000 Hz (N = 5, means $\pm$ S.D.). **c.** Individual best frequencies of the antennal sound receiver in the control and the mutant strains determined by converting the power spectra in panel (a) in velocity spectra. (N = 5, means $\pm$ S.D.). \*\*\* $p < 0.001$  by Mann-Whitney U-test.

### 3.1.1.2 Sound-evoked responses

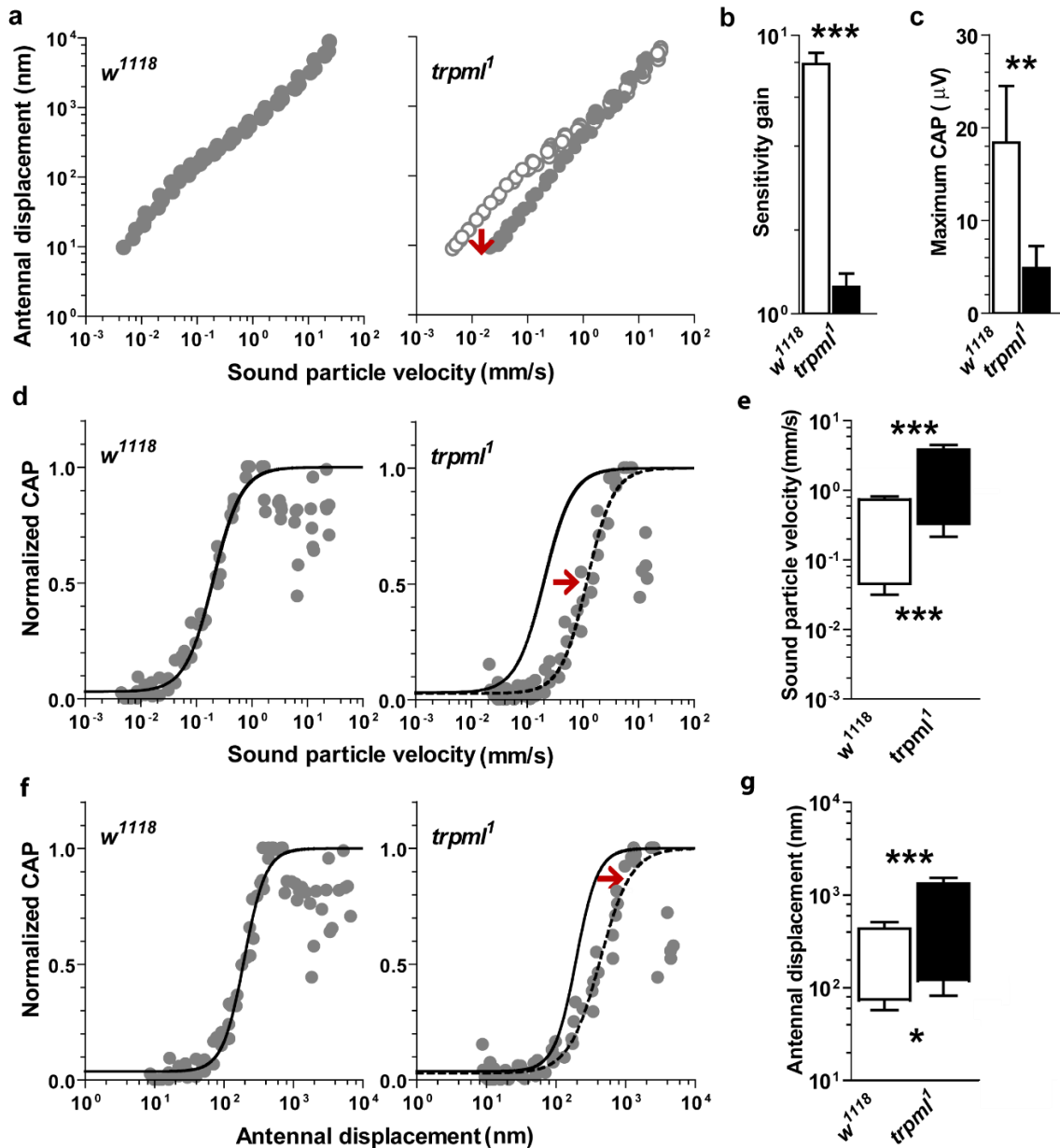


**Figure 7. Sound-evoked responses in *trpm1<sup>1</sup>* mutants suggest impairment in sensitive hearing.**

**a.** Sound-evoked displacement of the sound receivers in control (*w<sup>1118</sup>*) and mutant (*trpm1<sup>1</sup>*) strains as a function of the sound particle velocity, plotted in log-log coordinates. Filled circles, data from 5 individuals of the indicated strains; open circles, data from control added for comparison. **b.** Nonlinear amplification gain defined as (maximum sensitivity)/(minimum sensitivity) where sensitivity is calculated as (antennal displacement)/(sound particle velocity). **c.** Maximum CAP response. Normalized sound-evoked compound action potential (CAP) of antennal nerve as a function of the sound particle velocity (**d**) and the displacement of arista tip (**f**). Traces: grey traces, data points pooled from individuals of each strain; solid line, Hill fit of control strain, added also in the *trpm1<sup>1</sup>* panel for

(continued) comparison; dotted line, Hill fit of *trpm1<sup>1</sup>* mutants. Dynamic range for sound particle velocity (**e**) and for antennal displacement (**g**). Lower bound and upper bounds are defined as the sound particle velocity or antennal displacement corresponding to 10% and 90% of maximal amplitude deduced from Hill fits, respectively. \* ( $p < 0.05$ ), or \*\*\* ( $p < 0.001$ ) by Mann-Whitney U-test.

To quantify the gain of mechanical amplification that is provided by JO neurons, I exposed the flies to pure tones at the mechanical best frequency of their antennal receiver and measured the tone-evoked vibrations of this receiver and recorded the ensuing compound action potentials (CAPs) that are propagated by the axons of JONs within the antennal nerve. Plotting the phase-locked displacement of the antenna at the stimulus frequency against the corresponding sound-particle velocity (SPV) of the tone revealed the compressive nonlinearity that arises from mechanical amplification. (Figure 7a). Based on this nonlinearity, mechanical amplification gains were quantified as described by Göpfert et al. (2006). In controls, the nonlinear amplification was  $7.9 \pm 0.8$  (N=5), and in *trpm1<sup>1</sup>* mutants it was  $1.2 \pm 0.1$  (N=5) (Figure 7b). The latter value is close to one, denoting a complete loss of amplification.

The loss of amplification in *trpm1<sup>1</sup>* was associated with a loss of sensitive hearing. Maximum CAP amplitudes were strongly reduced in the mutants ( $4.9 \pm 2.4$   $\mu$ V versus  $18.4 \pm 6.1$   $\mu$ V in controls, N = 5 each), and the dynamic range of the CAP responses was shifted to higher SPVs (Figure 7d-e). Threshold SPVs were  $0.3 \pm 0.1$  mm/s in the mutants, which is significantly higher than that in controls ( $0.05 \pm 0.01$  mm/s). In the mutants, SPVs of  $3.8 \pm 0.6$  mm/s were required to evoke maximum CAP amplitudes, whereas they already occurred at SPVs of  $0.7 \pm 0.1$  mm/s in controls. Because the entire dynamic range shifts, there seems to be no effect on intensity resolution.

In addition to plotting relative CAP amplitudes against SPVs, I also plotted them directly against the corresponding antennal displacement (Figure 7f). In the mutants, CAP amplitudes increased for antennal displacements between  $123 \pm 40$  nm (threshold) and  $1,316 \pm 208$  nm (maximum), with both figures being significantly higher than in controls (*w<sup>1118</sup>*,  $75 \pm 17$  nm and  $432 \pm 75$  nm). Hence, the JO of *trpm1<sup>1</sup>* mutants shows both a lowered sound-sensitivity and a lowered sensitivity for antennal displacements.

### 3.1.2 Genomic rescue

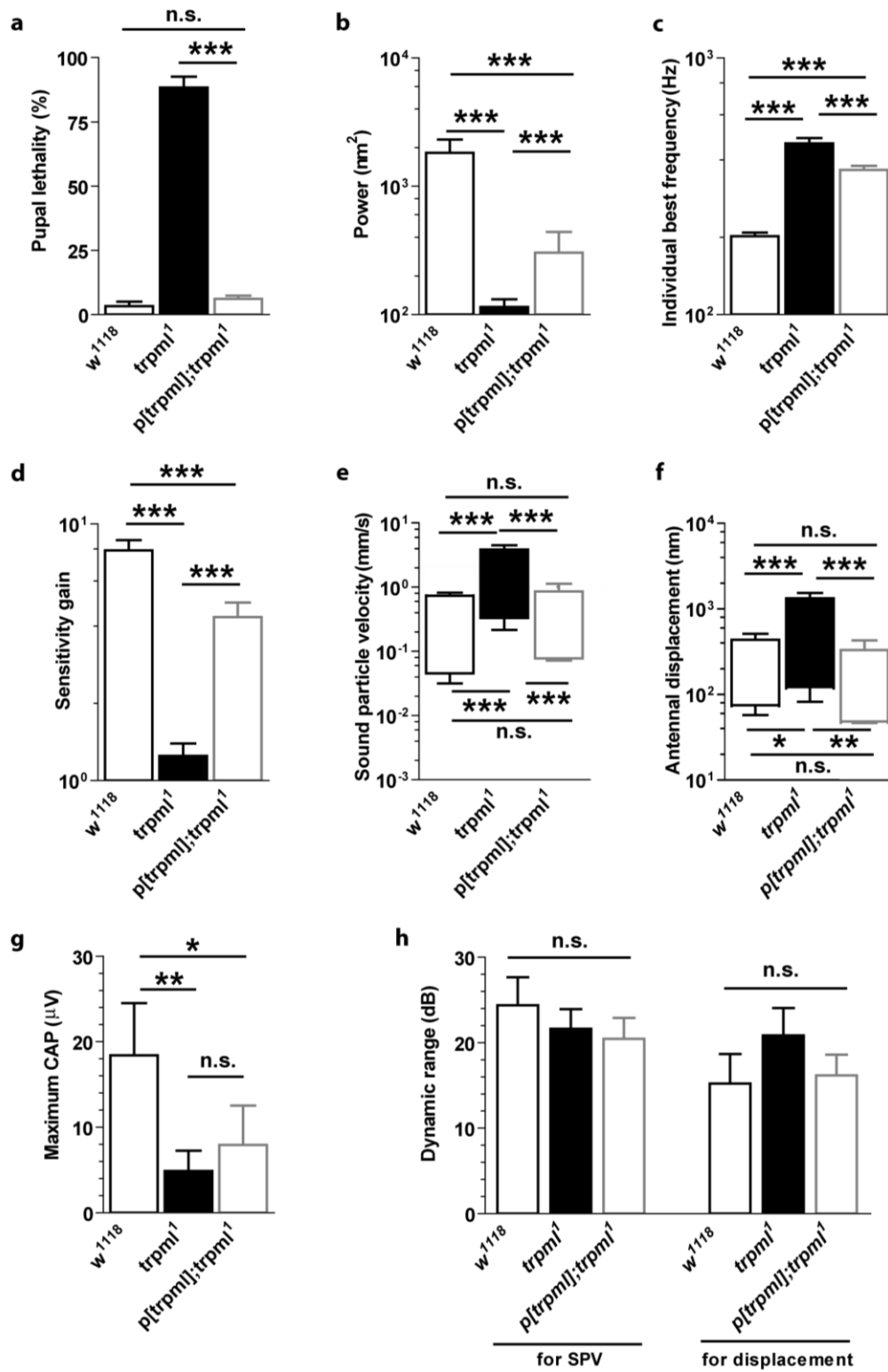


Figure 8. Introduction of genomic rescue construct partially restores sensitive hearing in *trpm1* mutants.



(continued) Comparisons were made among control ( $w^{1118}$ ), mutant ( $trpm1^1$ ) and genomic rescue ( $p[trpm1];trpm1^1$ ) strains. **a.** Pupal lethality, calculated as (number of dead pupae)/(number of all pupae) in % (N=5 vials, each with  $\geq 20$  pupae). **b.** Power of the receiver vibration, determined by integrating the power spectra between 100 and 1000 Hz. **c.** Individual best frequencies determined as the frequencies with the maximal velocity from the Fourier transform of antennal velocities. **d.** Sensitivity gain, calculated as ratio between maximum and minimum gain, where gain is defined as antennal displacement divided by stimulus intensity in sound particle velocity (SPV). Dynamic range of CAPs in relation to SPV **(e)** antennal displacement **(f)**. Dynamic ranges are deduced from Hill-fits such that lower boarder and upper boarder represent SPV or displacement corresponding to the 10% and 90% of maximal Hill-fit relative CAP amplitude, respectively. **g.** Maximum CAPs. **h.** Dynamic range of CAPs relative to antennal displacement and SPV in dB. All data are shown as means $\pm$ S.D. (N=5) and the statistical significances are indicated with \* ( $p < 0.05$ ), \*\* ( $p < 0.01$ ), \*\*\* ( $p < 0.001$ ), by Tuckey's multiple comparison test following one-way ANOVA. n.s.: not significant.

To confirm whether the  $trpm1^1$  mutation accounts for the auditory phenotypes, I tested the expression of a genomic rescue construct containing wild-type  $trpm1$  ( $p[trpm1]$ ) in the  $trpm1^1$  mutant background. In agreement with previous studies (Wong et al. 2012), I found that  $p[trpm1]$  rescues the pupal lethality, that arises from the incomplete autophagy in  $trpm1^1$  mutants:  $trpm1^1$  mutants showed a pupal lethality of  $88.4 \pm 4.2$  % (N=5 vials each with  $\geq 20$  pupae)), and this lethality was reduced to  $3.1 \pm 2.2$  % in  $p[trpm1];trpm1^1$  rescue flies, which is close to the values of  $w^{1118}$  controls ( $3.3 \pm 1.8$  %) (Figure 8a).  $p[trpm1]$  also partially rescued hearing in the  $trpm1^1$  mutants, including dynamic range of sound-evoked CAPs for SPV ( $0.077 \pm 0.005 - 0.85 \pm 0.027$  mm/s) and for antennal displacements ( $48.9 \pm 2.0 - 326.8 \pm 97.3$  nm) (Figure 9e-f). Also other parameters were partially reverted towards control-levels, such as the total fluctuation power of the antenna (Figure 8b.  $303.3 \pm 136.6$  nm<sup>2</sup>), its mechanical best frequency (Figure 9c.  $366.0 \pm 13.2$  Hz), the nonlinear amplification gain (Figure 8d.  $4.3 \pm 0.6$ ) and the amplitude of the maximal CAP response (Figure 8g.  $8.6 \pm 3.2$   $\mu$ V) (see also Table 3). Overall, genomic rescue restored all aspects of hearing, even though to different extents. The partial nature of this rescue might reflect site-specific properties of the  $p[trpm1]$  insertion site.

**Table 3. Comparison of hearing phenotypes in control (*w<sup>1118</sup>*), *trpm1<sup>1</sup>* mutants, and genomically rescued *trpm1<sup>1</sup>* mutants (N=5). SG, sensitivity gain.**

		Power (nm <sup>2</sup> )	iBF (Hz)	SG	Max CAP (μV)	SPV (mm/s)			Displacement (nm)		
						Thres- hold	Upper boarder	Dynamic range (dB)	Thres- hold	Upper boarder	Dynamic range (dB)
<i>w<sup>1118</sup></i>	Mean	1817.3	202.0	7.9	18.4	0.045	0.73	24.4	75.4	431.8	15.2
	S.D.	493.2	6.7	0.8	6.1	0.014	0.09	3.3	17.4	74.9	3.4
<i>trpm1<sup>1</sup></i>	Mean	114.7	463.6	1.2	4.9	0.330	3.83	21.6	123.2	1315.8	20.9
	S.D.	16.6	23.2	0.1	2.4	0.114	0.61	2.3	40.4	208.4	3.2
<i>p[trpm1]; trpm1<sup>1</sup></i>	Mean	303.3	366.0	4.3	7.9	0.077	0.85	20.5	48.9	326.8	16.2
	S.D.	136.6	13.2	0.6	4.6	0.005	0.27	2.5	2.0	97.3	2.4

### 3.1.3 Effects of *trpm1* mutation on morphology and cellular health of JO.

TRPML family channels in mammalian as well as in *Drosophila* have been implicated in apoptosis and lysosomal processes in numerous reports (reviewed in Cheng et al. 2010b, Venkatachalam et al. 2013b). To assess whether dTRPML is implicated in auditory organ anatomy, I tested for the integrity of JONs by visualizing them with the neuronal marker anti-Futsch antibody and Phalloidin, which binds to actin. The JON gross morphology in mutants was comparable to that of control, with the JONs projecting

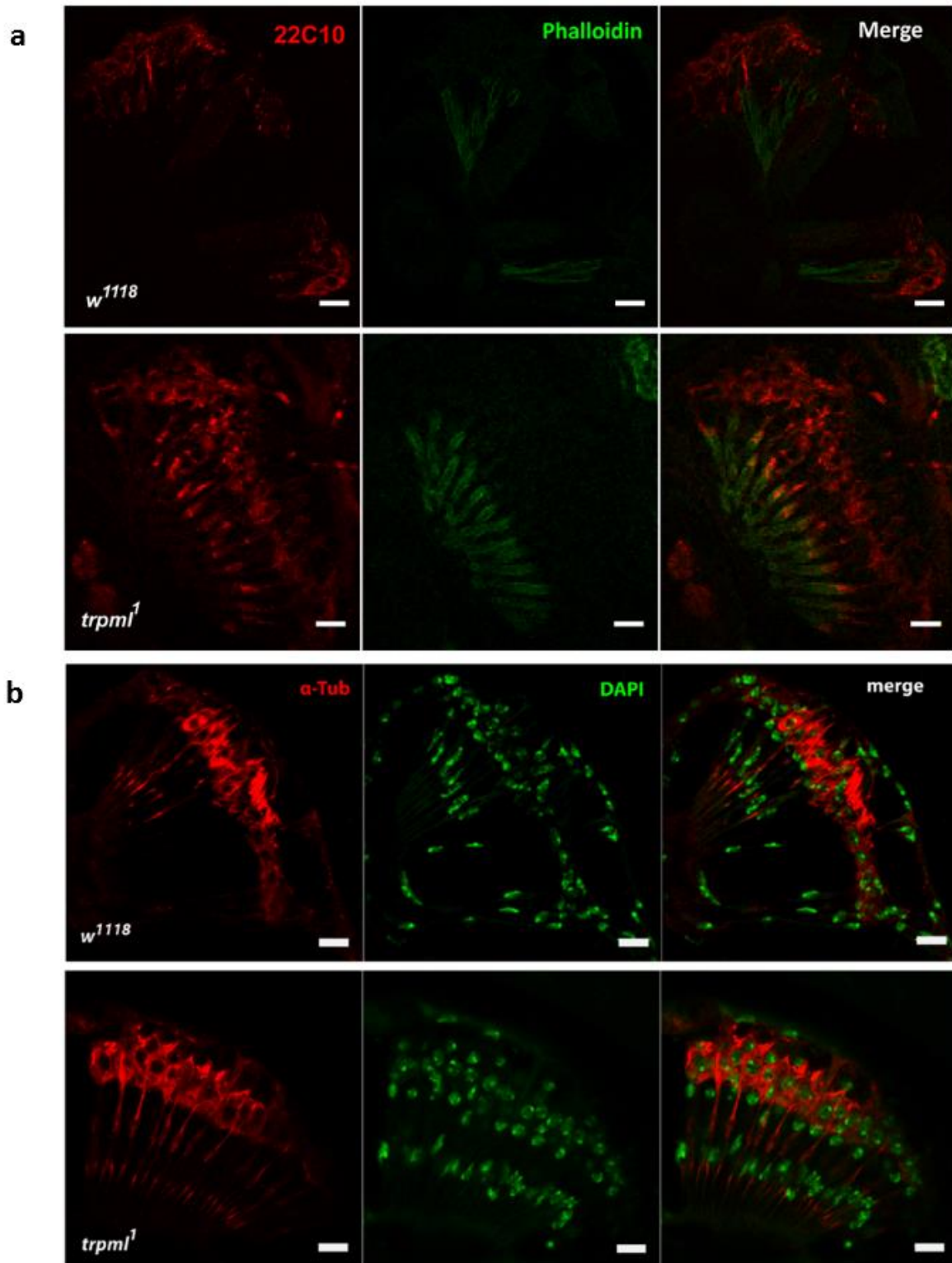


**Figure 9. Gross morphological integrity was maintained in *trpml<sup>1</sup>* mutant JO.**

**a.** Anatomy of JO. Neuronal cytoskeleton and actin-rich structures in supporting cells are marked with  $\alpha$ -HRP in red and Phalloidin in blue, respectively. **b.** Detection of later stage apoptosis. Scale bar: 10  $\mu$ m. DAPI and  $\alpha$ -Tubulin antibodies were used to detect the DNA condensation and cortical reorganization of microtubules, respectively.

ciliated dendrites that are surrounded by actin-based prongs that are secreted by accessory scolopale cells (Figure 9a). Progression of cell death was also monitored by staining JON nuclei with DAPI. No signs of significant chromosome condensation were observed in *trpm1<sup>1</sup>* mutants compared to controls that, in principle, should be visible with DAPI at late stages of cell death (Kim et al. 2012) (Figure 9b). During programmed cell death, the cells don't lose their membrane integrity and permeability until the late steps. This is possible by organization of apoptotic microtubule network, which delimits an area free of active caspases in the cellular cortex (Oropesa-Ávila et al. 2013). This significant cortical concentration of microtubules could not be found in the *trpm1<sup>1</sup>* mutants (Figure 9b).

Cells of MLIV patients show accumulation of lysosomes with lipofuscin, polymerized nondegradable protein and lipid residues that can be detected by strong autofluorescence (Goldin et al. 1995, Venkatachalam et al. 2008). Lipofuscin can block cell renewal and sensitize cells to oxidative stress due to binding of transition metals (Terman and Brunk 2004). To check the accumulation of undegraded waste, autofluorescence was observed at 488 nm emission. Compared to the controls, *trpm1<sup>1</sup>* mutants did not show significant difference (Figure 10), indicating minimal level of lysosomal overload, if there's any.

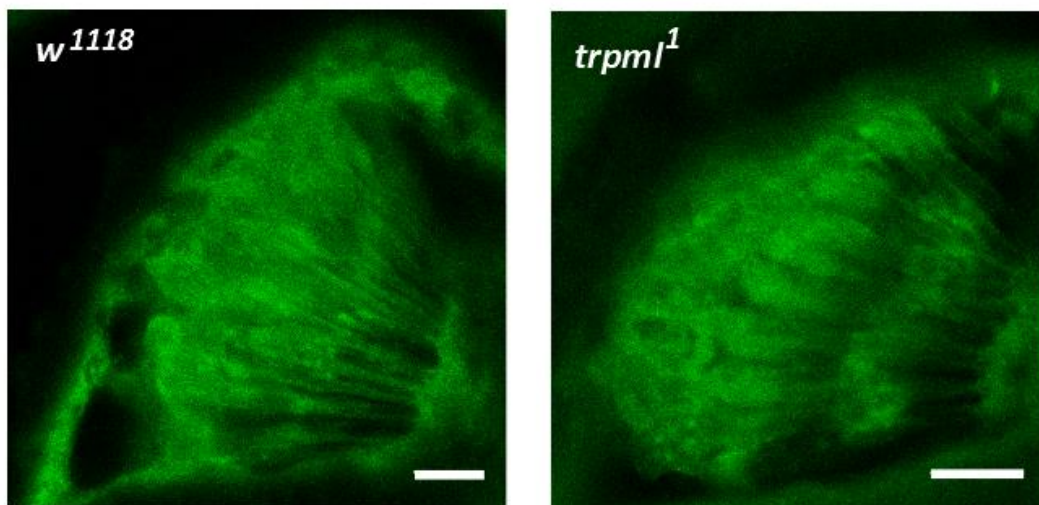


**Figure 10. Lipofuscin was not detected in *trpm1<sup>1</sup>* mutant JO.**

Confocal images of 488 nm emission with exaggerated gain was taken to autofluorescence. Scale bar: 10  $\mu$ m.

Venkatachalam et al. (2008) reported that autophagosomes accumulate in neuronal tissues of aged *trpm1<sup>1</sup>* mutants due to defective clearance, as visualized by increased ATG8-positive vesicles. In this study, however, young animals at the age of 1-3 days were used to minimize putative effects due to progressive neurodegeneration, I tested whether their hearing defects associate with ATG8-positive

vesicles in JONs. Within JO, ATG8 was almost undetectable, suggesting that the hearing defects observed at this age do not reflect a cellular overloading with undigested autophagosomes (Figure 11).

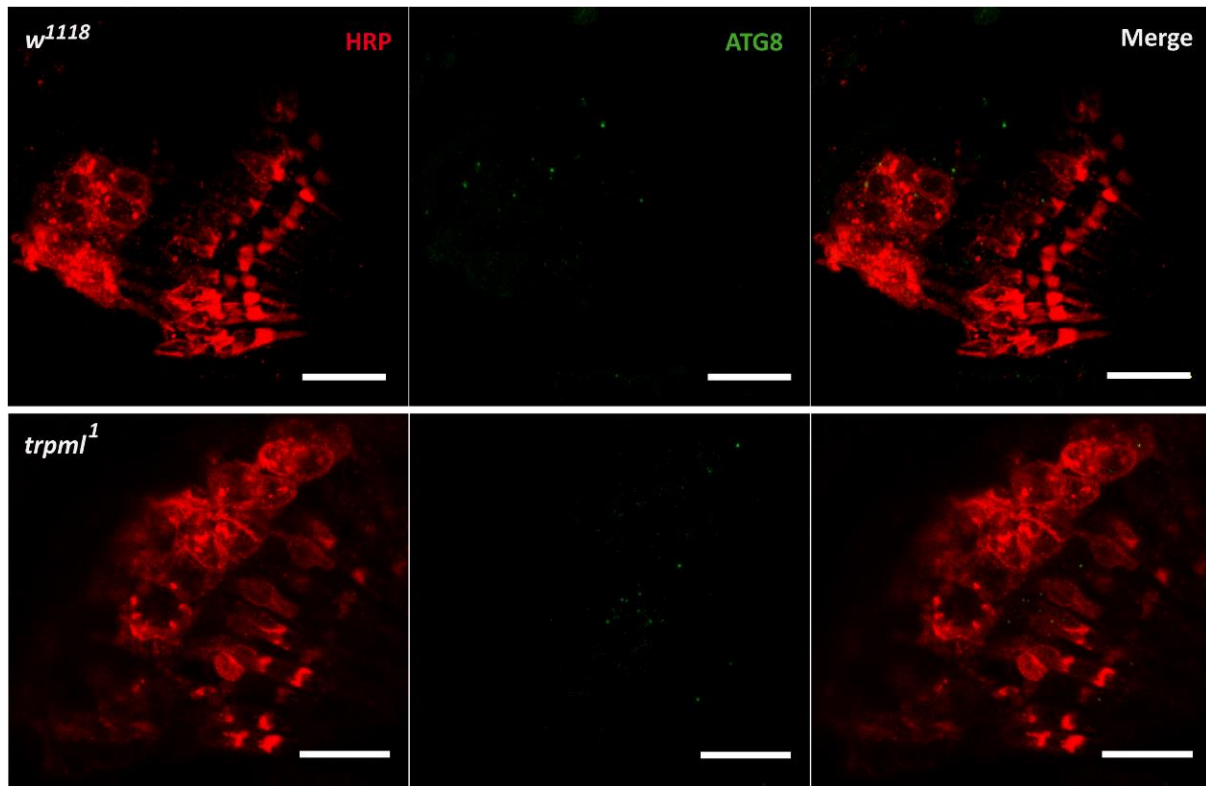


**Figure 11. Autophagosomal marker was not detected in *trpm1*<sup>1</sup> mutant JO.**

Level of autophagic processes. Autophagosomal marker ATG8 are represented in green, whereas neurons are counterstained with HRP, shown in red. Scale bar: 10  $\mu$ m.

### 3.2 TRPML, the place of action

To understand how TRPML operates on hearing, cellular expression and the subcellular localization of TRPML in JO was investigated using three different approaches: firstly, the *trpm1*<sup>1</sup> mutation was selectively rescued by expressing a *UAS-trpm1* rescue construct in a cell type-specific manner to delineate dTRPML-expressing cells within JO. Secondly, I generated a *trpm1* promoter fusion construct to assess the cellular expression of this gene. Thirdly, to probe the intracellular localization of the TRPML protein, I generated tagged versions of TRPML.

### 3.2.1 GAL4XUAS rescue

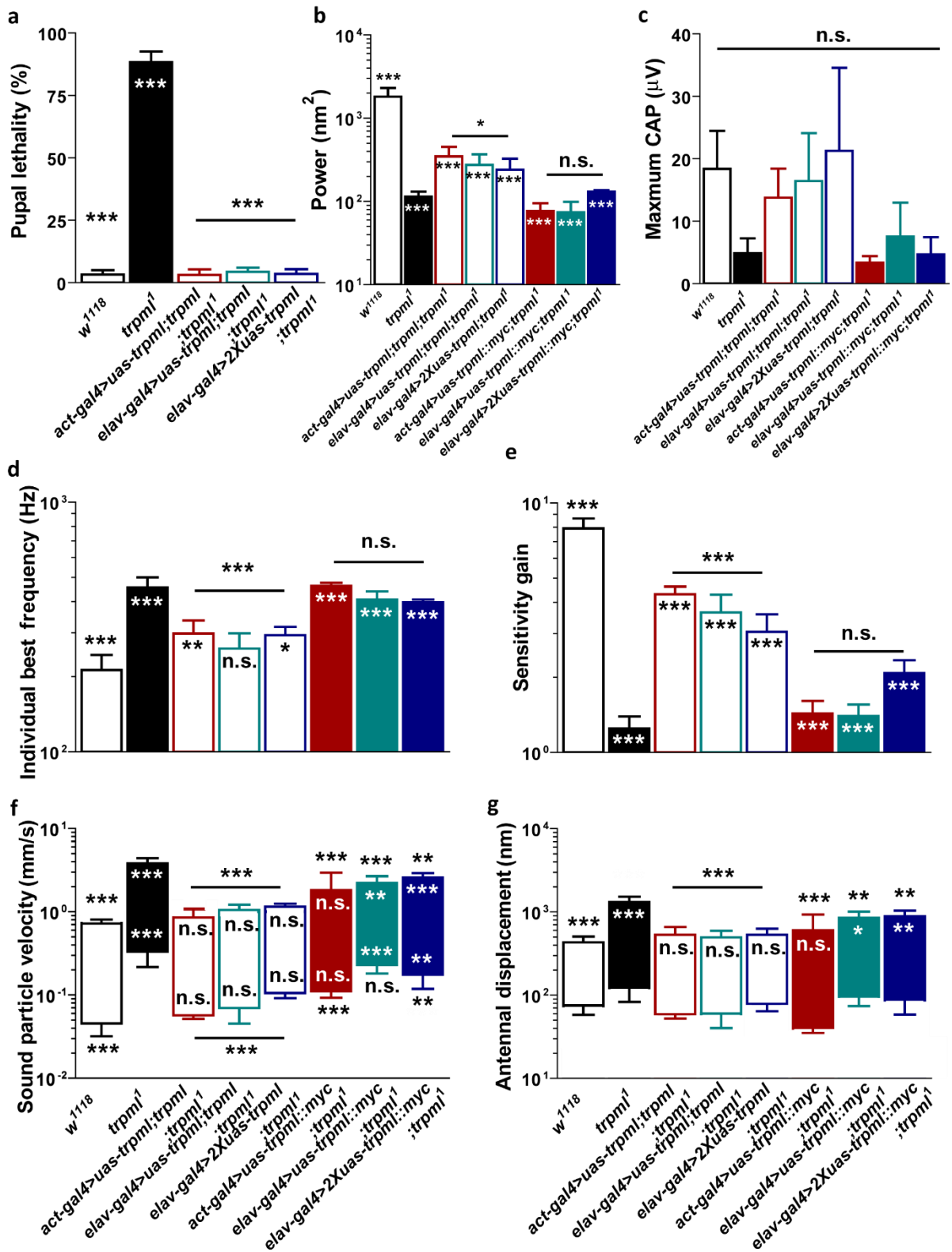


Figure 12. Neuronal expression of TRPML partially rescues the hearing phenotypes in *trpm1<sup>1</sup>* mutants.

(continued) **a.** Pupal lethality, calculated as (number of dead pupae)/(number of all pupae). **b.** Power of the receiver vibration, determined by integrating the power spectra between 100 and 1000 Hz. **c.** Maximum CAP response. **d.** Individual best frequencies determined as the frequencies with the maximal velocity from the Fourier transform of antennal velocities. **e.** Nonlinear amplification gain, calculated as ratio between maximum and minimum gain, where gain is defined as antennal displacement divided by stimulus intensity in sound particle velocity (SPV). Dynamic range of CAPs as functions of SPV (**f**) and antennal displacement (**g**). Dynamic ranges are deduced from Hill-fits such that lower boarder and upper boarder represent displacements or SPVs corresponding to the 10% and 90% of maximal Hill-fit CAP amplitude, respectively. All data are shown as means±S.D. (N=5 except for *act-gal4>uas-trpml::myc* (N=4) and *elav-gal4>uas-trpml::myc* (N=4)) and the statistical significances are indicated with \* (p<0.05), \*\* (p<0.01), \*\*\* (p<0.001), by Tuckey's multiple comparison test following one-way ANOVA, in the bars compared with the control and on the bars with the mutant. n.s.: not significant. *act-gal4* and *elav-gal4* were used to drive ubiquitous and neuronal expression. Note there is no lethality rescue by *uas-trpml::myc*: the insertion itself already reverted the pupal lethality phenotype.

To identify the JO cells that use TRPML, I expressed a *UAS-trpml* rescue construct in the *trpml<sup>1</sup>* mutant background flies using different GAL4 drivers. Pupal lethality (N=5 vials, ≥20 pupae per vial for all genotypes) was rescued to the control level by inducing expression of TRPML either ubiquitously (*act-gal4>uas-trpml;trpml<sup>1</sup>* (u as in ubiquitous), mean lethality = 3.1 ± 2.2 %) or neuronally (*elav-gal4>uas-trpml;trpml<sup>1</sup>* (n as in neuronal), 4.4±1.7 %) (Figure 12a), as previously described (Wong et al. 2012). Both ubiquitous and neuronal restoration of TRPML also completely rescued some aspects of hearing in the *trpml<sup>1</sup>* mutants, including dynamic ranges of SPV (Figure 12f. u, 0.057±0.005 – 0.86±0.23 mm/s ; n, 0.069±0.024 - 1.06±0.16 mm/s) and antennal displacement (Figure 12g. u, 59.0±6.6 – 532.4±125.5 nm ; n, 60.0±19.8 – 494.0±99.8 nm). In addition, some aspects were partially rescued by both ubiquitous and neuronal TRPML expression, including the free fluctuation (Figure 12b and d. u, total flucturation power, 347 ± 106 nm<sup>2</sup>; iBF 297.6±38.6 Hz; n, 274.3±94.1 nm<sup>2</sup>, 259.4±39.0 Hz) and sensitivity gain (Figure 12e. u, 4.3±0.3 ; n, 3.6±0.6). Although maximal CAP amplitudes did not show significant increases upon both ubiquitous and neuronal rescue, an overall tendency for such increase could be observed (Figure 12c. u, 18.4±6.1 μV ; n, 16.5±7.7 μV). This tendency was found to be significant when less stringent statistics were applied (p<0.01, Wilcoxon rank-sum test with Bonferroni correction). To test for effects of expression strength, I expressed two copies of the UAS-construct instead of one. Expressing two copies of this construct did not further increase the rescue (total

fluctuation power, 240.7±85.9; iBF: 293.0±23.4; nonlinear amplification gain, 3.0±0.5; dynamic range for SPV, 0.10±0.01 - 1.16±0.09 mm/s ; dynamic range for antennal displacement, 78.7±14.6 - 533.7±95.6; Maximum CAP, 21.3±13.3 μV) as well as the lethality (0.11±0.02). Hence, a partial rescue of hearing as observed in genomic rescue flies also ensues when dTRPML is selectively rescued in the neurons of JO.

**Table 4 . Comparison of hearing phenotypes in control (*w<sup>1118</sup>*), *trpml<sup>1</sup>* mutants, and ubiquitously and neuronally rescued *trpml<sup>1</sup>* mutants (N=5). SG, sensitivity gain.**

		Power (nm <sup>2</sup> )	iBF (Hz)	SG	Max CAP (μV)	SPV (mm/s)			Displacement (nm)		
						Thres-hold	Upper boarder	Dynamic range (dB)	Thres-hold	Upper boarder	Dynamic range (dB)
<i>w<sup>1118</sup></i>	Mean	1817.3	202.0	41889	41747	0.045	0.73	41753	75.4	431.8	41685
	S.D.	493.2	41826	0.8	41645	0.014	0.09	41701	41746	74.9	41732
<i>trpml<sup>1</sup></i>	Mean	114.7	463.6	41671	41886	0.330	30376	41811	123.2	1315.8	41902
	S.D.	41806	41693	0.1	41731	0.114	0.61	41700	40.4	208.4	41673
<i>act-gal4&gt;trpml</i>	Mean	346.8	297.6	41702	41864	0.057	0.86	41752	59.0	532.4	19.0
	S.D.	105.7	38.6	0.3	41794	0.005	0.23	41791	41796	125.5	41883
<i>elav-gal4&gt;trpml</i>	Mean	274.3	259.4	41793	41775	0.069	41791	24.0	60.0	494.0	41777
	S.D.	94.1	39.0	0.6	41827	0.024	0.16	41672	41870	99.8	41822
<i>elav-gal4&gt;2Xtrpml</i>	Mean	240.7	293.0	3.0	41719	0.105	42370	41902	78.7	533.7	41806
	S.D.	85.9	41752	0.5	41711	0.014	0.09	41791	41804	95.6	0.8
<i>act-gal4&gt;trpml::myc</i>	Mean	76.7	462.3	41730	41732	0.110	29952	41662	40.4	601.5	41751
	S.D.	41747	41772	0.2	41640	0.017	41640	41795	41675	331.6	41703
<i>elav-gal4&gt;trpml::myc</i>	Mean	74.4	408.0	41730	41766	0.229	44958	41870	96.1	846.8	19.0
	S.D.	41814	41670	0.2	41764	0.048	0.46	0.7	41720	161.2	1.0
<i>elav-gal4&gt;2Xtrpml::myc</i>	Mean	131.2	397.0	41641	41824	0.174	21582	41874	88.5	891.2	41749
	S.D.	41795	41739	0.3	41853	0.056	0.33	41823	41669	144.6	41793



### 3.2.2 Cellular expression

Rescue of hearing defects by ubiquitous and neuronal expression of TRPML alike suggests that TRPML function is strongly demanded for normal hearing in neuronal cell types. The question still remained,

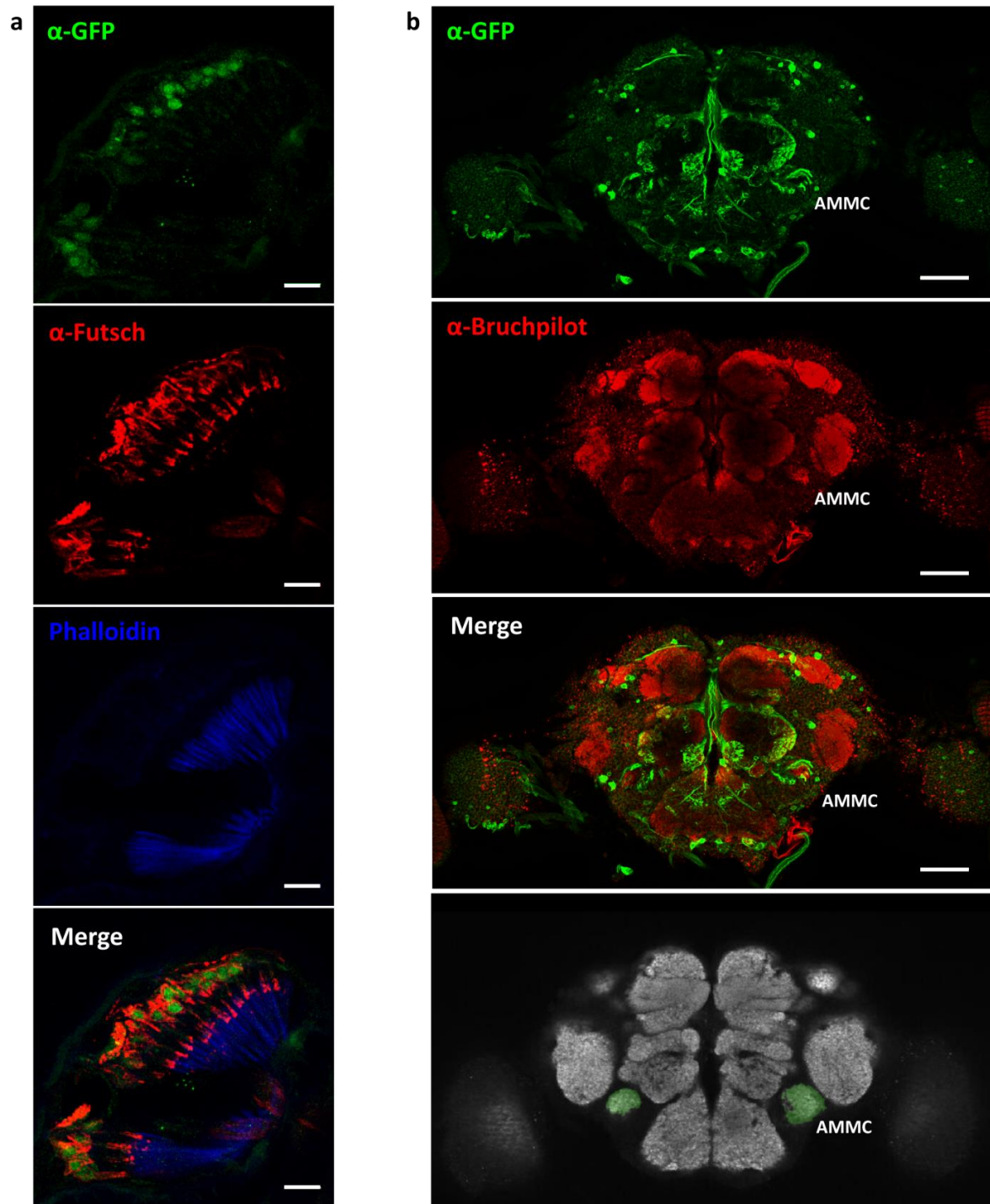


Figure 13. GFP expression driven by *trpml-gal4* suggests neuronal expression of TRPML in JO.

(continued) **a.** Expression of TRPML in JO (scale bar: 10  $\mu$ m). GFP is stained with anti-GFP antibody and shown in green, while anti-HRP antibody marking neurons and Phalloidin binding to F-actin-rich structures are presented in red and in blue, respectively. **b.** Projection of JO neurons to AMMC in brain anti-GFP antibody and anti-Bruchpilot antibody revealing neuropils stainings are shown in green and red, respectively. Lowermost picture is a screen shot from the browser provided by Virtual fly brain (<http://www.virtualflybrain.org>). (scale bar: 50  $\mu$ m).

however, whether the protein is expressed in the JO itself. To verify this point, I took ~2kb region upstream of *trpml* start codon and ligated it upstream of GAL4. This promoter fusion of *trpml* drove the reporter expression both in peripheral and central nervous system (Supplementary figure 1), corroborating the rescue of pupal lethality phenotypes by neuronal TRPML expression as reported previously (Venkatachalam et al. 2008). The reporter expression could be observed in the JONs. The projection of the neurons could be observed in antennal mechanosensory and motor center (AMMC), the brain center for auditory processing (Figure 13). Together with the hearing restoration observed in *trpml* mutants by neuronal TRPML expression, JON expression of the promoter fusion support the idea that dTRPML is required in the fly ear for sensitive hearing. But other fly strains carrying the promoter fusion construct in different chromosomal contexts revealed expression in non-neuronal cell types such as ligament cell (Supplementary figure 1), leaving the possibility that dTRPML is expressed also in other cell types.

### 3.2.3 Intracellular localization?

Previously, Vergarajauregui & Puertollano (2006) reported that three di-leucine motifs in the N- and C-terminal loops direct lysosomal transport, internalization, and/or membrane association of Mucolipin-1, one of three mammalian homologs of dTRPML. For recent reports indicate lysosomal requirement of dTRPML (Venkatachalam et al. 2008, Wong et al. 2012), I aligned the sequence of human Mucolipin-1 (hMucolipin-1) with dTRPML to figure out whether these are conserved. Among those, two (D/E)XXXL(L/I) motifs, N-terminal E<sup>11</sup>TERLL and the E<sup>573</sup>EHSLL, which mediate lysosomal sorting and internalization of hMucolipin-1, respectively, are not conserved in dTRPML. Palmitoylation consensus L<sup>563</sup>LCCC responsible for membrane association of hMucolipin-1, however, could be found in dTRPML. Especially, L<sup>564</sup>, the leucine residue necessary for the functionality of the whole motif, is substituted to isoleucine in dTRPML, which is strongly homologous in chemical nature to leucine,

```

hMucolipin-1  -----MTAPAGPRGSE-----TERLLT-----PNPGY  22
dTRPML       MQSYGPGAQTAPAVKRRDTSYEAAQQQQQSPESDEEYVNTRILRRQVQLQSTPVAVVPM  60
                **** * :; . *:* *

hMucolipin-1  GTQAGPSPAPPTPP-----EEDLRRRLKYFFMSPCDKFRAGRKPKCL  66
dTRPML       PISAGSGTAPPSVDGREEQPEFFPGSSAASYQEERMRRKLQFFMNPiEKWQAKRKFPYKE  120
                *.**.*.***: .** :***:***:* :*:** : * * :

                TM1
hMucolipin-1  MLQVVKILVVTQVQLILFGLSNQLAVTFREENTIAFRHLFLGYSYG-----ADDTFA  118
dTRPML       VVQIVKIFLVTMQLCLFAHSRYNHINITYTGDNRFAFSLHLFLRGWSSREVESYPPAVGPPA  180
                :*:***:***:* ** * . :; : * :** ***** *... * ..**

hMucolipin-1  AYTREQLYQAIHFAVDQYLALPDVSLGRYAYVRGGDPWTNGSGLALCQRYHRGHVDP  178
dTRPML       LYLKSEFFDTVQYAVNGYANVS-RSIGPYDYP---TPNNTMPEPLKLCQNYREGTIFGF  235
                * :*****: **:* * .: ** * * * * .. . * ** :*:* :

hMucolipin-1  NDTFDIDPMVVTDICIQVDPPEPFPFPPSDDLTLLESSSSYKNLTLKFHKLNVNTHFR  238
dTRPML       NESYIFDPHIDEVCERL-----PPNVTIGVENYLRQRDVEVNFASLVSALQTLFKIK  287
                *::: ** : * :; ** . :* . :; :* **.. :*:*

hMucolipin-1  TINLQSLIN-NEIPDCYTFSVLITFDNKAHSGRIPISLETQAHIQECKHPSVFQHG---D  294
dTRPML       TVNFKANGGPLSAPDCFRFDISITFNRRDHGQMLLSLDAEATRLKCHGATDFISDANFD  347
                *::: . . ***: *; ***: *.*: :*:** * :* : . *

                TM2
hMucolipin-1  NSFRLFDVVVILTCSLSFLCARSLLRGFLQNEFVGFMMWRQGRVISLWERLEFVNGW  354
dTRPML       SMLRSVLNIFVLLTICALSFALCTRALWRAYLLRCTTVNFFRSQFGKELSFQGRLEFV  407
                . :* :*:**:**** **:* ** *.:** : *:* * * :; :* ***:**

                TM3 TM4
hMucolipin-1  YILLVTSADVLTISGTIMKIGIEAKNLAS--YDVCSILLGTSTLLVWVGVIYRLTFF  412
dTRPML       YIMIIFNDVLLIIGSALKEQIEGRYLVVDQWDTCSLFLGIGNLLVWFGVLRYLGFEE  467
                **::: .** * * :; * ** : * . :* **:* ** ..**:* **:* **:*

                TM5
hMucolipin-1  ILIATLRVALPSVMRFCCCVAVIYLGFCFGWIVLGPYHVKFRSLSMVSECLFSLING  472
dTRPML       VVILTLLKKAAPKILRFILIAALLIYAGFVFCGWLILGPIHMKFRSLATTSECLFAL  527
                :* ** : * *.:** .. :** * : *****:*****:*****:*****

                TM6
hMucolipin-1  MFVTFAMQAQQGRSSLVWLFSQLYLYSFISLFYIMVLSLFIALITGAYDTIKHPGG  532
dTRPML       MFATFATLSS---KATLWFWFCQIYLYSFISLYIYVVLSLFIYVIMDAYDTIKAYY  584
                **.***::: :; :* *.*:*****:*****:*****:*****

hMucolipin-1  EESELQAYI-AQCQDSPTSGKFRRGSG-----SACSLCCCGR-----DPS EHSLL  578
dTRPML       PTTDLKAFVGRTRAE DISSGVFMTDLDDFDQTSFLDVVKSICCCGRGRHQEPAPNS  644
                :*:***: :; . :** * . . . . :***** :*: :*

hMucolipin-1  VN----- 580
dTRPML       TSLSSIMK 652
..

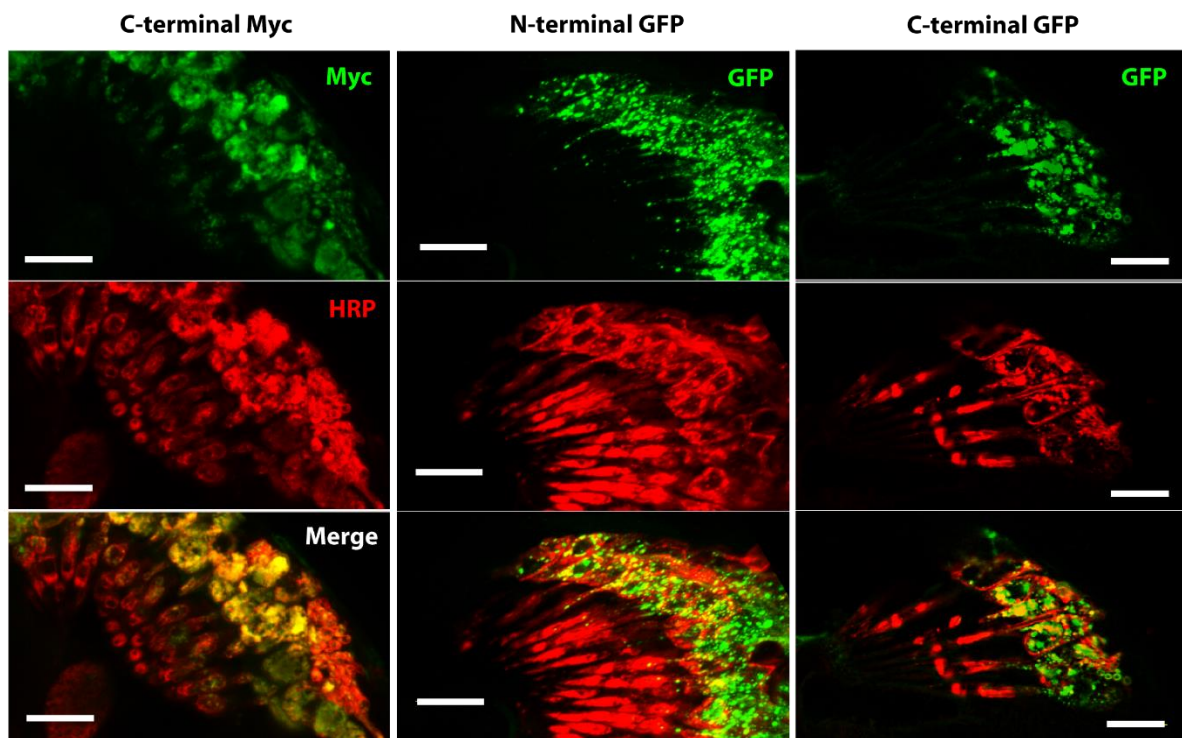
```

Figure 14. Targeting motif prediction suggest plasma membrane and lysosomal association.

Drosophila TRPML (dTRPML) was aligned with human Mucolipin-1 (hMucolipin-1). Symbols: \*, identical residues; :, strong homologous substitutions; ., weak homologous substitutions; boxes: predicted transmembrane domains. Bold characters: red, sequence motifs proven to be required for lysosomal targeting; blue, palmitoylation sites responsible for membrane association in hMucolipin-1, also present in dTRPML; green, possible lysosomal targeting consensus.

strongly hinting at functional conservation of the motif. Studies has been shown that cytosolic domains of most lysosomal proteins contain short signal peptides, namely tyrosine-based motifs (NPXY or YXXΦ,

where X means any amino acid and  $\Phi$  denotes a hydrophobic residue) or di-leucine motifs ((D/E)XXXL(L/I), DXXLL or LL) (Bonifacino and Traub 2003). Since the sequence motifs for lysosomal targeting sequences in hMucolipin-1 are not conserved in dTRPML, I searched for other possibilities (Figure 14). The results suggest five candidate positions, L<sup>378</sup>L in the intracellular loop between transmembrane domains (TM) 2-3, Y<sup>466</sup>NVV in the intracellular loop between TM4-5, Y<sup>644</sup>TSL in the C-terminal domain and less likely two, Y<sup>573</sup>DTI, for being homologous to hMucolipin-1 motif, which was tested to be irrelevant to lysosomal targeting (Vergarajauregui and Puertollano 2006), and Y<sup>118</sup>KFV, for having possible overlap with the transmembrane domain.



**Figure 15. Expression of TRPML with different tags might suggest lysosomal localization.**

Expression of TRPML::MYC (a), GFP::TRPML (b) and TRPML::GFP (c) were driven by neuronal driver in JO. Antibodies against tags (anti-MYC or anti-GFP antibodies) and anti-HRP antibody marking neurons were used for staining and presented in green and red, respectively. Scale bar: 10  $\mu$ m.

To gain insights on the molecular mechanism of TRPML action, three TRPML constructs with tags of different sizes (Myc, a 10aa peptide, and  $\sim$ 27kDa GFP) and locations (N'- and C'-termini) were tested for intracellular localization. I generated two constructs of TRPML tagged with GFP either at the N- or C- termini (GFP::TRPML and TRPML::GFP, respectively) and these were compared with already published C-terminally Myc tagged TRPML (TRPML::MYC, Wong et al. 2012). As the Myc-tagged TRPML in recent report described, all three versions of TRPML suggest endosomal localization when the

expression was driven into JO neurons. Indeed, TRPML family proteins in mammals as well as in *Drosophila* have been reported to be on vesicles of endosomal and exocytotic pathway as well as plasma membrane (Figure 15). Some signals were detectable in the dendritic region, which was not extending beyond basal body region demarcated by proximal band of HRP counterstaining (Senthilan et al. 2012), except for one antennal section expressing TRPML::GFP (data not shown). The localization revealed by the tagged form of proteins, however, should be taken with caution, because they might not be representing true location. For example, TRPML::MYC could hardly rescue the hearing phenotype (Figure 12; Table 4, other tagged TRPMLs are in preparation). This might be on account of altered multimerization/interaction or mislocalization, or combination of both. Ultimately, localization should be verified using antibodies raised against native TRPML (in progress).

### 3.3 Efforts to find the molecular mechanisms of TRPML action on hearing

#### 3.3.1 Analysis of gating compliance in *trpml<sup>1</sup>* mutants

Mechanotransduction channels are assumed to be directly gated by stimulus force. Result of this direct gating of the channels is nonlinear gating compliance: gating of these channels relax the structure involved in the coupling of the force to the channels, nonlinearizing the stiffness/stimulus relationship (Hudspeth 2008).

To gain insights into the mechanism of how TRPML is involved in auditory mechanics of *Drosophila*, I analyzed the nonlinear gating compliance seen in the antennal mechanics. Both gating spring models, i.e. that with one channel type and that with two channel types, were used to analyze the data. To determine which model better describes the data, I calculated the Akaike weights of the respective fits (Supplementary table 1). Judging from parameter values deduced with the gating spring model, the gating of the two distinct channel populations seen in controls persist in *trpml* mutants. However, the compliance appeared severely altered in mutants (Figure 16; Table 5), documenting alterations in channel gating. The asymptotic stiffness of the antenna was reduced, reflecting a drop of the combined gating spring stiffness by about 30 % and a small, but significant drop of the parallel stiffness. According to the gating spring model, the gating spring stiffness is proportional to the number of channels ( $N_s$  and  $N_i$ ) and  $\kappa$ , the stiffness of single gating spring, and the single channel gating force  $z$ . In *trpml<sup>1</sup>* mutants, the numbers of both the sensitive ( $N_s$ ) and insensitive channels ( $N_i$ ) were significantly



larger than in controls (mutants:  $N_s$ , 1042 (range: 548-1536);  $N_i$ , 69940 (52830-87060), (N=6)) controls:  $N_s$ , 341 (228-46);  $N_i$ , 41280 (35070-47500) in fN (N=6)). This increase alone could explain the higher  $K_{GS}$ . However, the single channel gating force showed sharp drop for both transducer types in the mutants ( $z_s$ , 14.43 (11.69-17.17);  $z_i$ , 2.368 (2.063-2.673) in fN (N=6)) when compared with the controls ( $z_s$ , 39.97 (34.00-45.95);  $z_i$ , 4.389 (4.035-4.743) in fN (N=6)), reducing the gating spring stiffness. This lowering of  $z$  decreases the sensitivity of the system, and the gating compliance suggests that loss of TRPML affects both types of mechanotransducer channels defined by Effertz et al. (2011), documenting that the mechanogating of channels in JONs and their numbers both depend on TRPML.

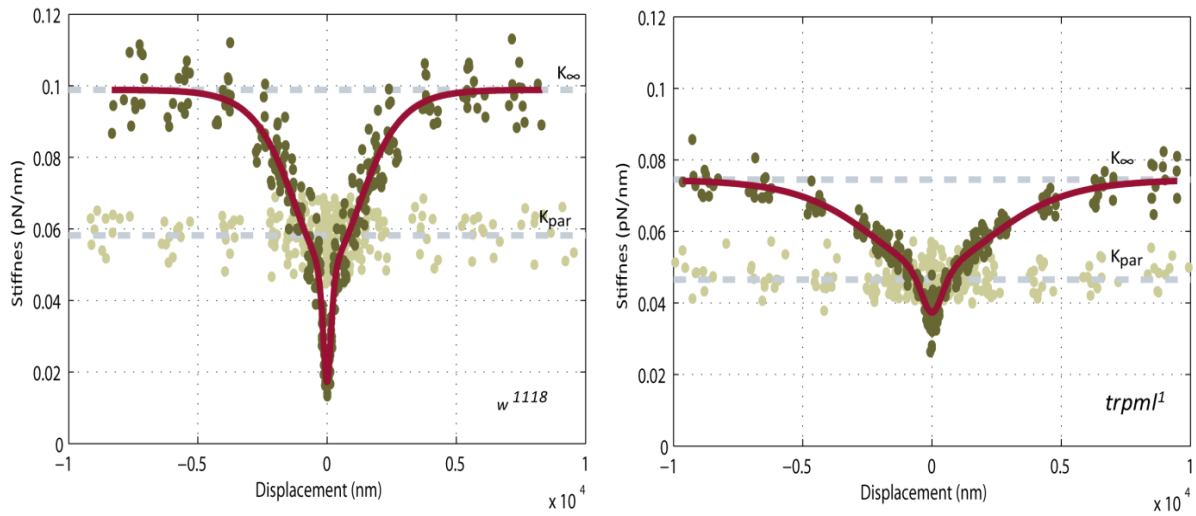


**Figure 16. *trpm1*<sup>1</sup> mutation affects the nonlinear gating compliance in the fly’s antenna.**

Stiffness of the antennal sound receiver as a function of antennal displacement. Symbols: dynamic slope stiffness (dark green symbols), steady-state slope stiffness (pale green symbols), fit of the dynamic slope stiffness data with the gating spring model (solid line), and parallel ( $K_{par}$ , lower dotted lines) and asymptotic ( $K_{\infty}$ , upper dotted lines) stiffnesses.

**Table 5. Comparison of parameters of gating spring model with two types of channels in control (*w*<sup>1118</sup> ( $R^2=0.9398$ )) and *trpm1*<sup>1</sup> mutants ( $R^2=0.9473$ ).**

Yeast		$N_s$		$Z_s$ (fN)		$N_i$		$Z_i$ (fN)		$K_{\infty}$ ( $\mu\text{N/m}$ )		$K_{par}$ ( $\mu\text{N/m}$ )		$K_{GS}$ ( $\mu\text{N/m}$ )	Number of flies
		Coefficient	95% confidence interval	Coefficient	95% confidence interval	Coefficient	95% confidence interval	Coefficient	95% confidence interval	Coefficient	95% confidence interval	Coefficient	Standard deviation	$K_{GS}$ $K_{par}$	
-	<i>w</i> <sup>1118</sup>	340.5	228 453	39.97	34 45.95	41280	35070 47500	4.389	4.035 4.743	98.87	97.18 100.6	58.162	3.575	40.708	6
-	<i>trpm1</i> <sup>1</sup>	1042	548.4 1536	14.43	11.69 17.17	69940	52830 87060	2.368	2.063 2.673	74.49	73.21 75.77	46.496	2.735	27.994	6

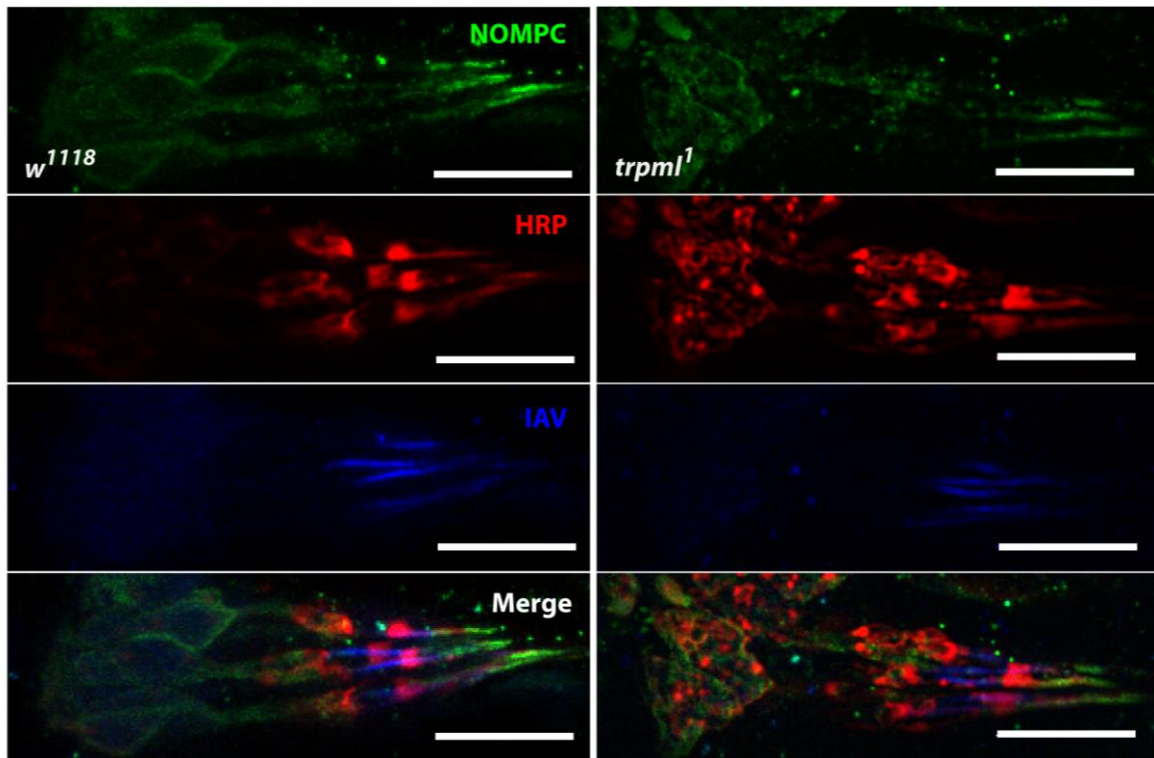


**Figure 17. NOMPC and IAV are localized properly in *trpml<sup>1</sup>* mutants.**

NOMPC and IAV are stained with  $\alpha$ -NOMPC and  $\alpha$ -IAV antibodies and indicated in green and blue, respectively.  $\alpha$ -HRP used for neuronal counterstaining is shown in red. Scale bar: 10  $\mu$ m.

NOMPC and IAV have been implied as auditory mechanotransducers in fly, with the key features of loss of the channels including elimination of amplificatory gain and sound-evoked nerve response, respectively (Göpfert et al. 2006 ; Effertz et al. 2012; Yan et al. 2013; Gong et al. 2013; Kim et al. 2003; Gong et al. 2004; Lehnert et al. 2013). Not only the expression per se but also the correct ciliary localization might be critical for the functionality of NOMPC and IAV/NAN in this process, as suggested by numerous evidence though none of them are conclusive (Lee et al. 2008, Cheng et al. 2010a, Park et al. 2013). For example, NOMPC with truncated Ankyrin repeat, which fail to be localized to the distal cilia by losing contact to microtubules, is not functional (Cheng et al. 2010a). *dtulp* mutants, which show spreading of NOMPC to proximal region and loss of IAV in the proximal cilia (Park et al. 2013) as well as *btv* mutants inducing expansion of IAV/NAN localization further to the distal from proximal cilia (Lee et al. 2008) don't have any nerve response by sound stimulation. According to the correlates deduced from gating compliance, TRPML seems to affect the numbers and single channel gating forces of both types of the 'mechanotransducer', whose identities are still elusive. Hence, whether *trpml<sup>1</sup>* mutants indeed behave as the model described was checked by visualizing the putative mechanotransduction channels in JONs. Staining the controls and mutants with NOMPC and IAV

antibodies, however, did not reveal any changes in localization nor quantity of protein (Figure 17), leaving the question open.

### 3.3.2 Epistatic analysis of TRPML and TRPV channels

#### 3.3.2.1 On the active process

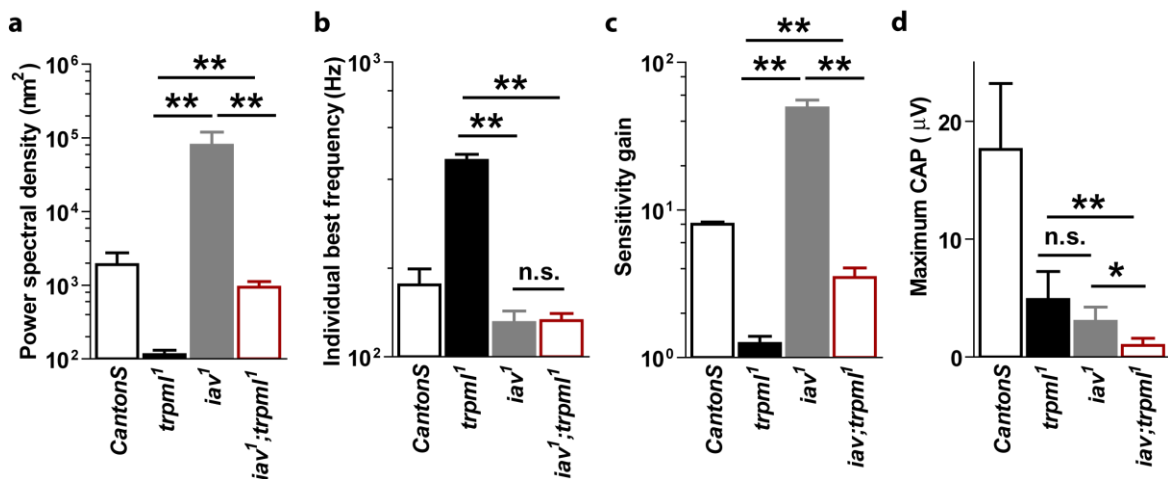


**Figure 18. Double mutants of *trpml*<sup>1</sup> and *iav*<sup>1</sup> channels show intermediate mechanical amplification of each single mutants.**

Comparisons were made among control (CantonsS), single mutants of *trpml*<sup>1</sup> and *iav*<sup>1</sup>, and double mutant (*iav*<sup>1</sup>;*trpml*<sup>1</sup>). **a.** Power of the receiver vibration, determined by integrating the power spectra between 100 and 1000 Hz. **b.** Individual best frequencies determined as the frequencies with the maximal velocity from the Fourier transform of antennal velocities. **c.** Sensitivity gain, calculated as a ratio between maximum and minimum gain, where gain is defined as antennal displacement divided by stimulus intensity in sound particle velocity (SPV). **d.** Maximum CAPs. Data in are shown as means±S.D. (N=5) and the statistical significances are indicated with n.s.: not significant, \* (p<0.05) or \*\* (p<0.01), by Wilcoxon rank-sum test with Bonferroni correction. Except for power of *iav*<sup>1</sup>;*trpml*<sup>1</sup>, all values were significantly different from those of controls, which is not indicated.

Previously, TRPVs Inactive (IAV) and Nanchung (NAN) has been shown to play significant roles in auditory process of *Drosophila* (Kim et al. 2003; Gong et al. 2004; Göpfert et al. 2006), controlling the



active amplification by JONs and the auditory nerve response. To see whether TRPML interacts with these TRPVs for auditory function in *Drosophila*, I compared the hearing phenotypes of double mutants carrying both *trpml<sup>1</sup>* and *iav<sup>1</sup>*. Because IAV and Nan interdependently localize within JONs (Gong et al., 2014), effect of mutation in only one of them was analyzed.

As described previously (Göpfert et al. 2006), the antennal sound receivers of *iav<sup>1</sup>* mutants displayed excessive self-sustained oscillations, resulting in a high total fluctuation power ( $79574.4 \pm 40265.2 \text{ nm}^2$ ) and excessive amplification gains ( $49.0 \pm 6.5$ ) (Figure 18; Table 6). In agreement with previous data, I also found that the nerve response is lost (maximum CAP amplitudes of  $3.0 \pm 1.2 \text{ } \mu\text{V}$ ). Introducing the *trpml<sup>1</sup>* mutation in the *iav<sup>1</sup>* mutant background yielded fluctuation powers of  $940.7 \pm 183.5 \text{ nm}^2$  and amplification gains of  $3.5 \pm 0.6$ . The intermediate values in double mutants compared with single mutants (*trpml<sup>1</sup>*, power,  $114.7 \pm 16.6 \text{ nm}^2$ ; sensitivity gain,  $1.2 \pm 0.1$ ) suggest that TRPML and TRPVs operate in parallel in the control of JON motility. The maximum CAP amplitudes were further reduced to  $1.0 \pm 0.6 \text{ } \mu\text{V}$  in the double mutants (*trpml<sup>1</sup>*,  $4.9 \pm 2.4$ ; *iav<sup>1</sup>*,  $3.0 \pm 1.2 \text{ } \mu\text{V}$ ), documenting an additive effect. This additive effect was significant, and are consistent with the idea that TRPML and TRPVs also function in parallel pathways in electrical signal generation.

**Table 6. Comparison of hearing phenotypes in control (*CantonS*), *trpml<sup>1</sup>* and *iav<sup>1</sup>* single and double mutants**

		Power ( $\text{nm}^2$ )	iBF (Hz)	Sensitivity gain	Max CAP ( $\mu\text{V}$ )
<i>CantonS</i>	Mean	1906.8	175.6	8.0	41807
	S.D.	853.6	41693	0.3	41795
<i>trpml<sup>1</sup></i>	Mean	114.7	463.6	41671	41886
	S.D.	41806	41693	0.1	41731
<i>iav<sup>1</sup></i>	Mean	79574.3	130.6	49.0	3.0
	S.D.	40265.2	41710	41765	41671
<i>iav<sup>1</sup>;trpml<sup>1</sup></i>	Mean	940.7	132.6	41762	1.0
	S.D.	183.5	41858	0.6	0.6

### 3.3.2.2 On transducer gating

Epistatic analysis of TRPML and TRPVs on amplification and nerve responses showed that those channels work in parallel to control these activities. To check whether this is the case for gating properties, I analyzed gating compliance and mechanical correlates deduced from it. First, effects of single *iav* mutation on mechanotransducer opening were characterized (Figure 19; Table 7). Gating compliance in *iav*<sup>1</sup> exhibited asymptotic stiffness of 103.2 (100.5-106.0) and parallel stiffness of 64.1±1.1 μN/m, which were comparable to those of controls ( $K_{\infty}$ , 103.1 (101.4-104.8);  $K_{par}$ , 67.0±2.6

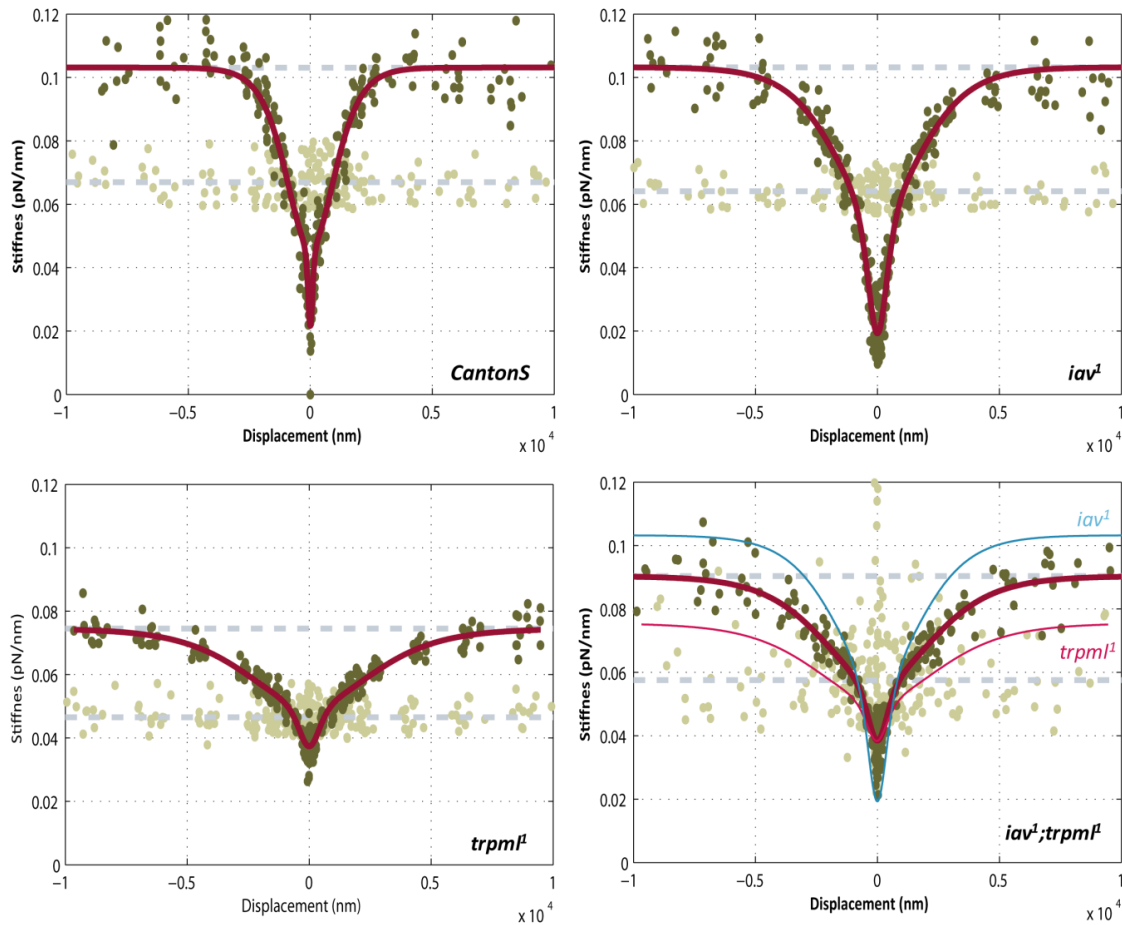


**Figure 19. Gating compliance in double mutants of *trpm*<sup>1</sup> and *iav*<sup>1</sup> reflect both aspects from single mutants.**

Stiffness of sound receiver is represented as a function of antennal displacement. Symbols: peak slope stiffness (dark green traces), steady-state slope stiffness (pale green traces), fit of peak slope stiffness data to gating spring model (solid line, red), parallel stiffness deduced from steady-state slope stiffness data (dotted line, lower), asymptotic stiffness obtained by fitting the peak slope stiffness data (dotted line, upper), gating spring model fits from *trpm*<sup>1</sup> (solid line, magenta) and *iav*<sup>1</sup> (solid line, cyan) added for comparison. Data for *CantonS* and *iav*<sup>1</sup> single mutants were provided by Christian Spalthoff.

$\mu\text{N/m}$ ). Fitting the data also revealed that the  $z$  values were 15.61 (12.07-19.16) fN for sensitive and 3.325 (2.665-3.985) fN for insensitive population of mechanotransducer channels, indeed much lower than in controls (*CantonS*,  $z_s$ , 68.13 (50.32-85.94);  $z_i$ , 6.145 (5.679-6.611) in fN). This change in single channel gating force of sensitive channels were comparable to those of *trpm1<sup>1</sup>* mutants (14.43 (11.69-17.17) fN), while  $z_i$  could be slightly higher than in *trpm1<sup>1</sup>* mutants (2.368 (2.063-2.673) fN). However, decrease in  $z$  values seems to be compensated not to lead to reduction in asymptotic stiffness, by increase in number of channels. Especially, change in the number of sensitive type of channels than those of insensitive population were drastic: in *iav<sup>1</sup>* mutants,  $N_s$  was suggested to be 2709 (1078-4339), which was by over the factor of 30 more than in controls (*CantonS*, 88 (40-136)), while  $N_i$  was just close to double of controls (*CantonS*, 24580 (21000-28170); *iav<sup>1</sup>*, 64760 (45540-83980)). While the change in  $N_s$  of *iav<sup>1</sup>* mutants could be more than in *trpm1<sup>1</sup>* mutants (1042 (548-1536)),  $N_i$  was comparable to 69940 (52830-87060) in *trpm1<sup>1</sup>* mutants.

**Table 7. Comparison of parameters of gating spring model with two types of channels in control (*CantonS* ( $R^2=0.9398$ )), single mutants (*trpm1<sup>1</sup>* ( $R^2=0.9473$ ) and *iav<sup>1</sup>* ( $R^2=0.9245$ )) and double mutants (*iav<sup>1</sup>;trpm1<sup>1</sup>* ( $R^2=0.9134$ )).**

	$N_s$			$Z_s$ (fN)			$N_i$			$Z_i$ (fN)			$K_\infty$ ( $\mu\text{N/m}$ )			$K_{\text{par}}$ ( $\mu\text{N/m}$ )		$K_{\text{GS}}$ ( $\mu\text{N/m}$ )	Number of flies
	Coefficient	95% confidence interval		Coefficient	95% confidence interval		Coefficient	95% confidence interval		Coefficient	95% confidence interval		Coefficient	Standard deviation	$K_\infty$ - $K_{\text{par}}$				
<i>CantonS</i>	87.76	39.99	135.5	68.13	50.32	85.94	24580	21000	28170	6.145	5.679	6.611	103.1	101.4	104.8	66.97	2.587	36.13	5
<i>trpm1<sup>1</sup></i>	1042	548.4	1536	14.43	11.69	17.17	69940	52830	87060	2.368	2.063	2.673	74.49	73.21	75.77	46.496	2.735	27.99	6
<i>iav<sup>1</sup></i>	2709	1078	4339	15.61	12.07	19.16	64760	45540	83980	3.325	2.665	3.985	103.2	100.5	106.0	64.10	1.108	39.10	5
<i>iav<sup>1</sup>;trpm1<sup>1</sup></i>	1360	349.8	2371	15.06	10.63	19.48	75720	52850	98590	2.676	2.214	3.138	90.35	88.21	92.49	57.56	10.83	32.79	5

Finally, gating compliance in sound receiver of fly was analyzed after introducing both of *iav<sup>1</sup>* and *trpm1<sup>1</sup>* mutations (Figure 19; Table 7). The linear terms which are not related to channel opening itself were shifted, i.e., the asymptotic stiffness, parallel stiffness and gating spring stiffness were suggested to be 90.35 (88.21-92.49), 57.56±10.83, and 32.79 fN, respectively, by the gating spring model, the values falling between those of the two single mutants. Single channel gating forces also appeared to be

intermediate to those of *iav*<sup>1</sup> and *trpm1*<sup>1</sup> single mutants, with  $z_s = 15.1$  (10.6-19.5) and  $z_i = 2.7$  (2.2-3.1). Number of channels, interestingly, were deduced to be 1360 (350-2371) and 75720 (52850-98590) for sensitive and insensitive channel types, the latter presenting synergistic effects of two mutations. Those intermediate as well as the synergistic features of two mutations shown in double mutants indicate that IAV and TRPML belong to parallel pathway for transducer gating modulation.

## 4 Discussion

TRPML first emerged as a candidate channel playing an auditory role by a report of the deafness phenotype in *varitint-waddler* mouse (Di Palma et al. 2002). The basis of this phenotype was revealed to be a point mutation rendering the TRPML3 channel constitutively active (Grimm et al. 2007, Kim et al. 2007, Nagata et al. 2008, van Aken et al. 2008). Genetic inactivation of TRPML3, however, did not lead to any hearing deficits (Jörs et al. 2010), leaving the engagement of TRPML in hearing ambiguous. In mammalian system, investigating roles of TRPML can be complicated by multiple homologs, always leaving the possibility of compensation by other homologs when one of them is lost. In this context, *Drosophila* carrying only one counterpart can be advantageous. Here, using *Drosophila* as a model system, I show that TRPML is expressed in the neurons of the antennal hearing organ and is required for sensitive hearing. The auditory mechanics in *trpml* mutant flies revealed that mechanical feedback amplification by auditory neurons is compromised, reducing the fluctuation power, shifting the tuned frequency and linearizing the mechanics of the sound receiver. This loss of mechanical amplification is associated with a reduced sensitivity of auditory nerve responses to both sound stimuli and sound-induced receiver displacements. Those defects were rescued when the mutants were introduced with genomic rescue construct of *trpml*. Also, the dTRPML expression driven into neurons could restore the normal hearing phenotypes, which, together with the *trpml* expression pattern demonstrated by the promoter fusion construct, suggest that dTRPML is required in the auditory neurons for sensitive hearing. Additionally, I show that the gating compliance is altered in the mutants. Analysis of correlates of transducer gating deduced from the gating compliance suggest that the loss of dTRPML increased the numbers and decreased the single channel gating forces of both sensitive and insensitive population of the channels suggested in Effertz et al. 2012, reducing the sensitivities to mechanical stimuli. Epistatic analysis showed that the dTRPML action on the active process of hearing as well as on the gating of mechanotransduction channels is in parallel with Nanchung/Inactive (NAN/IAV) channel complex, the modulator in this process. Lastly, I would like to discuss that involvement of dTRPML in the process of lysosomal signaling might link starvation response cascade to the quality of hearing.

## 4.1 Neuronal expression of TRPML in the *Drosophila* ear

The GAL4XUAS approach showed that ubiquitous or neuronal expression of TRPML could partially rescue the hearing phenotypes in *trpml* mutants. Together with the JON expression of reporter driven by *trpml* promoter fusion, these results indicate that TRPML is expressed at least in the auditory neurons in the fly ear and plays important roles in normal hearing. Whether it's sufficient to have TRPML only in the neurons of the ear, however, could not be confirmed in those rescue experiment, for the involvement of other supporting cells and the mechanisms of how they are controlled in the ear is not fully understood in the hearing process. Also, some fly strains carrying promoter constructs in different insertion sites as well as an enhancer trap line showed reporter expressions in some of the non-neuronal cell types (Supplementary figure 1; Joo 2011), which could be a part of the true expression pattern. Hence, evaluating the mechanical amplification in flies using *trpml* RNAi driven by drivers for different cellular components of JO, including JON, ligament cell, cap cell and scolopale cell as well as ubiquitous JO driver might be interesting. Especially, mechanical feedback amplification of sound stimuli in *Drosophila* is independent of efferent modulation, as demonstrated by lack of any chemical efferent synapse innervation to the auditory neurons and persistent mechanical amplification after pan-neuronal disruption of synaptic transmission (Kamikouchi et al. 2010). Thus selective knock-down of *trpml* in JO should be able to dissect the cellular involvement of *trpml* in this local process of mechanical amplification.

It should be also noted that none of the GAL4XUAS results, including TRPML expression in all cell types and in neurons with different doses, showed complete hearing rescue in the mutants. This might indicate that precise control of TRPML level is necessary for the proper hearing. This could be comparable with the observation that also in the genomic rescues, in which the construct was inserted in ectopic genomic context, hearing was never completely restored.

## 4.2 Intracellular localization of TRPML in *Drosophila*: on the lysosomes, on the plasma membrane and on the ciliary membrane?

Accumulating data on lysosomal proteins revealed that most of the proteins carry short signal peptides, including tyrosine-based motifs with the consensus of NPXY or YXXΦ (X and Φ denote any amino acid and a hydrophobic residue, respectively.), or di-leucine motifs ((D/E)XXXL(L/I), (D/E)XXLL or LL) (Bonifacino and Traub 2003). In mammalian Mucolipin-1, three di-leucine motifs in the N- and C-terminal loops were characterized to be essential for lysosomal targeting, internalization, and membrane association of the protein (Vergarajauregui and Puertollano 2006). Wong et al. 2012 reported that dTRPML::Myc is localized to endosomal compartments, like the dTRPML proteins with GFP tags at the N- or C-terminus tested in this study. The two N-terminal sequences mediating lysosomal transport and internalization of Mucolipin-1, however, are not conserved in dTRPML. Instead, the C-terminal palmitoylation motif, which is reported to be responsible for membrane association, is present, as revealed by sequence alignment (Figure 14). If these reflects the true localization of native dTRPML, it means that there are other mechanisms for dTRPML to be sorted into the lysosomes. I screened the dTRPML for candidate lysosomal targeting sequences, finding N-terminal Y<sup>118</sup>KFV, L<sup>378</sup>L in the intracellular loop between transmembrane domains (TM) 2-3, Y<sup>466</sup>NVV in the intracellular loop between TM4-5, Y<sup>644</sup>TSL and Y<sup>573</sup>DTI in the C-terminal domain. Interestingly, the sequence alignment revealed that human Mucolipin-3 (hMucolipin-3) also lacks the two N-terminal di-leucine motifs (data not shown). Overexpression studies in cell culture showed that hMucolipin-3 is mainly retained in the ER without the existence of its two other homologs, which are necessary for its lysosomal localization (Venkatachalam et al. 2006). At the endogenous expression level, however, the three TRPML proteins were coimmunoprecipitated and colocalized only partially (Zeevi et al. 2009). Also, in contrast to almost exclusive endosomal localization of two other human TRPMLs, hMucolipin-3 is localized to the cell surface as well as to the endosomes at the basal level, which could be entirely shifted to endosomal compartment upon cellular stress (Kim et al. 2009, Martina et al. 2009). The shift from plasma membrane to endosomes by stress was also reported in dTRPML (Wong et al. 2012). But none of the searched sequences were conserved between them, suggesting different regulatory mechanisms involved in spite of similar behavior in hMucolipin-3 and dTRPML.

Other than the two relatively well-established tyrosine-based and di-leucine motifs, Vergarajauregui and Puertollano (2006) also reviews 'acidic clusters', which are clusters of acidic amino acid residues containing the phosphorylation sites by casein kinase II ((S/T)XX(D/E)). Since those sequences are related to endosome-to-TGN sorting which might be relevant to the endosome-cell surface transition, I searched for the consensus in dTRPML and found T<sup>597</sup>AED. Interestingly, this motif was conserved in hMucolipin-2 (S<sup>506</sup>SKE), which was observed also on the plasma membrane (Dong et al. 2008, Samie et al. 2009, Lev et al. 2010, Zeevi et al. 2010, Grimm et al. 2012). But those predictions remain purely

hypothetical, since there has been no report on either the functionality or the involvement of casein kinase II in TRPML family proteins.

As mentioned above, the plasma membrane localization of dTRPML has been reported by Wong et al. 2012, which was not observed here (Figure 15). It could be due to the normal food condition I reared the flies under, which puts the pupae under starvation stress, leaving the question still open. The possible cell surface expression in JO brings a question: Does the surface include ciliary membrane? dTRPML has a predicted palmitoylation motif on the C-terminal loop. Interestingly, most of the known ciliary targeting motifs has been shown to be lipidated, either with myristoyl or palmitoyl moiety (Nanchury et al. 2010). These modifications facilitate the ciliary targeting via lipid raft association of the proteins, which can be blocked by mutations inhibiting the lipidations or removing the palmitoyltransferase (Godsel and Engman 1999, Tam et al. 2000, Tao et al. 2009, Follit et al. 2010). Also, there was an observation reporting stereociliary membrane localization of murine Mucolipin-3 (Di Palma et al. 2002), even though it should be noted that the stereocilia has low analogy to the cilia. Cilium is able to concentrate specific molecules due to the presence of periciliary diffusion barrier. Not surprisingly, the ciliary membrane seem to have a special lipid composition. Histochemistry combined with pharmacological techniques revealed that cilia of different organisms ranging from trypanosome to mammals are enriched with several sphingolipids and sterols (Montesano 1979, Souto-Pradón and de Souza 1983, Chailley and Boisvieux-Ulrich 1985, paramecium results reviewed in Kaneshiro 1987, Janich and Corbeil 2007). This was also proven by the observation that the ciliary membrane localization of a protein was facilitated via lipid raft association which was acylation-dependent (Tyler et al. 2009). Additionally, sequence analysis of dTRPML revealed one ciliary targeting consensus VXPX (V<sup>54</sup>APV). Also, according to the deduced correlates of transducer gating, loss of TRPML changes not only the number of channels but also the quality of them. Hence, it might be that dTRPML is also targeted to ciliary region to interact with and thus directly modulate the mechanotransduction channels, even though in this case the ciliary pool of modulatory dTRPML should be regulated differentially so that it doesn't undergo the reported dynamic shift between the plasma membrane and the endosomal compartments upon stress. To verify this point, generation of antibodies should be of the first priority (in progress).

### **4.3 TRPML mechanisms of action on fly hearing**



### 4.3.1 TRPML-TRPV interaction in the amplificatory gain and signal propagation

Recent study reported that heteromultimeric channels of TRPML3 and TRPV5 were formed by coexpressing them in a mammalian cell line (Guo et al. 2013), which were functionally distinct from either of the homomeric channels. While *trpml* null mutants show reduced active process demonstrated by loss of mechanical stimulus amplification as well as associated sensitivity of nerve response to sound stimulus, non-functional mutations in TRPVs causes enhanced active amplification and abolished nerve response in *Drosophila* (Göpfert et al. 2006). Heteromerization of TRPV and TRPML in mammalian system together with the mutant phenotypes of opposite directions in sensitivity gain in the mutants of *Drosophila* TRPVs and TRPML channels, albeit there is no evidence of colocalization so far, brought up the need to investigate epistatic relationship between dTRPML and dTRPVs. Since the functionality and localization of dTRPVs IAV and NAN in JONs are interdependent (Gong et al. 2004), only mutants of one of them was investigated. The parameters for active mechanical amplifications, i.e. total fluctuation power and amplification gains lay between those of caused by the loss of dTRPML or NAN/IAV, suggesting TRPML and TRPVs operate in parallel for mechanical amplification control. Reduced nerve response in both single mutants were aggravated in the double mutants, indicating the involvement of each channels in parallel pathways for nerve signal propagation.

### 4.3.2 TRPML on the correlates of transducer gating

Albert et al. (2007) showed that gating of auditory mechanotransduction channels in *Drosophila* and vertebrates share the common feature of direct gating, conforming to the gating spring model. This model supposes that the gate of each transduction channel is linked to an elastic gating spring bearing some tension at the resting position, which is increased upon forcing, changing the open probability of the channel (Corey and Hudspeth 1983). The opening of the channel, in turn, relaxes the spring, resulting in nonlinear gating compliance. The model divides the stiffness of the system into two parts, contributed by linear spring and gating spring. The contribution by the gating spring is further divided into linear stiffness corresponding to the stiffness of the gating spring itself and nonlinear stiffness, which correlates the stiffness with opening of the channel. Hence analyzing

gating compliance and correlates of transducer gating deduced from it by the gating spring model in mutants could provide a measure to evaluate the involvement of the protein of interest in the transducer gating process (Albert and Göpfert 2007). It should be noted that in *Drosophila*, the model is modified from the original gating spring model with one channel type to contain two types of channels with different force sensitivities to better fit the data (Effertz et al. 2012). According to the analysis of *trpml* mutants, other than still having two distinct populations with different sensitivities (indicated as *s*, sensitive and *i*, insensitive), loss of TRPML changes all the mechanical correlates of transducer gating significantly: it results in increase in numbers ( $N$ ) and reduction in single channel gating forces ( $z$ ) of both channel types and decrease in asymptotic stiffness ( $K_{\infty}$ ) due to reduction in both parallel ( $K_{par}$ ) and gating spring stiffness ( $K_{GS}$ ). Then what can be the detailed mechanisms behind these changes?

First, the number of channels for both channel types were augmented in *trpml* mutants. A recent report, which showed the link between dTRPML and TORC1 (Wong et al. 2012), might give us a hint on the mechanism behind it. TORC1, the master regulator of cell growth, is activated under rich nutritional conditions. Flies are highly dependent on autophagy for nutrients during pupal stage. The *trpml* mutant flies show high pupal lethality due to defective autophagy by failing to fuse lysosome-amphisome. Since TORC1 is activated by nutrient availability, aggravated starvation condition in *trpml* mutants lowers the activity of TORC1 (Wong et al. 2012). Previously, TORC1 is shown to positively regulate bulk endocytosis (Hennig et al. 2006) as well as ubiquitin-mediated endocytosis (MacGurn et al. 2011). Interestingly, ubiquitination has been implicated in the exit of protein from the cilia (Hurley and Emr 2006, Hu et al. 2007, Tanaka et al. 2008, Huang et al. 2009). Hence the general lowering of ubiquitin-mediated endocytosis caused by low TORC1 activity in *trpml* mutants could be setting the balance of ciliary mechanotransducer channels at the higher level. But it should be also noted that the immunohistochemistry on the two putative transducer candidates NOMPC and IAV did not show significant changes in the *trpml* mutants. This could be due to the penetration of antibodies to the relatively thick section, which should be improved by using different embedding material and method (in progress).

Second, the single channel gating force ( $z$ ) and the gating spring stiffness ( $K_{GS}$ ) are lowered in *trpml* mutants. While  $z$  is a term proportional to both the single gating spring stiffness  $\kappa$  and the gating swing  $d$  of the transducer channel associated with the spring,  $K_{GS}$  is proportional to the number of channels ( $N$ ) and  $\kappa$  (Howard and Hudspeth 1988, Hudspeth et al. 2000, Albert and Göpfert 2007). Since  $N$  increased both for the sensitive and the insensitive channel types, reduction in  $K_{GS}$  should be explained by decreased  $\kappa$ , which also could also explain the reduction in  $z$  value. The single gating

spring stiffness could be lowered by any change that can make the spring softer, such as amino acid mutation (Hudspeth et al. 2000). Since it is unlikely that the loss of TRPML mutates proteins, change in  $\kappa$  should imply altered chemical environment surrounding the gating spring. If TRPML is targeted to ciliary membrane, then interaction of TRPML might be keeping the gating spring more rigid, which is missing in the *trpml* mutant. Or as in case of the number of channels, the lower activity of TORC1 might have left too much of certain proteins, making them mislocalized or nonspecifically interact with the gating spring, which is yet to be identified but numerous reports suggested that it could be the 29 ankyrin repeats at the N-terminus of NOMPC (Howard and Bechstedt 2004, Sotomayor et al. 2005, Lee et al. 2006, Liang et al. 2013). Or suspending structure for mechanotransduction channels could have been changed. But could the gating spring be something else? In electron microscopy studies of stereocilia, tenting, the membrane at the top of the shorter stereocilium pulled away from the underlying actin cytoskeleton via tip link is often observed (Assad et al. 1991), suggesting force extension. A recent biophysical modeling study in the stereocilia have shown that this elasticity or compliance could be also derived from the membrane alone (Powers et al. 2012). If this is also the case in *Drosophila* JONs that the membrane is the gating spring, how can the change in single gating spring stiffness be explained? This point will be addressed in the following paragraphs.

*trpml<sup>1</sup>* mutants exhibited lower parallel stiffness ( $K_{par}$ ) of antenna than controls. By definition parallel stiffness represents “the combined elasticity of all the components that suspend the sound receiver but do not contribute to stimulus coupling (Albert and Göpfert 2007)”. Hence, the altered  $K_{par}$  implies gross changes in the attached structures, and this possibility was investigated. To evaluate the impact of the mutation on the general anatomy of hearing organ, I first checked the development of scolopidia by staining the neurons and supporting structures, which turned out to be normal in the mutants (Figure 9a). Also, I searched for the signs of cellular distress: Chromosomal and microtubular stainings confirmed that two major apoptotic events, including cortical organization of microtubular network that occurs during the execution stage and later stage DNA condensation, were not happening in the mutants (Figure 9b). Presence of autofluorescent lipofuscin, the indicative of lysosomal accumulation of waste, was also negative (Figure 10), in mutants and in controls alike. Finally, the organ was free of autophagic vesicles, which can be visualized with the antibodies against autophagosomal marker ATG8 (Figure 11). These results indicate that hearing defects in mutants of young age (1-3 days old) in this study did not arise from developmental defects or major cellular disturbance but rather from subtler changes.

In light of established lysosomal function of TRPML family channels in other organisms (reviewed in Luzio et al. 2007, Saftig and Klumperman 2009) and lysosomal involvement of *Drosophila* TRPML

suggested in recent reports (Venkatachalam et al. 2008, Wong et al. 2012), I speculate that the *trpml* mutant  $K_{par}$  phenotypes might arise from the involvement of lysosomal lipid trafficking. The idea is that changes in the ciliary membrane might be the cause behind the reduced linear stiffness: Cilium is able to concentrate specific molecules due to the presence of periciliary diffusion barrier (reviewed in Nachury et al. 2010). As mentioned earlier and not surprisingly, the ciliary membrane seems to have a special lipid composition. In this context, lysosomal function of TRPML might explain the reduced parallel stiffness. ML4 cells or cells with Mucolipin-1 knock-down show defective exit of lipids from LEL to TGN (Chen et al. 1998, Pryor et al. 2006, Thompson et al. 2007). Nieman-Pick C (NPC) proteins govern the transport of cholesterol/lipids out of lysosome and hence the mutation in this protein also causes accumulation of lipids in the lysosomes (Carstea et al. 1997). Those lipids include sphingomyelin and cholesterol and, interestingly, since Mucolipin-1 is directly inhibited by sphingomyelin (Shen et al. 2012), NPC and Mucolipin-1 mutations practically have the same effects on cholesterol dynamics in the cell. Interestingly, Garver et al. (2002) showed that cholesterol in plasma membrane caveolae isolated from NPC1 mutant cells had significantly decreased, whereas the average cholesterol concentration in the plasma membrane was unchanged. The depletion of cholesterol can be a shared feature in specialized membrane domains enriched with cholesterol in LSD cells, as also shown by Kruth et al. (2001), i.e. It might be that otherwise cholesterol-rich ciliary membrane is depleted with cholesterol by TRPML mutation, affecting the mechanics of antenna. Interestingly, Evans and Needham (1987) showed that the lipid compositions in the bilayer membrane can affect the mechanical properties of the membrane and, especially, that with the increasing cholesterol content, the membrane becomes stiff. Even though it does not agree with the lack of significant autofluorescence in the mutants of the young age I used in this study (1-3 days old), lags in lysosomal cholesterol efflux at the undetectable level might be already undergoing. Hence this defects in cholesterol exit from lysosomes, which might selectively deplete the cholesterol from those specialized membranes including ciliary, could provide less stiff suspending structures for the mechanotransducer channel and its gating spring coupling the force. Or if the membrane serves as the gating spring *per se*, which is yet to be investigated, the lowering of single gating spring stiffness in the *trpml* mutants could be also explained by the selective cholesterol depletion in ciliary membrane.

It might be also important to note that modulation by cholesterol in TRP family channels began to be reported (Picazo-Juárez et al. 2011, Klein et al. 2014). For example, capsaicin-mediated currents of rat TRPV1 were inhibited by high cholesterol and this cholesterol-sensitivity is conferred via the cholesterol binding motif in the 5<sup>th</sup> transmembrane domain of the channel (Picazo-Juárez et al. 2011). Sequence alignment of this channel with *Drosophila* TRPVs revealed that the residues essential for cholesterol binding in TRPV1 was not conserved (data not shown). The mouse TRPV3, however, could

be sensitized by high cholesterol (Klein et al. 2014), even though this channel did not have the conserved sequences for cholesterol binding. Furthermore, the homologous region of TRPV3 is more similar to that of the cholesterol-insensitive human ortholog TRPV1 (Picazo-Juárez et al. 2011), suggesting that the structure for cholesterol binding is more diverse and hence simple sequence prediction might not detect the module.

## 5 Conclusions

Here, I showed that TRPML is expressed in the auditory neurons of the antennal hearing organ of *Drosophila* and is required for sensitive hearing, positively regulating the mechanical amplification and afferent signal propagation. With the epistatic analysis with TRPVs, TRPML could be positioned in a parallel regulatory pathway for the auditory function. Additionally, analyses of the mechanical correlates of transducer gating suggested the possible mechanisms of TRPML action in mechanotransduction of *Drosophila* ear. Together, these results provide insights in a role of TRPML channels in *Drosophila* hearing and possible links between lysosomal process and hearing in *Drosophila*.

## 6 References

- Ake Flock, M. B., and A. J. Duvall. 1965. The ultrastructure of the kinocilium of the sensory cells in the inner ear and lateral line organs. *journal of cell biology* 25:1–8.
- Van Aken, A. F. J., M. Atiba-Davies, W. Marcotti, R. J. Goodyear, J. E. Bryant, G. P. Richardson, K. Noben-Trauth, and C. J. Kros. 2008. TRPML3 mutations cause impaired mechano-electrical transduction and depolarization by an inward-rectifier cation current in auditory hair cells of varitint-waddler mice. *The Journal of physiology* 586:5403–18.
- Albert, J. T., and M. C. Göpfert. 2007. Drosophila mechanotransduction: Linking proteins and functions. *Fly* 1:238–241.
- Albert, J. T., B. Nadrowski, and M. C. Göpfert. 2007. Mechanical signatures of transducer gating in the Drosophila ear. *Current biology : CB* 17:1000–6.
- Alberts, B., A. Johnson, J. Lewis, M. Raff, K. Roberts, and P. Walter. 2008. Transport from the Trans Golgi Network to the cell exterior: Exocytosis. Pages 799–808 in M. Anderson and S. Granum, editors. *Molecular biology of the cell*. 5th edition. Garland Science, New York, NY, U.S.A.,.
- Assad, J. A., G. M. Shepherd, and D. P. Corey. 1991. Tip-link integrity and mechanical transduction in vertebrate hair cells. *Neuron* 7:985–94.
- Baker, J. D., S. Adhikarakunnathu, and M. J. Kernan. 2004. Mechanosensory-defective, male-sterile unc mutants identify a novel basal body protein required for ciliogenesis in Drosophila. *Development (Cambridge, England)* 131:3411–22.
- Bechstedt, S., J. T. Albert, D. P. Kreil, T. Müller-Reichert, M. C. Göpfert, and J. Howard. 2010. A doublecortin containing microtubule-associated protein is implicated in mechanotransduction in Drosophila sensory cilia. *Nature communications* 1:11.
- Bechstedt, S., and J. Howard. 2008. Hearing mechanics: a fly in your ear. *Current biology : CB* 18:R869–70.
- Ben-arie, N., B. A. Hassan, N. A. Bermingham, and D. M. Malicki. 2000. Functional conservation of atonal and Math1 in the CNS and PNS 1048:1039–1048.
- Bennet-Clark, H. C. 1971. Acoustics of Insect Song. *Nature* 234:255–259.
- Bermingham, N. A., B. A. Hassan, S. D. Price, M. A. Vollrath, N. Ben-Arie, R. A. Eatock, H. J. Bellen, A. Lysakowski, and H. Y. Zoghbi. 1999. Math1: an essential gene for the generation of inner ear hair cells. *Science (New York, N.Y.)* 284:1837–41.
- Blott, E. J., and G. M. Griffiths. 2002. Secretory lysosomes. *Nature reviews. Molecular cell biology* 3:122–31.
- Boekhoff-Falk, G. 2005. Hearing in Drosophila: development of Johnston’s organ and emerging parallels to vertebrate ear development. *Developmental dynamics : an official publication of the American Association of Anatomists* 232:550–8.

- Bonifacino, J. S., and L. M. Traub. 2003. Signals for sorting of transmembrane proteins to endosomes and lysosomes. *Annual review of biochemistry* 72:395–447.
- Burnet, B., K. Connolly, and L. Dennis. 1971. The function and processing of auditory information in the courtship behaviour of *Drosophila melanogaster*. *Animal behaviour* 19:409–15.
- Burnham, K. P., and D. R. Anderson. 2002. Model Selection and Multimodel Inference - A Practical Information-Theoretic Approach. Page 488. 2nd edition. Springer-Verlag New York, Inc.
- Cachero, S., T. I. Simpson, P. I. Zur Lage, L. Ma, F. G. Newton, E. E. Holohan, J. D. Armstrong, and A. P. Jarman. 2011. The gene regulatory cascade linking proneural specification with differentiation in *Drosophila* sensory neurons. *PLoS biology* 9:e1000568.
- Carlson, S. D., S. L. Hilgers, and J. L. Juang. 1997a. First developmental signs of the scolopale (glial) cell and neuron comprising the chordotonal organ in the *Drosophila* embryo. *Glia* 19:269–74.
- Carlson, S. D., S. L. Hilgers, and J. L. Juang. 1997b. Ultrastructure and blood-nerve barrier of chordotonal organs in the *Drosophila* embryo. *Journal of neurocytology* 26:377–88.
- Carstea, E. D., J. A. Morris, K. G. Coleman, S. K. Loftus, D. Zhang, C. Cummings, J. Gu, M. A. Rosenfeld, W. J. Pavan, D. B. Krizman, J. Nagle, M. H. Polymeropoulos, S. L. Sturley, Y. A. Ioannou, M. E. Higgins, M. Comly, A. Cooney, A. Brown, C. R. Kaneski, E. J. Blanchette-Mackie, N. K. Dwyer, E. B. Neufeld, T. Y. Chang, L. Liscum, J. F. Strauss, K. Ohno, M. Zeigler, R. Carmi, J. Sokol, D. Markie, R. R. O'Neill, O. P. van Diggelen, M. Elleder, M. C. Patterson, R. O. Brady, M. T. Vanier, P. G. Pentchev, and D. A. Tagle. 1997. Niemann-Pick C1 disease gene: homology to mediators of cholesterol homeostasis. *Science (New York, N.Y.)* 277:228–31.
- Chailley, B., and E. Boisvieux-Ulrich. 1985. Detection of plasma membrane cholesterol by filipin during microvillogenesis and ciliogenesis in quail oviduct. *Journal of Histochemistry & Cytochemistry* 33:1–10.
- Chen, C. S., G. Bach, and R. E. Pagano. 1998. Abnormal transport along the lysosomal pathway in mucopolipidosis, type IV disease. *Proceedings of the National Academy of Sciences of the United States of America* 95:6373–8.
- Chen, D., and S. W. Whiteheart. 1999. Intracellular localization of SNAP-23 to endosomal compartments. *Biochemical and biophysical research communications* 255:340–6.
- Cheng, L. E., W. Song, L. L. Looger, L. Y. Jan, and Y. N. Jan. 2010a. The role of the TRP channel NompC in *Drosophila* larval and adult locomotion. *Neuron* 67:373–80.
- Cheng, X., D. Shen, M. Samie, and H. Xu. 2010b. Mucopolipins: Intracellular TRPML1-3 channels. *FEBS letters* 584:2013–21.
- Christensen, A. P., and D. P. Corey. 2007. TRP channels in mechanosensation: direct or indirect activation? *Nature reviews. Neuroscience* 8:510–21.
- Chung, Y. D., J. Zhu, Y. Han, and M. J. Kernan. 2001. *nompA* encodes a PNS-specific, ZP domain protein required to connect mechanosensory dendrites to sensory structures. *Neuron* 29:415–28.

- Cook, B., R. W. Hardy, W. B. McConnaughey, and C. S. Zuker. 2008. Preserving cell shape under environmental stress. *Nature* 452:361–4.
- Corey, D. P., and A. J. Hudspeth. 1983. Kinetics of the receptor current in bullfrog saccular hair cells. *The Journal of neuroscience : the official journal of the Society for Neuroscience* 3:962–76.
- Dong, X., D. Shen, X. Wang, T. Dawson, X. Li, Q. Zhang, X. Cheng, Y. Zhang, L. S. Weisman, M. Delling, and H. Xu. 2010. PI(3,5)P(2) controls membrane trafficking by direct activation of mucolipin Ca(2+) release channels in the endolysosome. *Nature communications* 1:38.
- Dong, X.-P., X. Cheng, E. Mills, M. Delling, F. Wang, T. Kurz, and H. Xu. 2008. The type IV mucopolipidosis-associated protein TRPML1 is an endolysosomal iron release channel. *Nature* 455:992–6.
- Eberl, D. F., and G. Boekhoff-Falk. 2007. Development of Johnston's organ in *Drosophila*. *The International journal of developmental biology* 51:679–87.
- Eberl, D. F., R. W. Hardy, and M. J. Kernan. 2000. Genetically Similar Transduction Mechanisms for Touch and Hearing in *Drosophila*. *The journal of neuroscience* 20:5981–5988.
- Effertz, T. 2011. Candidate mechanosensitive transduction channels in *Drosophila melanogaster*. Georg-August-Universität Göttingen, Göttingen, Germany.
- Effertz, T., B. Nadrowski, D. Piepenbrock, J. T. Albert, and M. C. Göpfert. 2012. Direct gating and mechanical integrity of *Drosophila* auditory transducers require TRPN1. *Nature neuroscience* 15:1198–200.
- Effertz, T., R. Wiek, and M. C. Göpfert. 2011. NompC TRP channel is essential for *Drosophila* sound receptor function. *Current biology : CB* 21:592–7.
- Evans, E., and D. Needham. 1987. Physical properties of surfactant bilayer membranes: thermal transitions, elasticity, rigidity, cohesion, and colloidal interactions. *Journal of physical chemistry* 91:4219–4228.
- Feng, X., Y. Huang, Y. Lu, J. Xiong, C.-O. Wong, P. Yang, J. Xia, D. Chen, G. Du, K. Venkatachalam, X. Xia, and M. X. Zhu. 2014. *Drosophila* TRPML forms PI(3,5)P2-activated cation channels in both endolysosomes and plasma membrane. *The Journal of biological chemistry* 289:4262–72.
- Follit, J. A., L. Li, Y. Vucica, and G. J. Pazour. 2010. The cytoplasmic tail of fibrocystin contains a ciliary targeting sequence. *The Journal of cell biology* 188:21–8.
- Garver, W. S., K. Krishnan, J. R. Gallagos, M. Michikawa, G. A. Francis, and R. A. Heidenreich. 2002. Niemann-Pick C1 protein regulates cholesterol transport to the trans-Golgi network and plasma membrane caveolae. *Lipid research* 43:579–589.
- Godsel, L. M., and D. M. Engman. 1999. Flagellar protein localization mediated by a calcium-myristoyl/palmitoyl switch mechanism. *The EMBO journal* 18:2057–65.
- Goldin, E., E. J. Blanchette-Mackie, N. K. Dwyer, P. G. Pentchev, and R. O. Brady. 1995. Cultured skin fibroblasts derived from patients with mucopolipidosis 4 are auto-fluorescent. *Pediatric research* 37:687–92.



- Gong, J., Q. Wang, and Z. Wang. 2013. NOMPC is likely a key component of *Drosophila* mechanotransduction channels. *The European journal of neuroscience* 38:2057–64.
- Gong, Z., W. Son, Y. D. Chung, J. Kim, D. W. Shin, C. a McClung, Y. Lee, H. W. Lee, D.-J. Chang, B.-K. Kaang, H. Cho, U. Oh, J. Hirsh, M. J. Kernan, and C. Kim. 2004. Two interdependent TRPV channel subunits, inactive and Nanchung, mediate hearing in *Drosophila*. *The Journal of neuroscience : the official journal of the Society for Neuroscience* 24:9059–66.
- Göpfert, M. C., J. T. Albert, B. Nadrowski, and a Kamikouchi. 2006. Specification of auditory sensitivity by *Drosophila* TRP channels. *Nature neuroscience* 9:999–1000.
- Göpfert, M. C., and D. Robert. 2002. The mechanical basis of *Drosophila* audition 1208:1199–1208.
- Göpfert, M. C., and D. Robert. 2003. Motion generation by *Drosophila* mechanosensory neurons. *Proceedings of the National Academy of Sciences* 100:5514–5519.
- Göpfert, M. C., and D. Robert. 2008. Active processes in insect hearing. Pages 191–209 in G. A. Manley, R. R. Fay, and A. N. Popper, editors. *Active Processes and Otoacoustic Emissions in Hearing*. Springer Science+Business Media, LLC, New York, NY, U.S.A.
- Grimm, C., M. P. Cuajungco, A. F. J. Van Aken, M. Schnee, S. Jo, A. J. Ricci, and S. Heller. 2007. A helix-breaking mutation in TRPML3 leads to constitutive activity underlying deafness in the varitint-waddler mouse 104:19583–19588.
- Grimm, C., S. Jörs, Z. Guo, A. G. Obukhov, and S. Heller. 2012. Constitutive activity of TRPML2 and TRPML3 channels versus activation by low extracellular sodium and small molecules. *The Journal of biological chemistry* 287:22701–8.
- Guicciardi, M. E., M. Leist, and G. J. Gores. 2004. Lysosomes in cell death. *Oncogene* 23:2881–90.
- Guo, Z., C. Grimm, L. Becker, A. J. Ricci, and S. Heller. 2013. A novel ion channel formed by interaction of TRPML3 with TRPV5. *PLoS one* 8:e58174.
- Han, Y.-G., B. H. Kwok, and M. J. Kernan. 2003. Intraflagellar transport is required in *Drosophila* to differentiate sensory cilia but not sperm. *Current biology : CB* 13:1679–86.
- Harteneck, C., T. D. Plant, and G. Schultz. 2000. From worm to man: three subfamilies of TRP channels. *Trends in neurosciences* 23:159–66.
- Hellmich, U. A., and R. Gaudet. 2014. Structural biology of TRP channels. *Handbook of experimental pharmacology* 223:963–90.
- Hennig, K. M., J. Colombani, and T. P. Neufeld. 2006. TOR coordinates bulk and targeted endocytosis in the *Drosophila melanogaster* fat body to regulate cell growth. *The Journal of cell biology* 173:963–74.
- Howard, J., and S. Bechstetd. 2004. Hypothesis : A helix of ankyrin repeats of the NOMPC-TRP ion channel is the gating spring of tors. *Current biology* 14:224–226.
- Howard, J., and a. J. Hudspeth. 1988. Compliance of the hair bundle associated with gating of mechano-electrical transduction channels in the Bullfrog's saccular hair cell. *Neuron* 1:189–199.

- Hu, J., S. G. Wittekind, and M. M. Barr. 2007. STAM and Hrs down-regulate ciliary TRP receptors. *Molecular biology of the cell* 18:3277–89.
- Huang, K., D. R. Diener, and J. L. Rosenbaum. 2009. The ubiquitin conjugation system is involved in the disassembly of cilia and flagella. *The Journal of cell biology* 186:601–13.
- Hudspeth, a J. 2008. Making an effort to listen: mechanical amplification in the ear. *Neuron* 59:530–45.
- Hudspeth, a J., Y. Choe, a D. Mehta, and P. Martin. 2000. Putting ion channels to work: mechano-electrical transduction, adaptation, and amplification by hair cells. *Proceedings of the National Academy of Sciences of the United States of America* 97:11765–72.
- Humphris, A. D. L., J. T. Albert, D. Robert, O. Hendrich, and M. C. Go. 2005. Power gain exhibited by motile mechanosensory neurons in *Drosophila* ears 102.
- Hurley, J. H., and S. D. Emr. 2006. The ESCRT complexes: structure and mechanism of a membrane-trafficking network. *Annual review of biophysics and biomolecular structure* 35:277–98.
- Jacquet, B. V., R. Salinas-Mondragon, H. Liang, B. Therit, J. D. Buie, M. Dykstra, K. Campbell, L. E. Ostrowski, S. L. Brody, and H. T. Ghashghaei. 2009. FoxJ1-dependent gene expression is required for differentiation of radial glia into ependymal cells and a subset of astrocytes in the postnatal brain. *Development (Cambridge, England)* 136:4021–31.
- Janich, P., and D. Corbeil. 2007. GM1 and GM3 gangliosides highlight distinct lipid microdomains within the apical domain of epithelial cells. *FEBS letters* 581:1783–7.
- Jarman, A. P. 2014. Development of the auditory organ (Johnston’s organ) in *Drosophila*. Pages 32–61 in R. Romand and I. Varela-Nieto, editors. *Development of Auditory and Vestibular Systems*. Fourth edition. Academic Press, Waltham, MA, U.S.A.
- Jarman, A. P., Y. Sun, L. Y. Jan, and Y. N. Jan. 1995. Role of the proneural gene, *atonal*, in formation of *Drosophila* chordotonal organs and photoreceptors. *Development (Cambridge, England)* 121:2019–30.
- Joo, S. 2011. The role of *trpml* in hearing of *Drosophila melanogaster*. Georg-August-Universität Göttingen, Göttingen, Germany.
- Jörs, S., C. Grimm, L. Becker, and S. Heller. 2010. Genetic inactivation of *Trpml3* does not lead to hearing and vestibular impairment in mice. *PLoS one* 5:e14317.
- Kamikouchi, A., J. T. Albert, and M. C. Göpfert. 2010. Mechanical feedback amplification in *Drosophila* hearing is independent of synaptic transmission. *The European journal of neuroscience* 31:697–703.
- Kamikouchi, A., H. K. Inagaki, T. Effertz, O. Hendrich, A. Fiala, M. C. Göpfert, and K. Ito. 2009. The neural basis of *Drosophila* gravity-sensing and hearing. *Nature* 458:165–71.
- Kamikouchi, A., T. Shimada, and K. E. I. Ito. 2006. Comprehensive Classification of the Auditory Sensory Projections in the Brain of the Fruit Fly *Drosophila melanogaster* 356:317–356.

- Kaneshiro, E. S. 1987. Lipids of Paramecium. *Journal of lipid research* 28:1241–1258.
- Kavlie, R. G., M. J. Kernan, and D. F. Eberl. 2010. Hearing in Drosophila requires TilB, a conserved protein associated with ciliary motility. *Genetics* 185:177–88.
- Kedei, N., T. Szabo, J. D. Lile, J. J. Treanor, Z. Olah, M. J. Iadarola, and P. M. Blumberg. 2001. Analysis of the native quaternary structure of vanilloid receptor 1. *The Journal of biological chemistry* 276:28613–9.
- Kernan, M., D. Cowan, and C. Zuker. 1994. Genetic dissection of mechanosensory transduction: mechanoreception-defective mutations of Drosophila. *Neuron* 12:1195–206.
- Kernan, M. J. 2007. Mechanotransduction and auditory transduction in Drosophila. *Pflügers Archiv : European journal of physiology* 454:703–20.
- Kikuchi, T., T. Takasaka, A. Tonosaki, and H. Watanabe. (n.d.). Fine structure of guinea pig vestibular kinocilium. *Acta oto-laryngologica* 108:26–30.
- Killick, R., P. K. Legan, C. Malenczak, and G. P. Richardson. 1995. Molecular cloning of chick beta-tectorin, an extracellular matrix molecule of the inner ear. *The Journal of cell biology* 129:535–47.
- Kim, D. S., B. K. Jeon, Y. E. Lee, W. H. Woo, and Y. J. Mun. 2012. Diosgenin Induces Apoptosis in HepG2 Cells through Generation of Reactive Oxygen Species and Mitochondrial Pathway. *Evidence-based complementary and alternative medicine : eCAM* 2012:981675.
- Kim, H. J., Q. Li, S. Tjon-Kon-Sang, I. So, K. Kiselyov, and S. Muallem. 2007. Gain-of-function mutation in TRPML3 causes the mouse Varitint-Waddler phenotype. *The Journal of biological chemistry* 282:36138–42.
- Kim, H. J., A. A. Soyombo, S. Tjon-Kon-Sang, I. So, and S. Muallem. 2009. The Ca<sup>2+</sup> channel TRPML3 regulates membrane trafficking and autophagy. *Traffic* 10:1157–1167.
- Kim, J., Y. D. Chung, D. Park, and S. Choi. 2003. A TRPV family ion channel required for hearing in Drosophila. *Nature* 424:81–84.
- Klein, A. S., A. Tannert, and M. Schaefer. 2014. Cholesterol sensitises the transient receptor potential channel TRPV3 to lower temperatures and activator concentrations. *Cell calcium* 55:59–68.
- Kroemer, G., and M. Jäättelä. 2005. Lysosomes and autophagy in cell death control. *Nature reviews. Cancer* 5:886–97.
- Kruth, H. S., I. Ifrim, J. Chang, L. Addadi, D. Perl-Treves, and W. Y. Zhang. 2001. Monoclonal antibody detection of plasma membrane cholesterol microdomains responsive to cholesterol trafficking. *Journal of lipid research* 42:1492–500.
- LaPlante, J. M., J. Falardeau, M. Sun, M. Kanazirska, E. M. Brown, S. A. Slaugenhaupt, and P. M. Vassilev. 2002. Identification and characterization of the single channel function of human mucolipin-1 implicated in mucopolipidosis type IV, a disorder affecting the lysosomal pathway. *FEBS letters* 532:183–7.

- Laplante, M., and D. M. Sabatini. 2012. mTOR signaling in growth control and disease. *Cell* 149:274–93.
- Larroux, C., G. N. Luke, P. Koopman, D. S. Rokhsar, S. M. Shimeld, and B. M. Degnan. 2008. Genesis and expansion of metazoan transcription factor gene classes. *Molecular biology and evolution* 25:980–96.
- Latorre, R., C. Zaelzer, and S. Brauchi. 2009. Structure-functional intimacies of transient receptor potential channels. *Quarterly reviews of biophysics* 42:201–46.
- Lee, E., E. Sivan-Loukianova, D. F. Eberl, and M. J. Kernan. 2008. An IFT-A protein is required to delimit functionally distinct zones in mechanosensory cilia. *Current biology : CB* 18:1899–906.
- Lee, G., K. Abdi, Y. Jiang, P. Michaely, V. Bennett, and P. E. Marszalek. 2006. Nanospring behaviour of ankyrin repeats. *Nature* 440:246–9.
- Lee, J., S. Moon, Y. Cha, and Y. D. Chung. 2010. Drosophila TRPN(=NOMPC) channel localizes to the distal end of mechanosensory cilia. *PLoS one* 5:e11012.
- Legan, P. K., A. Rau, J. N. Keen, and G. P. Richardson. 1997. The mouse tectorins. Modular matrix proteins of the inner ear homologous to components of the sperm-egg adhesion system. *The Journal of biological chemistry* 272:8791–801.
- Lehnert, B. P., A. E. Baker, Q. Gaudry, A.-S. Chiang, and R. I. Wilson. 2013. Distinct roles of TRP channels in auditory transduction and amplification in Drosophila. *Neuron* 77:115–28.
- Lev, S., D. a Zeevi, A. Frumkin, V. Offen-Glasner, G. Bach, and B. Minke. 2010. Constitutive activity of the human TRPML2 channel induces cell degeneration. *The Journal of biological chemistry* 285:2771–82.
- Liang, X., J. Madrid, R. Gärtner, J.-M. Verbavatz, C. Schiklenk, M. Wilsch-Bräuninger, A. Bogdanova, F. Stenger, A. Voigt, and J. Howard. 2013. A NOMPC-dependent membrane-microtubule connector is a candidate for the gating spring in fly mechanoreceptors. *Current biology : CB* 23:755–63.
- Liang, X., J. Madrid, H. S. Saleh, and J. Howard. 2011. NOMPC, a member of the TRP channel family, localizes to the tubular body and distal cilium of Drosophila campaniform and chordotonal receptor cells. *Cytoskeleton (Hoboken, N.J.)* 68:1–7.
- Liu, B., H. Du, R. Rutkowski, A. Gartner, and X. Wang. 2012. LAAT-1 is the lysosomal lysine/arginine transporter that maintains amino acid homeostasis. *Science (New York, N.Y.)* 337:351–4.
- Lloyd-Evans, E., A. J. Morgan, X. He, D. A. Smith, E. Elliot-Smith, D. J. Sillence, G. C. Churchill, E. H. Schuchman, A. Galione, and F. M. Platt. 2008. Niemann-Pick disease type C1 is a sphingosine storage disease that causes deregulation of lysosomal calcium. *Nature medicine* 14:1247–55.
- Lu, Q., P. R. Senthilan, T. Effertz, B. Nadrowski, and M. C. Göpfert. 2009. Using Drosophila for studying fundamental processes in hearing. *Integrative and comparative biology* 49:674–80.
- Lu, S. Q. 2011. The virtual ear: deducing transducer function in the Drosophila ear. Georg-August-Universität Göttingen, Göttingen, Germany.

- Luzio, J. P., P. R. Pryor, and N. A. Bright. 2007. Lysosomes: fusion and function. *Nature reviews. Molecular cell biology* 8:622–32.
- MacGurn, J. A., P.-C. Hsu, M. B. Smolka, and S. D. Emr. 2011. TORC1 regulates endocytosis via Npr1-mediated phosphoinhibition of a ubiquitin ligase adaptor. *Cell* 147:1104–17.
- Mariño, G., M. Niso-Santano, E. H. Baehrecke, and G. Kroemer. 2014. Self-consumption: the interplay of autophagy and apoptosis. *Nature reviews. Molecular cell biology* 15:81–94.
- Martina, J. A., B. Lelouvier, and R. Puertollano. 2009. The calcium channel mucolipin-3 is a novel regulator of trafficking along the endosomal pathway. *Traffic (Copenhagen, Denmark)* 10:1143–56.
- Mazet, F., J. K. Yu, D. A. Liberles, L. Z. Holland, and S. M. Shimeld. 2003. Phylogenetic relationships of the Fox (Forkhead) gene family in the Bilateria. *Gene* 316:79–89.
- McNeil, P. L., and T. Kirchhausen. 2005. An emergency response team for membrane repair. *Nature reviews. Molecular cell biology* 6:499–505.
- Montesano, R. 1979. Inhomogeneous distribution of filipin-sterol complexes in the ciliary membrane of rat tracheal epithelium. *The American journal of anatomy* 156:139–45.
- Moreau, K., M. Renna, and D. C. Rubinsztein. 2013. Connections between SNAREs and autophagy. *Trends in biochemical sciences* 38:57–63.
- Mosavi, L. K., T. J. Cammett, D. C. Desrosiers, and Z.-Y. Peng. 2004. The ankyrin repeat as molecular architecture for protein recognition. *Protein science : a publication of the Protein Society* 13:1435–48.
- Mullock, B. M., C. W. Smith, G. Ihrke, N. A. Bright, M. Lindsay, E. J. Parkinson, D. A. Brooks, R. G. Parton, D. E. James, J. P. Luzio, and R. C. Piper. 2000. Syntaxin 7 is localized to late endosome compartments, associates with Vamp 8, and is required for late endosome-lysosome fusion. *Molecular biology of the cell* 11:3137–53.
- Nachury, M. V., E. Seeley, and H. Jin. 2010. Trafficking to the ciliary membrane: How to get across the periciliary diffusion barrier? *Annual review of cell and developmental biology* 10:59–87.
- Nadrowski, B., J. T. Albert, and M. C. Göpfert. 2008. Transducer-based force generation explains active process in Drosophila hearing. *Current biology : CB* 18:1365–72.
- Nadrowski, B., and M. C. Göpfert. 2009. Level-dependent auditory tuning. *Communicative & Integrative Biology* 2:1:7–10.
- Nagata, K., L. Zheng, T. Madathany, A. J. Castiglioni, J. R. Bartles, and J. Garci. 2008. The varitint-waddler (Va) deafness mutation in TRPML3 generates constitutive, inward rectifying currents and causes cell degeneration 105.
- Nanchury, M., E. Seeley, and H. Jin. 2010. Trafficking to the ciliary membrane: how to get across the periciliary diffusion barrier? *Annual review of cell and developmental biology* 26:59–87.

- Newton, F. G., P. I. zur Lage, S. Karak, D. J. Moore, M. C. Göpfert, and A. P. Jarman. 2012. Forkhead transcription factor Fd3F cooperates with Rfx to regulate a gene expression program for mechanosensory cilia specialization. *Developmental cell* 22:1221–33.
- Novikoff, A. B., H. Beaufay, and C. de Duve. 1956. Electron microscopy of lysosomeric fractions from rat liver. *The Journal of biophysical and biochemical cytology* 2:179–84.
- Oropesa-Ávila, M., a Fernández-Vega, M. de la Mata, J. G. Maraver, M. D. Cordero, D. Cotán, M. de Miguel, C. P. Calero, M. V Paz, a D. Pavón, M. a Sánchez, a P. Zaderenko, P. Ybot-González, and J. a Sánchez-Alcázar. 2013. Apoptotic microtubules delimit an active caspase free area in the cellular cortex during the execution phase of apoptosis. *Cell death & disease* 4:e527.
- Di Palma, F., I. a Belyantseva, H. J. Kim, T. F. Vogt, B. Kachar, and K. Noben-Trauth. 2002. Mutations in Mcoln3 associated with deafness and pigmentation defects in varitint-waddler (Va) mice. *Proceedings of the National Academy of Sciences of the United States of America* 99:14994–9.
- Park, J., J. Lee, J. Shim, W. Han, J. Lee, Y. C. Bae, Y. D. Chung, C. H. Kim, and S. J. Moon. 2013. dTULP, the *Drosophila melanogaster* homolog of tubby, regulates transient receptor potential channel localization in cilia. *PLoS genetics* 9:e1003814.
- Peña-Llopis, S., S. Vega-Rubin-de-Celis, J. C. Schwartz, N. C. Wolff, T. A. T. Tran, L. Zou, X.-J. Xie, D. R. Corey, and J. Brugarolas. 2011. Regulation of TFEB and V-ATPases by mTORC1. *The EMBO journal* 30:3242–58.
- Peterson, M. R., C. G. Burd, and S. D. Emr. 1999. Vac1p coordinates Rab and phosphatidylinositol 3-kinase signaling in Vps45p-dependent vesicle docking/fusion at the endosome. *Current biology : CB* 9:159–62.
- Picazo-Juárez, G., S. Romero-Suárez, A. Nieto-Posadas, I. Llorente, A. Jara-Oseguera, M. Briggs, T. J. McIntosh, S. a Simon, E. Ladrón-de-Guevara, L. D. Islas, and T. Rosenbaum. 2011. Identification of a binding motif in the S5 helix that confers cholesterol sensitivity to the TRPV1 ion channel. *The Journal of biological chemistry* 286:24966–76.
- Powers, R. J., S. Roy, E. Atilgan, W. E. Brownell, S. X. Sun, P. G. Gillespie, and A. a Spector. 2012. Stereocilia membrane deformation: implications for the gating spring and mechanotransduction channel. *Biophysical journal* 102:201–10.
- Pryor, P. R., F. Reimann, F. M. Gribble, and J. P. Luzio. 2006. Mucolipin-1 is a lysosomal membrane protein required for intracellular lactosylceramide traffic. *Traffic (Copenhagen, Denmark)* 7:1388–98.
- Puertollano, R., and K. Kiselyov. 2009. TRPMLs: in sickness and in health. *American journal of physiology. Renal physiology* 296:F1245–54.
- Reitsma, S., D. W. Slaaf, H. Vink, M. A. M. J. van Zandvoort, and M. G. A. oude Egbrink. 2007. The endothelial glycocalyx: composition, functions, and visualization. *Pflügers Archiv : European journal of physiology* 454:345–59.
- Ren, J., L. Wen, X. Gao, C. Jin, Y. Xue, and X. Yao. 2008. CSS-Palm 2.0: an updated software for palmitoylation sites prediction. *Protein engineering, design & selection : PEDS* 21:639–44.

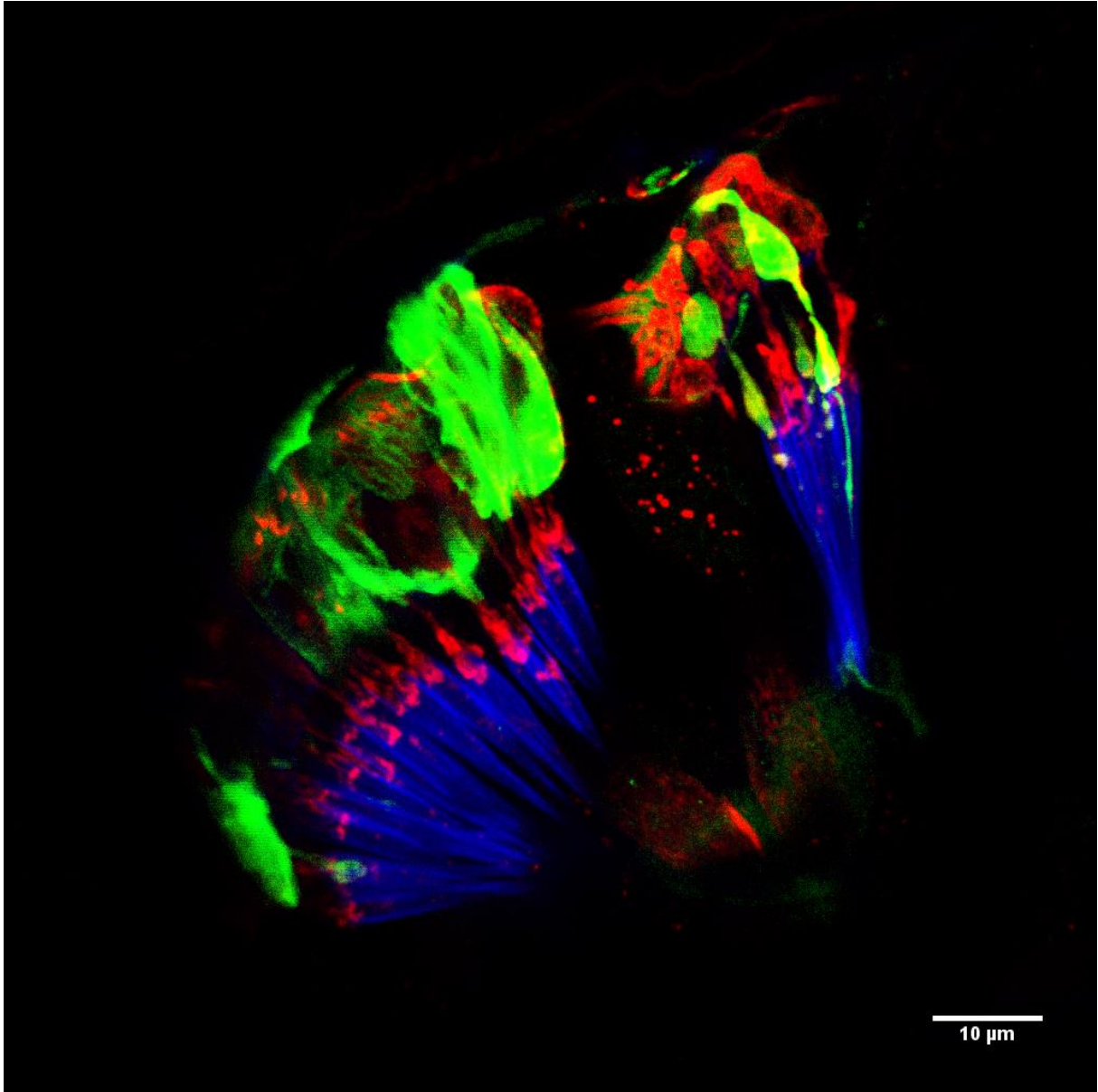
- Saftig, P., and J. Klumperman. 2009. Lysosome biogenesis and lysosomal membrane proteins: trafficking meets function. *Nature reviews. Molecular cell biology* 10:623–35.
- Samie, M. A., C. Grimm, J. A. Evans, C. Curcio-Morelli, S. Heller, S. A. Slaugenhaupt, and M. P. Cuajungco. 2009. The tissue-specific expression of TRPML2 (MCOLN-2) gene is influenced by the presence of TRPML1. *Pflügers Archiv : European journal of physiology* 459:79–91.
- Sardiello, M., M. Palmieri, A. di Ronza, D. L. Medina, M. Valenza, V. A. Gennarino, C. Di Malta, F. Donaudy, V. Embrione, R. S. Polishchuk, S. Banfi, G. Parenti, E. Cattaneo, and A. Ballabio. 2009. A gene network regulating lysosomal biogenesis and function. *Science (New York, N.Y.)* 325:473–7.
- Sedgwick, S. G., and S. J. Smerdon. 1999. The ankyrin repeat: a diversity of interactions on a common structural framework. *Trends in biochemical sciences* 24:311–6.
- Senthilan, P. R., D. Piepenbrock, G. Ovezmyradov, B. Nadrowski, S. Bechstedt, S. Pauls, M. Winkler, W. Möbius, J. Howard, and M. C. Göpfert. 2012. Drosophila auditory organ genes and genetic hearing defects. *Cell* 150:1042–54.
- Settembre, C., and A. Ballabio. 2014. Lysosome: regulator of lipid degradation pathways. *Trends in Cell Biology*:1–8.
- Settembre, C., A. Fraldi, D. L. Medina, and A. Ballabio. 2013. Signals from the lysosome: a control centre for cellular clearance and energy metabolism. *Nature reviews. Molecular cell biology* 14:283–96.
- Settembre, C., C. Di Malta, V. A. Polito, M. Garcia Arencibia, F. Vetrini, S. Erdin, S. U. Erdin, T. Huynh, D. Medina, P. Colella, M. Sardiello, D. C. Rubinsztein, and A. Ballabio. 2011. TFEB links autophagy to lysosomal biogenesis. *Science (New York, N.Y.)* 332:1429–33.
- Shen, D., X. Wang, X. Li, X. Zhang, Z. Yao, X. Dong, T. Yu, A. P. Lieberman, and H. D. Showalter. 2012. Lipid storage disorders block lysosomal trafficking by inhibiting TRP channel and calcium release. *Nature communications* 3.
- Sotomayor, M., D. P. Corey, and K. Schulten. 2005. In search of the hair-cell gating spring elastic properties of ankyrin and cadherin repeats. *Structure (London, England : 1993)* 13:669–82.
- Souto-Padrón, T., and W. de Souza. 1983. Freeze-fracture localization of filipin-cholesterol complexes in the plasma membrane of *Trypanosoma cruzi*. *The Journal of parasitology* 69:129–37.
- Sun, M., E. Goldin, S. Stahl, J. L. Falardeau, J. C. Kennedy, J. S. Acierno, C. Bove, C. R. Kaneski, J. Nagle, M. C. Bromley, M. Colman, R. Schiffmann, and S. A. Slaugenhaupt. 2000. Mucopolidosis type IV is caused by mutations in a gene encoding a novel transient receptor potential channel. *Human molecular genetics* 9:2471–8.
- Sun, Y., L. Liu, Y. Ben-Shahar, J. S. Jacobs, D. F. Eberl, and M. J. Welsh. 2009. TRPA channels distinguish gravity sensing from hearing in Johnston's organ. *Proceedings of the National Academy of Sciences of the United States of America* 106:13606–11.
- Tabuchi, K., M. Suzuki, A. Mizuno, and A. Hara. 2005. Hearing impairment in TRPV4 knockout mice. *Neuroscience letters* 382:304–8.

- Takumida, M., and M. Anniko. 2010. Expression of transient receptor potential channel mucolipin (TRPML) and polycystine (TRPP) in the mouse inner ear. *Acta oto-laryngologica* 130:196–203.
- Tam, B. M., O. L. Moritz, L. B. Hurd, and D. S. Papermaster. 2000. Identification of an outer segment targeting signal in the COOH terminus of rhodopsin using transgenic *Xenopus laevis*. *The Journal of cell biology* 151:1369–80.
- Tanaka, N., M. Kyuuma, and K. Sugamura. 2008. Endosomal sorting complex required for transport proteins in cancer pathogenesis, vesicular transport, and non-endosomal functions. *Cancer science* 99:1293–303.
- Tao, B., S. Bu, Z. Yang, B. Siroky, J. C. Kappes, A. Kispert, and L. M. Guay-Woodford. 2009. Cystin localizes to primary cilia via membrane microdomains and a targeting motif. *Journal of the American Society of Nephrology : JASN* 20:2570–80.
- Terman, A., and U. T. Brunk. 2004. Lipofuscin. *The international journal of biochemistry & cell biology* 36:1400–4.
- Thomas, J., L. Morlé, F. Soulavie, A. Laurençon, S. Sagnol, and B. Durand. 2010. Transcriptional control of genes involved in ciliogenesis: a first step in making cilia. *Biology of the cell / under the auspices of the European Cell Biology Organization* 102:499–513.
- Thompson, E. G., L. Schaheen, H. Dang, and H. Fares. 2007. Lysosomal trafficking functions of mucolipin-1 in murine macrophages. *BMC cell biology* 8:54.
- Todi, S. V., Y. Sharma, and D. F. Eberl. 2004. Anatomical and molecular design of the *Drosophila* antenna as a flagellar auditory organ. *Microscopy research and technique* 63:388–399.
- Todi, S. V., E. Sivan-Loukianova, J. S. Jacobs, D. P. Kiehart, and D. F. Eberl. 2008. Myosin VIIA, important for human auditory function, is necessary for *Drosophila* auditory organ development. *PLoS one* 3:e2115.
- Tyler, K. M., A. Fridberg, K. M. Toriello, C. L. Olson, J. a Cieslak, T. L. Hazlett, and D. M. Engman. 2009. Flagellar membrane localization via association with lipid rafts. *Journal of cell science* 122:859–66.
- Venkatachalam, K., T. Hofmann, and C. Montell. 2006. Lysosomal localization of TRPML3 depends on TRPML2 and the mucopolidosis-associated protein TRPML1. *The Journal of biological chemistry* 281:17517–27.
- Venkatachalam, K., a A. Long, R. Elsaesser, D. Nikolaeva, K. Broadie, and C. Montell. 2008. Motor deficit in a *Drosophila* model of mucopolidosis type IV due to defective clearance of apoptotic cells. *Cell* 135:838–51.
- Venkatachalam, K., and C. Montell. 2007. TRP channels. *Annual review of biochemistry* 76:387–417.
- Venkatachalam, K., C.-O. Wong, and C. Montell. 2013. Feast or Famine: Role of TRPML in preventing cellular amino acid starvation. *Autophagy* 9:1–3.
- Vergarajauregui, S., and R. Puertollano. 2006. Two di-leucine motifs regulate trafficking of mucolipin-1 to lysosomes. *Traffic (Copenhagen, Denmark)* 7:337–53.



- Wagenmakers, E.-J., and S. Farrell. 2004. AIC model selection using Akaike weights. *Psychonomic Bulletin & Review* 11:192–196.
- Wang, V. Y., B. A. Hassan, H. J. Bellen, and H. Y. Zoghbi. 2002. Drosophila atonal fully rescues the phenotype of Math1 null mice: new functions evolve in new cellular contexts. *Current biology : CB* 12:1611–6.
- Wang, W., X. Zhang, Q. Gao, and H. Xu. 2014. TRPML1: an ion channel in the lysosome. *Handbook of experimental pharmacology* 222:631–45.
- Wong, C.-O., R. Li, C. Montell, and K. Venkatachalam. 2012. Drosophila TRPML is required for TORC1 activation. *Current biology : CB* 22:1616–21.
- Yan, Z., W. Zhang, Y. He, D. Gorczyca, Y. Xiang, L. E. Cheng, S. Meltzer, L. Y. Jan, and Y. N. Jan. 2013. Drosophila NOMPC is a mechanotransduction channel subunit for gentle-touch sensation. *Nature* 493:221–5.
- Yu, F. H., and W. A. Catterall. 2004. The VGL-chanome: a protein superfamily specialized for electrical signaling and ionic homeostasis. *Science's STKE : signal transduction knowledge environment* 2004:re15.
- Zanini, D., and M. C. Göpfert. 2014. TRPs in hearing. Pages 899–916 in B. Nilius and V. Flockerzi, editors. *Handbook of experimental pharmacology*. Springer.
- Zeevi, D. a, S. Lev, A. Frumkin, B. Minke, and G. Bach. 2010. Heteromultimeric TRPML channel assemblies play a crucial role in the regulation of cell viability models and starvation-induced autophagy. *Journal of cell science* 123:3112–24.
- Zeevi, D. A., A. Frumkin, V. Offen-glasner, A. Kogot-levin, and G. Bach. 2009. A potentially dynamic lysosomal role for the endogenous TRPML proteins. *Journal of pathology* 219:153–162.
- Zimoń, M., J. Baets, M. Auer-Grumbach, J. Berciano, A. Garcia, E. Lopez-Laso, L. Merlini, D. Hilton-Jones, M. McEntagart, A. H. Crosby, N. Barisic, E. Boltshauser, C. E. Shaw, G. Landouré, C. L. Ludlow, R. Gaudet, H. Houlden, M. M. Reilly, K. H. Fischbeck, C. J. Sumner, V. Timmerman, A. Jordanova, and P. De Jonghe. 2010. Dominant mutations in the cation channel gene transient receptor potential vanilloid 4 cause an unusual spectrum of neuropathies. *Brain : a journal of neurology* 133:1798–809.

## 7 Supplementary data



**Supplementary figure 1. GFP expression driven by another *trpml-gal4* line.** GFP stained with anti-GFP antibodies is shown in green, while anti-Futsch antibody marking neurons and Phalloidin binding to F-actin-rich structures are presented in red and in blue, respectively.

Supplementary table 1. Akaike test results for comparison of two-transducer vs one-transducer type based gating spring models.

Yeast supplement	Age (days old)	Strain	Number of data points (n)	Number of parameters (k)	Residual sum of squares (rss)	$AIC_c$	$\Delta_i(AIC)$	Akaike weight ( $w_i$ )
-	1-3	<i>CantonS</i>	268	5	0,0131	-2650,2	0	1
			268	3	0,02	-2540,81	109,3962	0
-	1-3	<i>trpml<sup>1</sup></i>	324	5	0,0029	-3756,11	0	1
			324	3	0,0047	-3603,66	152,444	0
-	1-3	<i>iav<sup>1</sup></i>	268	5	0,0197	-2540,86	0	1
			268	3	0,0271	-2459,39	81,46924	0
-	1-3	<i>lav;trpml<sup>1</sup></i>	270	5	0,0088	-2779,48	0	1
			270	3	0,0119	-2702	77,4824	0
-	1-3	<i>w<sup>1118</sup></i>	324	5	0,0131	-3267,55	0	1
			324	3	0,028	-3025,44	242,1079	0
+	1-3	<i>w<sup>1118</sup></i>	162	5	0,0027	-1772,34	0	1
			162	3	0,0118	-1537,41	234,9253	0
-	1-3	<i>trpml<sup>1</sup></i>	324	5	0,0029	-3756,11	0	1
			324	3	0,0047	-3603,66	152,444	0
+	1-3	<i>trpml<sup>1</sup></i>	162	5	0,00089	-1951,4	0	1
			162	3	0,0019	-1833,27	118,1378	0
-	21	<i>w<sup>1118</sup></i>	162	5	0,0025	-1784,81	0	1
			162	3	0,0068	-1626,71	158,1024	0
-	21	<i>trpml<sup>1</sup></i>	162	5	0,0019	-1829,27	0	1
			162	3	0,0023	-1802,32	26,95095	0

## List of abbreviations

AIC, Akaike information criterion

AICc, Akaike information criterion with correction for finite sample size

AMMC, antennal mechanosensory and motor center

CAP, compound action potential

iBF, individual best frequency

IAV, Inactive

JO, Johnston's organ

JON, Johnston's organ neuron

ML4 or MLIV, Mucolipidosis IV

NAN, Nanchung

LDV, Laser Doppler yibrometer

LSD, lysosomal storage disorder

NPC, Niemann-Pick C

PSD, power spectral density

TM, transmembrane

TRP, transient receptor potential

TRPML, transient receptor potential mucolipin

UAS, upstream activating sequences

## Acknowledgements

It is a great honor to have this opportunity to thank the people who made my way through about 4 years of PhD possible. First of all, I would like to show my gratitude my supervisor and thesis committee member Prof. Martin Göpfert for his supervision and support. I thank him deeply for his endless patience and the opportunity and freedom of academic pursuits he provided. I also owe my gratitudes to two other thesis committee members, Prof. André Fiala and Dr. Tina Pangrsic, for their insights into my project.

I would like to thank my former colleague Dr. Thomas Effertz who started this project and established the methods. At the same time, I thank Dr. Qianhao Simon Lu for building the setup and making the program for data processing. I thank Dr. Christian Spalthoff, who kindly shared his gating compliance data from *CantonS* and *iav* mutants, scripts, and knowledge regarding the measurements, setup and statistics. Without Simon and Christian, I wouldn't even have made the plots in time.

I would like to thank Stephanie Pauls, Margret Winkler and Silvia Guberti for their technical support as well as for their extraordinary kindness. In addition, I owe my thanks to Gudrun Matthes for her administrative guidance, for making it possible for a foreigner with absolutely no idea on the matter to stay legally in this country famous for its bureaucracy.

I thank my previous and current office mates Dr. Somdatta Karak, Natasa Miljus, Dr. Marta Andres and Paule Lefebvre plus Dr. Damiano Zanini for all the cultural and emotional as well as scientific moments we shared together. I am also grateful to my colleague Philipp Jähde for helping me try out different ideas and providing small technical advices which were always turned out to be very helpful. I thank Dr. Christian Spalthoff, Dr. David Piepenbrock and Radoslaw Katana for letting me use their setup and learn the methods from them. And I'd like to thank all my colleagues for giving me different ideas and making me laugh and smile.

I thank Dr. Venkatachalam for sharing *trpml* fly strains, which were already carrying the mutation and *uas* constructs together, sparing me some crosses. I also thank Prof. Changsoo Kim and Dr. Katja Köhler for kindly providing their precious antibodies.

It is a pleasure for me to thank my former supervisors Prof. Jung-Ha Lee and Prof. Reinhard Schuh for showing me how exciting it can be to study science and providing me unconditional support and guidance as mentors. I give my special thanks to Prof. Lee for introducing me into the field of ion channels and Reinhard for letting me experience the fun of working with *Drosophila*, the great experimental organism.

Last but not least, I'd like to show my deepest gratitude to my friends and family for being there, with their limitless support and trust.

## Curriculum vitae

### Personal information

<b>Name</b>	Seol-hee Joo
<b>Date of Birth</b>	23 <sup>rd</sup> of November, 1981
<b>Place of Birth</b>	Seoul
<b>Nationality</b>	South Korea

### Education

06.2011-present	PhD candidate in Sensory and motor neuroscience, Göttingen University, Göttingen, Germany, Thesis title: Probing roles of TRPML in <i>Drosophila</i> hearing.
09.2009-05.2011	M.S. in Molecular biology, Göttingen University, Göttingen, Germany, Thesis title: The role of <i>trpml</i> in hearing of <i>Drosophila melanogaster</i> .
09.2006-02.2009	M. eng. in Integrated biotechnology (with honors), Sogang University Seoul, South Korea, Thesis title: Interaction of $\beta$ Subunits with $Ca_v3.1$ T-type $Ca^{2+}$ Channels.

02.2000-08.2006

B.S. in Life science and B.B.A. in Business administration (with honors), Sogang University, Seoul, South Korea.

## **Publications**

Jaspers MH, Nolde K, Behr M, Joo SH, Plessmann U, Nikolov M, Urlaub H, Schuh R, The claudin Megatrachea protein complex, *J. Biol. chem.*, 2012.

Kang HW, Moon HJ, Joo SH, Lee JH, Histidine residues in the IS3-IS4 loop are critical for nickel-sensitive inhibition of the Cav2.3 calcium channel, *FEBS lett.*, 2007.